Density Cumulant Theory for Ground and Excited Electronic states

by

Andreas Victor Copan

(Under the Direction of Henry F. Schaefer III)

Abstract

Density cumulant theory (DCT) describes the state of an electronic system by variationally optimizing a parametrization of the two-particle density cumulant. The cumulant is a statistical descriptor of the electronic density distribution which naturally decouples independent subsystems, leading to desirable properties like size-extensivity which have given the coupled-cluster methods pride of place in electronic structure theory. We present benchmarks calculations demonstrating the superior performance of density cumulant theory relative to coupled-cluster theory for the description of ground-state properties. Next, we extend this method for the description of excited states using linear response theory. Finally, we develop algorithms for the new excited state model which enable us to study larger systems.

Index words: Electronic structure theory, cumulants, density matrices, linear response theory, excited states, coupled-cluster theory

Density Cumulant Theory for Ground and Excited Electronic states

by

Andreas Victor Copan

B.A., Bethel University, 2013

A Dissertation Submitted to the Graduate Faculty
of The University of Georgia in Partial Fulfillment
of the
Requirements for the Degree

Doctor of Philosophy

Athens, Georgia

2018

Density Cumulant Theory for Ground and Excited Electronic states

by

Andreas Victor Copan

Approved:

Major Professor: Henry F. Schaefer III

Committee: Gary E. Douberly
Henning Meyer

Electronic Version Approved:

Suzanne Barbour
Dean of the Graduate School
The University of Georgia
May 2018

In memory of Valery Andreiyevich and Valtraut Kirsch Copan

Contents

Chapter 1

Introduction and Literature Review

1.1 Naive Electronic Structure Theory

As an entry point to electronic structure theory, let us begin by forgetting what we know about electrons from the standard model of particle physics. From the standpoint of Heisenberg and others developing the new quantum theory in 1925[2] chemical matter was described by nimble, negatively-charged electrons orbiting heavy, positively-charged nuclei. This theory would be conceptually clarified in the following year by Schrödinger's development of wave mechanics,[3–5] which described the possible states of electrons in a molecule as eigenfunctions of the quantum-mechanical Hamiltonian, oscillating in time with a frequency proportional to their energy. In atomic units:

$$\Psi(t) = \Psi e^{-iEt} \qquad \hat{H}\Psi = E\Psi. \tag{1.1}$$

Crudely speaking, this Hamiltonian is derived from its classical counterpart by replacing its momentum variables with del operators divided by the imaginary

unit, $\hat{\mathbf{p}} = \frac{1}{i}\nabla$. It can be written as a sum over one- and two-electron terms

$$\hat{H} = \sum_{i}^{\text{electrons}} \hat{h}_i + \sum_{i<j}^{\substack{\text{electron}\\ \text{pairs}}} \hat{g}_{ij} \tag{1.2}$$

where the one-electron operator $\hat{h}_i$ describes the kinetic energy of the i^{th} electron and its electrostatic (Coulomb's law) attraction to the nuclei, and the two-electron operator $\hat{g}_{ij}$ describes the Coulombic repulsion between electrons i and j.

$$\hat{h}_i \equiv \tfrac{1}{2}\hat{\mathbf{p}}_i^2 - \sum_{A}^{\text{nuclei}} \frac{Z_A}{|\mathbf{r}_A - \mathbf{r}_i|} \qquad \hat{g}_{ij} \equiv \frac{1}{|\mathbf{r}_i - \mathbf{r}_j|} \tag{1.3}$$

The vector space containing the wavefunction Ψ is the system's Hilbert space, $\mathcal{H}$, which in this case is the space of square integrable functions of n position variables, $L^2(\mathbb{R}^{3n})$, one for each electron in the molecule. Since this space is infinite-dimensional, the only way forward in most cases is to determine a basis that approximately spans the states of interest. Here we are helped by the fact that a function of n position variables can be written as a linear combination of products

$$\Psi(\mathbf{r}_1, \ldots, \mathbf{r}_n) = \sum_{p_1 \cdots p_n} c_{p_1 \cdots p_n}\, \phi_{p_1}(\mathbf{r}_1) \cdots \phi_{p_n}(\mathbf{r}_n) \tag{1.4}$$

where the one-electron functions or *orbitals* in this expansion span a one-electron Hilbert space, $\mathcal{H}_{\text{e}} = L^2(\mathbb{R}^3)$. More generally, the Hilbert space of a system is always given by a tensor product of the Hilbert spaces for its constituent particles.

$$\mathcal{H} = \mathcal{H}_{\text{e}} \otimes \mathcal{H}_{\text{e}} \otimes \cdots \tag{1.5}$$

In words, this says that the states of a system are spanned by all possible combinations of the states its components exhibit in isolation. This enables a general strategy for bootstrapping the electronic structure problem:

1. The states of a single electron orbiting a single nucleus are determined by the spherical symmetry of the nuclear potential to have a degenerate shell structure where the energy of the state increases with the number of nodal surfaces in the function. These 1s, 2s, 2p, ... atomic orbitals have analytically known functional forms.

2. Treating the other electrons in a molecule as static fields which partially shield the nuclear charges, the states of individual electrons in a molecule are well described as linear combinations of atomic one-electron functions centered on each nucleus. The dominant contributions to these molecular orbitals come from atomic orbitals with a similar energy, so that the lowest energy molecular orbital typically looks like the 1s orbital of the nucleus with the greatest charge, with very little contribution from, say, the 42g orbital of another atom. The higher energy states are linear combinations of higher energy atomic orbitals with increasing numbers of nodes.

3. Finally, the total electronic wavefunction is described by a linear combination of products of these molecular orbitals, and the electronic ground-state will be spanned to a good approximation by products of the low-energy molecular orbitals. When the molecular orbitals are weakly interacting, the mean-field approximation of step 2 furnishes a good description of their motions, and

the wavefunction will be heavily dominated by a single one of these products. From a statistical perspective, this means that the electron probability density of the wavefunction approximately separates into a product of one-electron densities, because the molecular orbitals are *weakly correlated*.

At the end of this procedure, we have a matrix equation in the product basis.

$$\mathbf{Hc} = E\mathbf{c} \qquad (\mathbf{H})_{PQ} = \langle \phi_{p_1} \cdots \phi_{p_n} | \hat{H} | \phi_{q_1} \cdots \phi_{q_n} \rangle \tag{1.6}$$

In the limit of a complete expansion, this eigenvalue equation is exactly equivalent to the Schrödinger equation and the coefficients of the solution vector correspond to the components of the wavefunction along our product functions. In order to stack the deck in favor of one product in the expansion, we can determine the molecular orbitals in step 2 to minimize its energy expectation value

$$\langle \phi_1 \cdots \phi_n | \hat{H} | \phi_1 \cdots \phi_n \rangle = \sum_{i=1}^{\text{orbitals}} h_i^i + \sum_{i<j}^{\substack{\text{orbital} \\ \text{pairs}}} g_{ij}^{ij} \tag{1.7}$$

where we have defined the all-important *one- and two-electron integrals*.

$$h_p^q \equiv \langle \phi_p | \hat{h}_1 | \phi_q \rangle = \int d^3\mathbf{r}_1 \, \phi_p^*(\mathbf{r}_1) \hat{h}_1 \phi_q(\mathbf{r}_1) \tag{1.8}$$

$$g_{pq}^{rs} \equiv \langle \phi_p \phi_q | \hat{g}_{12} | \phi_r \phi_s \rangle = \int d^3\mathbf{r}_1 d^3\mathbf{r}_2 \, \phi_p^*(\mathbf{r}_1) \phi_q^*(\mathbf{r}_2) \hat{g}_{12} \phi_r(\mathbf{r}_1) \phi_s(\mathbf{r}_2) \tag{1.9}$$

For an orthonormal orbital basis, this minimization leads to an effective Schrödinger equation for one-electron states

$$(\hat{h}_1 + \hat{v}_1)\phi_i(\mathbf{r}_1) = \epsilon_i\,\phi_i(\mathbf{r}_1) \tag{1.10}$$

where $\hat{v}_1$ is the mean electrostatic field of the other electrons in the molecule.

$$\hat{v}_1 \equiv \sum_{j\neq i} \int d\mathbf{r}_2\, \frac{\phi_j^*(\mathbf{r}_2)\phi_j(\mathbf{r}_2)}{|\mathbf{r}_1 - \mathbf{r}_2|} \tag{1.11}$$

This is the mean-field approximation described in step 2 above. We complete the bootstrapping cycle by expanding these unknown molecular orbitals in the basis of the atomic orbitals described in step 1 and solving for the expansion coefficients.

The general strategy we have just outlined carries over into modern electronic structure theory, but it is missing two essential ingredients: the spin of the electron, and the antisymmetric permutational symmetry of electrons as indistinguishable particles. We turn to these next.

1.2 Spin

The non-relativistic theory of one-electron states was in a sense completed with Pauli's publication solution of the spectrum of hydrogen at the start of 1926.[6] His work concludes with a discussion of the recent work by Goudsmit and Uhlenbeck[7] showing that the anomalous Zeeman splitting of the alkali metals could be explained by positing an intrinsic source of angular momentum and magnetism for the electron besides that generated by its orbital motion about the nucleus. This

was the electron's spin. The need for such a theory had already been understood by Pauli in his analysis of alkali metal spectra earlier in the previous year:

> In alkali metals the angular momentum values of the atom, and its energy changes in the presence of an external magnetic field, are appropriately interpreted as the sole working of the optically active electron, and the same situation is thought to be the case in the observations of the anomalous Zeeman effect. *From this standpoint, the doublet structure of the alkali spectra, as well as the breakdown of Larmor's theorem, must therefore come from some intrinsic, classically non-describable type of two-valuedness that is a characteristic of the optically active electron.* (Translated from Ref. 8 with emphasis added.)

In hindsight, the Stern-Gerlach experiment[9] had already shown in 1922 that the 5s electron of the silver atom was quantized into two magnetic states, whereas the new quantum theory predicted an odd number of magnetic states $(0, \pm 1, \pm 2, \ldots)$ for the spatial orbits of a charged particle. This new source of angular momentum was characterized by half-integer values whose eigenfunctions cannot exist in $L^2(\mathbb{R}^3)$.

$$\hat{s}_z \psi = \pm \tfrac{1}{2} \psi \tag{1.12}$$

The new "spinor" component of the electron's state is represented in $\mathbb{C}^2$ as

$$\hat{s}_z = \frac{1}{2} \begin{pmatrix} 1 & 0 \\ 0 & -1 \end{pmatrix} \qquad \alpha = \begin{pmatrix} 1 \\ 0 \end{pmatrix} \qquad \beta = \begin{pmatrix} 0 \\ 1 \end{pmatrix} \tag{1.13}$$

where α is the "spin-up" state and β is the "spin-down" state, and the states of individual electrons are described not by orbitals but by spin-orbitals:

$$\psi(\mathbf{r},\sigma) = \phi(\mathbf{r})\,\omega_\sigma \qquad \omega_\sigma \equiv \begin{cases} \alpha_\sigma & \text{if spin projection is } +1/2 \\ \beta_\sigma & \text{if spin projection is } +1/2 \end{cases} \tag{1.14}$$

which live in an extended Hilbert space, $\mathcal{H}_\mathrm{e} = L^2(\mathbb{R}^3) \otimes \mathbb{C}^2$. The new spin-variable σ refers to the first or second vector component of the spinor, which is 1 or 0 depending on whether the state is spin-up or spin-down.

1.3 Antisymmetry

Pauli exclusion[10]

> By considering the case of strong magnetic fields we can reduce [earlier observations] that the number of electrons in a completed subgroup is the same as the number of corresponding terms of the Zeeman effect of the alkali spectra, to the following more general rule about the occurrence of equivalent electrons in an atom: There can never be two or more equivalent electrons in an atom for which in strong fields the values of all quantum numbers n, l, k, m_l (or, equivalently, n, l, m_l, m_s) are the same. If an electron is present in the atom for which these quantum numbers (in an external field) have definite values, this state is "occupied." ... We cannot give a further justification for this rule, but it seems to be a very plausible one.

Exchange symmetry[11]

The aspects of de Broglie's theory of waves that lead to Bose-Einstein statistics[12–14] appear to have no analogue in quantum mechanics; Ad hoc rules like Pauli's ban on equivalent orbitals have no expression in the mathematical formalism of quantum mechanics as it stands. ... Finally there is one known difficulty in the quantitative interpretation of spectra that we should remind ourselves of: The splitting of singlet and triplet states in the spectra of the alkaline earth metals and in helium is too big by an order of magnitude to be explained as a difference in the magentic interaction energies of two spinning electrons.

$$\Phi_{p_1 \cdots p_n}(1, \ldots, n) = \tfrac{1}{\sqrt{n!}} \sum_{\pi} (-)^{\pi} \psi_{p_1}(\pi_1) \cdots \psi_{p_n}(\pi_n) \tag{1.15}$$

1.4 Modern Electronic Structure Theory

$$a_p \Psi(1, \ldots, n) \equiv \sqrt{n} \int d(1)\, \psi_p^*(1) \Psi(1, \ldots, n) \tag{1.16}$$

$$1_n = \tfrac{1}{\sqrt{n}} \sum_{p} \psi_p(1)\, a_p \tag{1.17}$$

$$\langle \Psi | \hat{H} | \Psi \rangle = \sum_{pq} h_p^q \langle \Psi | a_p^\dagger a_q | \Psi \rangle + \tfrac{1}{2} \sum_{pqrs} g_{pq}^{rs} \langle \Psi | a_p^\dagger a_q^\dagger a_s a_r | \Psi \rangle \tag{1.18}$$

1.5 Prospectus

Hydrogen or silver or alkali metals

$$(\hat{h} + \hat{v}_{\mathrm{e}})|\psi\rangle = \epsilon|\psi\rangle \qquad \hat{h} = \tfrac{1}{2}\hat{\mathbf{p}}^2 + \hat{v}_{\mathrm{n}} \qquad \hat{v}_{\mathrm{n}} = \sum_a^{\text{nuclei}} \frac{q_a}{|\mathbf{r}_a - \hat{\mathbf{r}}|} \tag{1.19}$$

$$\mathcal{H} = L^2(\mathbb{R}^3) \tag{1.20}$$

1.5.1 Symmetry

Symmetry properties of the potential give us spatial symmetries

$$\hat{o}|\psi\rangle = o|\psi\rangle \tag{1.21}$$

point groups and lattice groups. For one electron atoms the O(3) symmetries are described by the conservation of angular momentum, $\hat{\mathbf{j}}^2$ and $\hat{j}_z$.

Atoms: angular momentum (s, p, d)

Free electrons: plane waves

Molecules and crystals are described by symmetry adapted combinations of these functions

Goudsmit-Uhlenbeck (Uhlenbeck:1926p264) give us spin, which is a constant intrinsic to the electron as a particle

$$\hat{s}^2|\psi\rangle = \tfrac{3}{4}|\psi\rangle \tag{1.22}$$

The earlier Stern-Gerlach experiment (Gerlach:1922p349) showed in hindsight that spin can be oriented up or down along a given axis

$$\hat{s}_z|\psi\rangle = \pm\tfrac{1}{2}|\psi\rangle \tag{1.23}$$

$$\hat{s}_z = \tfrac{1}{2}(|\alpha\rangle\langle\alpha| - |\beta\rangle\langle\beta|) \tag{1.24}$$

$$\mathcal{H} = L^2(\mathbb{R}^3) \otimes \mathrm{SU}(2) \tag{1.25}$$

Two problems led to particle stats: the anomalous Zeeman effect, and the absence of electron *bunching*. In an orbital picture, you would expect all of the electrons to fall in the lowest energy state, such that the ground state is qualitatively described by a product

$$\Psi_0(1, \ldots, n) \approx \psi_0(1) \cdots \psi_0(n) \tag{1.26}$$

which is indeed what you find for bosons.

Paul describing spin before people knew what it was (Pauli:1925p373): "The closed energy configurations contribute nothing to the magnetic moment or angular momentum of the atom. In particular, in alkali metals the angular momentum values of the atom and its energy changes in the presence of an external magnetic field are appropriately interpreted as the sole working of the optically active electron, and the same situation is thought to be the case in the observations of

the anomalous Zeeman effect. From this standpoint, the doublet structure of the alkali spectra, as well as the breakdown of Larmor's theorem, must therefore come from some intrinsic, classically non-describable type of two-valuedness that is a characteristic of the optically active electron's state." Pauli proposed this without proposing any model for this extra degree of freedom. That was the contribution of Uhlenbeck and Goudsmit in 1926.

Pauli exlusion (Pauli:1925p756): "By considering the case of strong magnetic fields we can reduce [E. C.] Stoner's result, that the number of electrons in a completed subgroup [of an atom] is the same as the number of the corresponding terms of the Zeeman effect of the alkali spectra, to the following more general rule about the occurrence of equivalent electrons in an atom: *There can never be two or more equivalent electrons in an atom for which in strong fields the values of all quantum numbers* n, k_1, k_2, m_1 *(or, equivalently* n, k_1, m_1, m_2*) are the same. If an electron is present in the atom for which these quantum numbers (in an external field) have definite values, this state is "occupied."* ... We cannot give a further justification for this rule, but it seems to be a very plausible one. It refers, as mentioned, first of all to the case of strong field. However, from thermodynamic arguments (the invariance of statistic weights under adiabatic transformations of the system) it follows that the number of stationary states of an atom must be the same in strong and weak fields for given values of the number k_1 and k_2 of the separate electrons and a value of $\overline{m_1} = \sum m_1$ for the whole atom."

This is in contrast to photons in stimulated emission, where they are all forced to occupy the same state.

1.5.2 Antisymmetry

Heisenberg to Pauli (May 5, 1926) on the connection between Pauli exclusion and the singlet triplet gap in helium (Mehra:1982): *I want to write to you that I have found a rather decisive argument that your exclusion of equivalent orbitals is connected with the singlet-triplet separation [in helium].*

Heisenberg to Born (May 26, 1926) on the challenge of calculating the energy states of helium (Mehra:1982): *The large separation between the singlet and triplet systems could not be explained by a magnetic interaction of the spinning electrons; one had therefore to assume with Hund a large force of unknown origin between the magnets [Hund's rule].*

He explains everything by qualitative arguments in his paper on "The Many-Body Problem and Resonance in Quantum Mechanics" (Heisenberg:1926p411), which *aims to lay the groundwork for a quantum-mechanical treatment of the many-body problem.*

He is the first to propose the form of the Slater determinant.

1.6 Fock Space

$$\hat{H} = \sum_{i=1}^{n} \hat{h}(i) + \sum_{i=1}^{n} \sum_{j=i+1}^{n} \hat{g}(i,j) \tag{1.27}$$

$$\hat{g}(i,j) = \frac{1}{|\hat{\mathbf{r}}_i - \hat{\mathbf{r}}_j|} \tag{1.28}$$

$$\mathcal{H}^n = \mathcal{H}(1) \otimes \cdots \otimes \mathcal{H}(n) \tag{1.29}$$

$$|\Psi\rangle = \sum_{p_1 \cdots p_n} c_{p_1 \cdots p_n} |\psi_{p_1}\rangle \otimes \cdots \otimes |\psi_{p_n}\rangle \tag{1.30}$$

Chapter 2

Benchmark Study of Density Cumulant Functional Theory: Thermochemistry and Kinetics*

*A. V. Copan, A. Y. Sokolov, and H. F. Schaefer, *J. Chem. Theory Comput.* 10, 2389 (2014). Reprinted here with permission of the publisher.

2.1 Abstract

We present an extensive benchmark study of density cumulant functional theory (DCFT) for thermochemistry and kinetics of closed- and open-shell molecules. The performance of DCFT methods (DC-06, DC-12, ODC-06, and ODC-12) is compared to that of coupled-electron pair methods ($CEPA_0$ and $OCEPA_0$) and coupled-cluster theory (CCSD and CCSD(T)) for the description of noncovalent interactions (A24 database), barrier heights of hydrogen-transfer reactions (HTBH38), radical stabilization energies (RSE30), adiabatic ionization energies (AIE), and covalent bond stretching in diatomic molecules. Our results indicate that out of four DCFT methods the ODC-12 method is the most reliable and accurate DCFT formulation to date. Compared to CCSD, ODC-12 shows superior results for all benchmark tests employed in our study. With respect to coupled-pair theories, ODC-12 outperforms $CEPA_0$, and shows similar accuracy to the orbital-optimized $CEPA_0$ variant ($OCEPA_0$) for systems at equilibrium geometries. For covalent bond stretching, ODC-12 is found to be more reliable than $OCEPA_0$. For the RSE30 and AIE datasets, ODC-12 shows competitive performance with CCSD(T). In addition to benchmark results, we report new reference values for the RSE30 dataset computed using coupled cluster theory with up to perturbative quadruple excitations.

2.2 Introduction

Recent developments in *ab initio* quantum chemistry have resulted in a variety of computational models for studying molecules. Apart from concerns about efficiency and accuracy, several concepts have evolved as criteria for judging the merits of a particular method. Energy-based criteria typically define an "ideal" approximation as one yielding correlation energies that are size-consistent, extensive[15], well-defined (giving continuous, unique potential surfaces), and variational.[16] While it has been argued that the practical benefits of variationality are rather limited,[17] the efficiency of gradient computations, at least, is improved by formulating a theory in terms of a Hermitian and stationary energy functional.[18] With respect to scope and stability, methods that show consistent performance for open-shell systems, strongly correlated states, and non-equilibrium geometries are particularly valuable.[17]

The incorrect scaling of truncated configuration interaction (CI) energies with system size has inspired the development of size-extensive alternatives. Among the earliest formulations, the coupled electron pair approximations (CEPAs)[19–23] attracted much attention in 1970s,[24–28] offering rigorous extensivity and size-consistency while retaining much of the linearity[29] of CI in their equations. CEPA methods, however, have been shown to rapidly deteriorate as the molecular geometry deviates from equilibrium[29] and yield energies that vary under the rotation of the occupied orbitals.[22] Partly in light of such defects, CEPA has been largely displaced by coupled-cluster (CC) theory.[17;30–36] In addition to size-extensivity, CC offers orbital invariance and improved stability for non-equilibrium structures[29],

but has a non-Hermitian energy functional and non-linear equations which are not readily amenable to parallel implementation. Although neither class of methods is strictly variational, VCEPA (variational CEPA) has been shown to be effectively equivalent to its non-variational counterpart.[37] Various other modifications to resolve the deficiencies of traditional CEPA have been explored, including self-consistent size-consistent CI,[38;39] orbital-invariant CEPA,[40;41] and orbital-optimized CEPA formulations.[42–45] Recently, the CEPA methods have been revived by Neese and co-workers[37;46;47] who developed the local pair-natural-orbital CEPA (LPNO-CEPA) methods and have implemented them for massively parallel computer architectures.

It has recently been demonstrated[48–51] that CEPA methods naturally arise in the context of theories that obtain the molecular energies from density cumulants, the connected and extensive components of the reduced density matrices (RDMs).[52–57] The advantage of cumulant-based theories is that, unlike their RDM-based counterparts,[58–60] they are naturally size-extensive and size-consistent.[55;61] We have recently achieved the first implementation[62;63] of density cumulant functional theory (DCFT), proposed by Kutzelnigg in 2006.[48] In DCFT, the molecular energy is obtained in terms of a mean-field one-particle RDM and the two-particle density cumulant, constrained to be at least approximately N-representable (*i.e.* to correspond to a physical N-electron wavefunction). Like traditional CC theory, DCFT is size-extensive and orbital-invariant, but it has the additional advantage of a stationary and Hermitian energy functional, which simplifies the computation of molecular properties. In the original DCFT formulation (DC-06)[48;62;63] N-

representability conditions derived from second-order Møller-Plesset perturbation theory (MPPT) were used,[64] yielding equations similar to those of the simplest CEPA model ($CEPA_0$),[21;23] but including higher-order terms in the description of one-particle correlation effects. Using the same set of conditions, we have developed new formulations of DCFT that take advantage of an improved description of the one-particle density matrix (DC-12)[65] and full orbital optimization (ODC-06 and ODC-12 methods).[66]

Our previous studies[62;63;65;66] demonstrated for a limited set of systems that the DC-06, DC-12, ODC-06 and ODC-12 methods generally yield molecular energies and properties competitive with those obtained by CCSD and CCSD(T), but may exhibit unstable performance due to imbalances in the description of electron correlation. Herein, we present an extensive benchmark of the DCFT methods with respect to thermochemical and kinetic molecular properties, including noncovalent interactions, barrier heights in hydrogen-transfer reactions, radical stabilization energies, and adiabatic ionization energies for challenging electron-dense systems. We conclude our benchmark study by testing the performance of DCFT for covalent bond stretching in diatomic molecules.

2.3 Overview of DCFT

In this section a short overview of DCFT is presented. For details on the theory the reader is referred to our earlier publications.[62;65;66] In the RDM methods[67] the exact molecular energy is expressed as a functional of the one- and two-particle

reduced density matrices, $\boldsymbol{\gamma}_1$ and $\boldsymbol{\gamma}_2$ (1-RDM and 2-RDM):

$$E = h^q_p \gamma^p_q + \tfrac{1}{2} g^{rs}_{pq} \gamma^{pq}_{rs} \,, \qquad [\boldsymbol{\gamma}_1]^p_q \equiv \gamma^p_q \,, \qquad [\boldsymbol{\gamma}_2]^{pq}_{rs} \equiv \gamma^{pq}_{rs} \,. \tag{2.1}$$

In Eq. (2.1), h^q_p and g^{rs}_{pq} are the usual one- and two-electron integrals in the orthonormal spin-orbital basis $\{\psi_p\}$ and summation over the repeated indices is implied. Expressing $\boldsymbol{\gamma}_1$ through $\boldsymbol{\gamma}_2$ via the partial trace relation $\sum_r \gamma^{pr}_{qr} = (N-1)\gamma^p_q$, the energy functional (2.1) can be minimized by varying $\boldsymbol{\gamma}_2$ subject to N-representability constraints. This is the essence of the variational 2-RDM approach.[67]

In DCFT, some of the challenges of the 2-RDM approach are circumvented by expanding $\boldsymbol{\gamma}_2$ in terms of its irreducible components – the 1-RDM and the two-particle cumulant (denoted by $\boldsymbol{\lambda}_2$):

$$\gamma^{pq}_{rs} = \gamma^p_r \gamma^q_s - \gamma^q_r \gamma^p_s + \lambda^{pq}_{rs} \,. \tag{2.2}$$

In Eq. (2.2), $\boldsymbol{\lambda}_2$ describes the correlated part of $\boldsymbol{\gamma}_2$ that cannot be expressed via $\boldsymbol{\gamma}_1$. The cumulant also determines the correlation contribution to $\boldsymbol{\gamma}_1$, allowing the 1-RDM to be decomposed as the sum of an idempotent 1-RDM ($\boldsymbol{\kappa}$) and a correlation correction ($\boldsymbol{\tau}$):

$$\boldsymbol{\gamma}_1 = \boldsymbol{\kappa} + \boldsymbol{\tau} \,. \tag{2.3}$$

The correlation component $\boldsymbol{\tau}$ is fully specified by $\boldsymbol{\lambda}_2$, whereas $\boldsymbol{\kappa}$ is independent of $\boldsymbol{\lambda}_2$. Eqs. (2.2) and (2.3) allow us to write an equivalent energy expression with $\boldsymbol{\kappa}$

and $\boldsymbol{\lambda}_2$ as independent functional parameters:

$$E[\boldsymbol{\kappa}, \boldsymbol{\lambda}_2] = \tfrac{1}{2}(h_p^q + f_p^q)(\kappa_q^p + \tau_q^p) + \tfrac{1}{4}\overline{g}_{pq}^{rs}\lambda_{pq}^{rs} \tag{2.4}$$

$$f_p^q = h_p^q + \overline{g}_{pr}^{qs}(\kappa_s^r + \tau_s^r) \qquad \overline{g}_{rs}^{pq} = g_{rs}^{pq} - g_{rs}^{qp} \tag{2.5}$$

Here, the generalized Fock operator $\boldsymbol{f}$ differs from that of Hartree-Fock theory by the presence of an external potential $\overline{g}_{pr}^{qs}\tau_s^r$ due to electron correlation.[48]

To date, all DCFT formulations make the energy (2.4) stationary with respect to variations of $\boldsymbol{\lambda}_2$, subject to cumulant N-representability constraints derived from second-order Møller-Plesset perturbation theory (MPPT).[64] To account for orbital relaxation effects, the two earliest DCFT methods, DC-06[48;62;63] and DC-12[65], determined the orbitals by diagonalizing the generalized Fock operator $\boldsymbol{f}$ defined in Eq. (2.4). These two methods differ in their description of 1-RDM N-representability. Whereas DC-06 employs an approximate expression for $\boldsymbol{\tau}$ in terms of $\boldsymbol{\lambda}_2$, DC-12 uses the exact relationship. Recently, we proposed orbital-optimized variants of DC-06 and DC-12 (ODC-06 and ODC-12),[66] which fully account for orbital relaxation effects.

2.4 Computational Details

All computations were performed using the Psi4 package.[68] The results were benchmarked against coupled cluster theory with single and double excitations (CCSD)[34–36], CCSD with perturbative triple excitations [CCSD(T)],[69;70] coupled electron pair approximation zero (CEPA_0),[21;23] and the orbital-optimized variant

of $CEPA_0$ ($OCEPA_0$)[43]. All electrons were correlated in all computations. The cc-pCVXZ[71;72] and aug-cc-pVXZ[73] basis sets (X = T, Q) were used (see text for details). Noncovalent interaction energies, hydrogen-transfer barrier heights, and radical stabilization energies were computed using geometries from the A24[74], HTBH38[75], and RSE30[76] benchmark databases, respectively, available in Psi4. Adiabatic ionization energies were computed from neutral and cation geometries optimized at each level of theory, with added harmonic zero-point vibrational energy corrections. Harmonic frequencies were computed by numerical differentiation of analytic energy gradients. Single-point energies were converged to 10^{-8} E_h, while the root mean square of the energy gradient was converged to 10^{-6} E_h/a_0 for geometry optimizations.

2.5 Results

2.5.1 Noncovalent Interactions

We begin by testing the accuracy of DCFT methods for the description of noncovalent interactions in 24 closed-shell molecular dimers, which are listed in Table 2.1. These molecular complexes comprise the A24 dataset[74] developed by Řezáč and Hobza to include a variety of noncovalent interactions, including hydrogen bonding and π-π stacking. Although Řezáč and Hobza reported the interaction energies at the CCSD(T) complete basis set (CBS) limit, we use CCSD(T)/aug-cc-pVTZ energies as reference values in order to effectively exclude basis-set incompleteness error from the comparison.

Table 2.1: Errors in interaction energies (kcal mol^{-1}) for 24 noncovalently bound molecular dimers comprising the A24 database[74] computed using seven methods with the aug-cc-pVTZ basis set. The errors are relative to CCSD(T) reference values (kcal mol^{-1}) shown in the rightmost column. For each method the mean absolute deviations from CCSD(T) (Δ_{MAE}, kcal mol^{-1}) and the standard deviations from the mean signed error (Δ_{SD}, kcal mol^{-1}) are also shown.

Complex (Sym.)	ΔCEPA$_0$	ΔDC-06	ΔDC-12	ΔCCSD	ΔOCEPA$_0$	ΔODC-06	ΔODC-12	CCSD(T)
$H_2O\cdots NH_3$ (C_s)	0.26	0.24	0.22	0.36	0.19	0.20	0.18	-7.18
$H_2O\cdots H_2O$ (C_s)	0.19	0.18	0.16	0.25	0.13	0.14	0.12	-5.71
$HCN\cdots HCN$ (C_s)	0.21	0.27	0.16	0.15	0.18	0.26	0.14	-7.12
$HF\cdots HF$ (C_s)	0.14	0.13	0.11	0.16	0.08	0.09	0.07	-5.20
$NH_3\cdots NH_3$ (C_{2h})	0.15	0.13	0.14	0.26	0.12	0.12	0.12	-3.43
$HF\cdots CH_4$ (C_{3v})	0.17	0.16	0.20	0.23	0.12	0.12	0.16	-2.30
$NH_3\cdots CH_4$ (C_{3v})	0.07	0.05	0.05	0.13	0.05	0.05	0.04	-1.08
$H_2O\cdots CH_4$ (C_s)	0.06	0.05	0.04	0.11	0.05	0.05	0.04	-1.03
$CH_2O\cdots CH_2O$ (C_s)	0.89	0.99	0.65	0.46	0.62	0.87	0.46	-5.23
$H_2O\cdots C_2H_4$ (C_s)	0.15	0.16	0.15	0.31	0.20	0.26	0.21	-3.33
$CH_2O\cdots C_2H_4$ (C_s)	0.21	0.18	0.14	0.27	0.19	0.24	0.16	-2.24
$HCCH\cdots HCCH$ (C_{2v})	0.07	0.05	0.05	0.20	0.10	0.12	0.10	-2.57

Complex (Sym.)	ΔCEPA$_0$	ΔDC-06	ΔDC-12	ΔCCSD	ΔOCEPA$_0$	ΔODC-06	ΔODC-12	CCSD(T)
$NH_3\cdots C_2H_4$ (C_s)	0.09	0.06	0.08	0.24	0.12	0.15	0.13	-2.07
$C_2H_4\cdots C_2H_4$ (C_{2v})	0.10	0.02	0.07	0.33	0.14	0.13	0.15	-1.81
$CH_4\cdots C_2H_4$ (C_s)	0.02	-0.02	0.01	0.14	0.05	0.04	0.06	-0.92
$BH_3\cdots CH_4$ (C_s)	0.23	0.18	0.24	0.37	0.18	0.16	0.22	-2.52
$CH_4\cdots C_2H_4$ (C_s)	0.13	0.09	0.13	0.23	0.10	0.09	0.09	-1.37
$CH_4\cdots C_2H_6$ (C_s)	0.09	0.06	0.09	0.17	0.07	0.06	0.09	-1.14
$CH_4\cdots CH_4$ (D_{3d})	0.08	0.06	0.08	0.14	0.06	0.05	0.08	-0.93
$Ar\cdots CH_4$ (C_{3v})	0.07	0.05	0.07	0.10	0.05	0.05	0.06	-0.78
$Ar\cdots C_2H_4$ (C_{2v})	0.03	-0.01	0.02	0.11	0.05	0.03	0.05	-0.63
$C_2H_4\cdots HCCH$ (C_{2v})	-0.02	-0.19	-0.01	0.38	0.07	-0.06	0.11	0.43
$C_2H_4\cdots C_2H_4$ (D_{2h})	-0.05	-0.30	-0.03	0.43	0.04	-0.16	0.11	0.41
$HCCH\cdots HCCH$ (D_{2h})	0.01	-0.09	0.02	0.34	0.10	0.02	0.12	0.91
Δ_{MAE}:	0.14	0.16	0.12	0.25	0.13	0.15	0.13	
Δ_{SD}:	0.18	0.23	0.13	0.11	0.12	0.18	0.09	

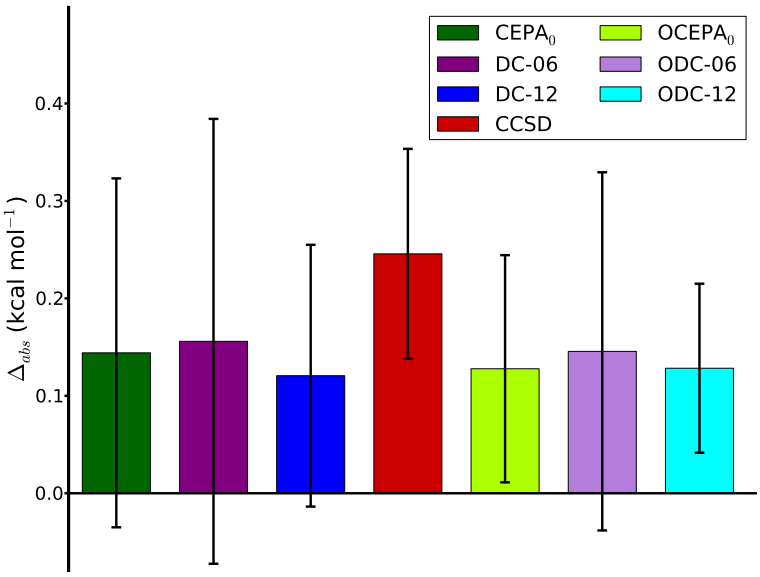

Figure 2.1: Mean absolute deviations (Δ_{MAE}, kcal mol^{-1}) and the standard deviations from the mean signed error (Δ_{SD}, kcal mol^{-1}) of the interaction energies for 24 noncovalently bound molecular dimers (A24 database) computed using seven methods with the aug-cc-pVTZ basis set. The errors are relative to CCSD(T)/aug-cc-pVTZ reference values. The Δ_{MAE} value is represented as a height of each colored box, while the Δ_{SD} value is depicted as a radius of the black vertical bar. See Table 2.1 for data on individual database members.

Figure 2.1 depicts mean absolute error (Δ_{MAE}) relative to CCSD(T) in the binding energies of CEPA$_0$, OCEPA$_0$, CCSD, and the four DCFT methods (DC-06, DC-12, ODC-06, and ODC-12), as well as the root mean square deviation from the average signed error (Δ_{SD}). All methods but CCSD give similar Δ_{MAE} values (0.14 ± 0.02 kcal mol^{-1}), and a comparison between CEPA$_0$, DC-06, and DC-12 and their orbital-optimized variants (OCEPA$_0$, ODC-06, and ODC-12) shows negligible 0.01 kcal mol^{-1} differences in each case. CCSD gives a significantly larger Δ_{MAE}

(0.25 kcal mol^{-1}) than the other methods, exceeding the DC-12 Δ_{MAE} by a factor of two (0.12 kcal mol^{-1}). The Δ_{SD} values are much more sensitive to the choice of method than the Δ_{MAE} values, and are noticeably affected by orbital optimization. ODC-12 gives the smallest standard deviation ($\Delta_{\mathrm{SD}} = 0.09$ kcal mol^{-1}), while the largest Δ_{SD} value was found for DC-06 (0.23 kcal mol^{-1}). The OCEPA$_0$, ODC-06, and ODC-12 methods ($\Delta_{\mathrm{SD}} = 0.12$, 0.18, and 0.09 kcal mol^{-1}, respectively) exhibit much more consistent performance than their non-orbital-optimized analogues, with Δ_{SD} smaller by 0.05 ± 0.01 kcal mol^{-1} in each case. CCSD also exhibits a relatively small Δ_{SD} value (0.11 kcal mol^{-1}), possibly due to its inclusion of single excitations which partly account for orbital relaxation.

Errors in interaction energy and CCSD(T) reference values for each molecular complex are shown in Table 2.1. The largest deviations from CCSD(T) were obtained for the formaldehyde dimer ($CH_2O \cdots CH_2O$, complex 9 in Table 2.1), for which DC-06, CEPA$_0$, and OCEPA$_0$ yield errors of 0.99, 0.89, and 0.87 kcal mol^{-1}, respectively. For this system, the best performance is shown by CCSD and ODC-12, both of which give an error of 0.46 kcal mol^{-1}. For systems with π-stacking interactions (complexes 22-24 in Table 2.1), CCSD shows large errors (0.38, 0.43, 0.34 kcal mol^{-1}) relative to the magnitude of the interaction energy (0.43, 0.41, 0.91 kcal mol^{-1}, respectively). Here CEPA$_0$, DC-12, and their orbital-optimized variants offer much better agreement with CCSD(T), with errors ranging from 0.01 to 0.15 kcal mol^{-1}.

Table 2.2: Errors in barrier heights (kcal mol^{-1}) for 18 hydrogen-transfer reactions ($R_1 + R_2H \rightarrow R_1H + R_2$) comprising the HTBH38 database[77] computed using five methods with the aug-cc-pVTZ basis set. The errors are relative to CCSD(T) reference values (kcal mol^{-1}) shown in the rightmost column. Each reaction includes barrier heights in the forward ($R_1 + R_2H \rightarrow [R_1R_2H]^*$) and reverse ($[R_1R_2H]^* \leftarrow R_1H + R_2$) directions, respectively, except in the case of $R_1 = R_2 = H$ where they are the same. The mean absolute (Δ_{MAE}, kcal mol^{-1}) and the mean percent (Δ_{rel}, %) errors with respect to CCSD(T), as well as the standard deviations from the mean signed error (Δ_{SD}, kcal mol^{-1}) are also shown.

	Reaction Barrier	ΔCEPA$_0$	ΔDC-12	ΔCCSD	ΔOCEPA$_0$	ΔODC-12	CCSD(T)
1	$H + HCl \rightarrow [HHCl]^*$	0.74	0.49	0.09	-0.41	-0.28	5.22
2	$OH + H_2 \rightarrow [OHH_2]^*$	3.77	3.38	1.82	0.88	1.24	4.99
3	$CH_3 + H_2 \rightarrow [CH_3H_2]^*$	1.60	1.46	1.37	0.46	0.70	11.29
4	$OH + CH_4 \rightarrow [OHCH_4]^*$	4.26	3.85	2.61	1.22	1.65	5.64
5	$H + H_2 \rightarrow [HH_2]^*$	0.80	0.69	0.30	-0.27	-0.05	9.77
6	$OH + NH_3 \rightarrow [OHNH_3]^*$	6.02	5.25	3.54	1.18	1.82	3.17
7	$HCl + CH_3 \rightarrow [HClCH_3]^*$	1.93	1.78	1.79	0.68	0.92	0.10
8	$OH + C_2H_6 \rightarrow [OHC_2H_6]^*$	4.66	4.21	2.69	1.28	1.72	2.69
9	$F + H_2 \rightarrow [FH_2]^*$	3.40	3.14	1.20	0.52	0.78	1.13
10	$O + CH_4 \rightarrow [OHCH_3]^*$	3.40	3.12	2.37	0.70	1.20	13.62
11	$H + PH_3 \rightarrow [HPH_3]^*$	0.93	0.86	0.59	-0.16	0.10	2.29
12	$H + HO \rightarrow [OHH]^*$	2.03	1.59	0.44	-0.61	-0.26	10.25
13	$H + H_2S \rightarrow [HH_2S]^*$	1.01	0.92	0.65	-0.11	0.14	3.17
14	$O + HCl \rightarrow [OHCl]^*$	6.33	6.01	3.58	0.79	1.51	9.74
15	$NH_2 + CH_3 \rightarrow [CH_3NH_2]^*$	2.48	2.22	1.99	0.49	0.86	7.66
16	$NH_2 + C_2H_5 \rightarrow [NH_2C_2H_5]^*$	2.48	2.22	2.09	0.55	0.92	8.21
17	$C_2H_6 + NH_2 \rightarrow [C_2H_6NH_2]^*$	3.30	3.00	2.73	1.23	1.62	10.39
18	$NH_2 + CH_4 \rightarrow [NH_2CH_4]^*$	2.98	2.72	2.55	1.11	1.48	13.23

	Reaction Barrier	ΔCEPA$_0$	ΔDC-12	ΔCCSD	ΔOCEPA$_0$	ΔODC-12	CCSD(T)
1	$[HHCl]^* \leftarrow H_2 + Cl$	1.44	1.31	1.61	0.53	0.77	7.39
2	$[OHH_2]^* \leftarrow H + H_2O$	2.09	1.66	0.09	-0.91	-0.58	21.07
3	$[CH_3H_2]^* \leftarrow H + CH_4$	0.95	0.80	0.38	-0.38	-0.11	14.91
4	$[OHCH_4]^* \leftarrow CH_3 + H_2O$	3.23	2.80	1.87	0.27	0.65	18.09
6	$[OHNH_3]^* \leftarrow H_2O + NH_2$	5.46	4.62	3.14	0.79	1.33	13.17
7	$[HClCH_3]^* \leftarrow Cl + CH_4$	1.97	1.94	2.31	0.78	1.16	5.89
8	$[OHC_2H_6]^* \leftarrow H_2O + C_2H_5$	3.34	2.89	1.85	0.28	0.64	18.49
9	$[FH_2]^* \leftarrow HF + H$	1.27	0.88	-0.78	-1.47	-1.33	32.95
10	$[OHCH_3]^* \leftarrow OH + CH_3$	2.62	2.29	1.82	0.32	0.68	7.43
11	$[HPH_3]^* \leftarrow PH_2 + H_2$	1.14	1.11	1.37	0.39	0.63	23.21
12	$[OHH]^* \leftarrow H_2 + O$	3.47	3.08	1.99	0.62	1.07	12.81
13	$[HH_2S]^* \leftarrow H_2 + HS$	1.51	1.51	1.88	0.65	0.97	16.41
14	$[OHCl]^* \leftarrow OH + Cl$	5.59	5.35	3.55	0.51	1.24	9.35
15	$[CH_3NH_2]^* \leftarrow CH_4 + NH$	2.77	2.49	2.26	0.73	1.12	21.32
16	$[NH_2C_2H_5]^* \leftarrow C_2H_6 + NH$	3.06	2.75	2.46	0.85	1.26	18.52
17	$[C_2H_6NH_2]^* \leftarrow NH_3 + C_2H_5$	2.54	2.30	2.30	0.63	1.02	16.20
18	$[NH_2CH_4]^* \leftarrow CH_3 + NH_3$	2.51	2.29	2.21	0.56	0.96	15.69
	Δ_{MAE}:	2.77	2.49	1.84	0.67	0.94	
	Δ_{SD}:	1.51	1.39	1.06	0.62	0.71	
	Δ_{rel} %:	99	90	77	29	40	

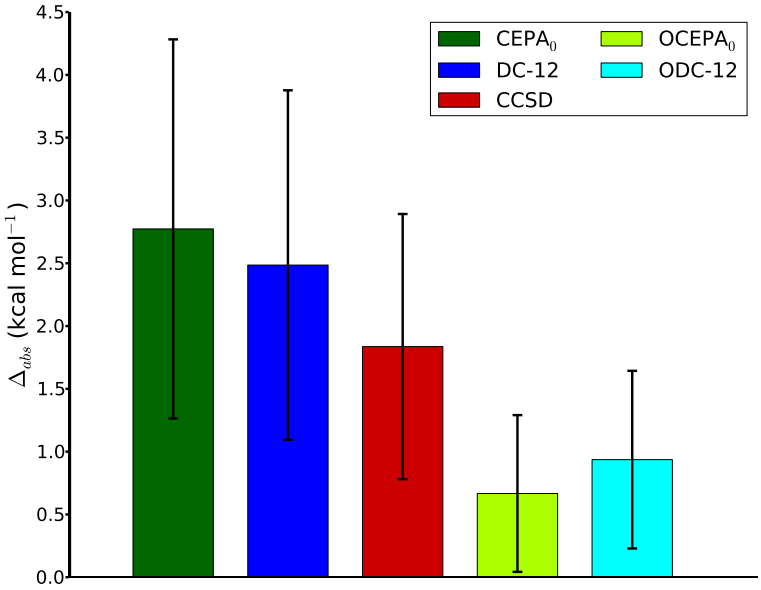

Figure 2.2: Mean absolute deviations (Δ_{MAE}, kcal mol^{-1}) and the standard deviations from the mean signed error (Δ_{SD}, kcal mol^{-1}) of barrier heights for 18 hydrogen-transfer reactions ($\mathrm{R_1 + R_2H \rightarrow R_1H + R_2}$, HTBH38 database) computed using five methods with the aug-cc-pVTZ basis set. The errors are relative to CCSD(T)/aug-cc-pVTZ reference values. The Δ_{MAE} value is represented as a height of each colored box, while the Δ_{SD} value is depicted as a radius of the black vertical bar. See Table 2.2 for data on individual database members.

2.5.2 Hydrogen-Transfer Reaction Barrier Heights

We continue by assessing the performance of DCFT methods in predicting barrier heights for 18 hydrogen-transfer reactions from the HTBH38 database:[75]

$$\mathrm{R_1 + R_2H \longrightarrow [R_1R_2H]^* \longrightarrow R_1H + R_2} \tag{2.6}$$

These reactions[†] involve molecules (R_1 and R_2) and transition states ($[R_1R_2H]^*$) with open-shell character, making their properties more sensitive to electron correlation effects. We employ barrier heights computed at the CCSD(T)/aug-cc-pVTZ level of theory as our reference rather than the values provided by Lynch[77] in order to effectively exclude basis-set incompleteness effects. We also omit the DC-06 and ODC-06 methods, which encounter frequent convergence problems due to the poor description of N-representability (see Supporting Information for incomplete DC-06 results).

Mean absolute deviations (Δ_{MAE}) and standard deviations (Δ_{SD}) for the hydrogen-transfer barrier heights are presented in Table 2.2 and plotted in Figure 2.2. The largest Δ_{MAE} values come from CEPA_0 and DC-12 (2.77 and 2.49 kcal mol^{-1}, respectively). Orbital optimization greatly improves the accuracy of these methods, resulting in Δ_{MAE} values of just 0.67 and 0.94 kcal mol^{-1} for OCEPA_0 and ODC-12, respectively. The CCSD method shows intermediate performance with Δ_{MAE} = 1.84 kcal mol^{-1}. A similar trend is observed for the Δ_{SD} values, with OCEPA_0 (0.62 kcal mol^{-1}) and ODC-12 (0.71 kcal mol^{-1}) significantly improving upon CEPA_0 (1.51 kcal mol^{-1}), DC-12 (1.39 kcal mol^{-1}), and CCSD (1.06 kcal mol^{-1}). In addition to Δ_{MAE} and Δ_{SD}, Table 2.2 includes mean percent error (Δ_{rel}) values, which are commonly used to benchmark performance for reaction kinetics. The smallest Δ_{rel} values are 29% and 40% for OCEPA_0 and ODC-12, respectively.

Turning to barrier heights for individual hydrogen-transfer reactions (Table 2.2), the largest errors are observed for reactions 6 and 14, both involving the OH radi-

[†]Reaction 19 in HTBH38, the cis-trans isomerization of piperylene, is omitted in the present study.

cal, for which $CEPA_0$ and DC-12 give errors of $\sim$ 5-6 kcal mol^{-1}. The best results for these reactions are obtained from $OCEPA_0$, with errors ranging from 0.51 to 1.18 kcal mol^{-1}. The ODC-12 method tends to predict larger barrier heights than $OCEPA_0$, yielding smaller errors only when $OCEPA_0$ underestimates the barrier heights.

2.5.3 Radical Stabilization Energies

In this section we study the performance of DCFT methods for predicting radical stabilization energies (RSEs). An R-group's RSE is defined as the enthalpy of a homodesmotic reaction

$$RH + {}^{\cdot}CH_3 \longrightarrow {}^{\cdot}R + CH_4 \tag{2.7}$$

where exothermic (negative) values indicate that the radical $^{\cdot}R$ is more thermodynamically stable than $^{\cdot}CH_3$.[78] For our benchmark we use the RSE30 dataset[76], which provides a diverse variety of $^{\cdot}R$ species (listed in Table 2.3). Since the performance of CCSD(T) is known to deteriorate for strongly spin-contaminated UHF references,[79–83] we augment CCSD(T) energies with a quadruples correction ($\Delta Q = E_{CCSDT(Q)} - E_{CCSD(T)}$) and use these as our benchmark. CBS-extrapolated CCSD(T) reference values have been published for this dataset,[44] but we use CCSD(T) values computed with the cc-pCVTZ basis set to avoid basis-set incompleteness effects. The δQ correction was evaluated using the cc-pCVDZ basis set. As in the previous Section, DC-06 and ODC-06 computations cannot be converged

Table 2.3: Errors in radical stabilization energies (RSEs, kcal mol^{-1}) for 30 open-shell doublet species ($^{\cdot}$R) comprising the RSE30 database[76] computed using six methods with the cc-pCVTZ basis set. The errors are relative to CCSD(T) with an added quadruples correction ($\delta Q = E_{\mathrm{CCSDT(Q)}} - E_{\mathrm{CCSD(T)}}$) shown in the rightmost column in kcal mol^{-1}. The δQ correction was computed using the cc-pCVDZ basis set. RSE is defined as the reaction enthalpy for the homodesmotic reaction $^{\cdot}CH_3 + RH \rightarrow CH_4 + {}^{\cdot}R$. To indicate the degree of spin-contamination in the UHF reference, the spin expectation values ($\langle \hat{S}^2 \rangle_{\mathrm{SCF}}$) are also shown in units of $\hbar^2$. For each method the mean absolute deviations from CCSD(T)+δQ (Δ_{MAE}, kcal mol^{-1}) and the standard deviations from the mean signed error (Δ_{SD}, kcal mol^{-1}) are also presented.

$^{\cdot}$R	$\langle \hat{S}^2 \rangle_{\mathrm{SCF}}$	ΔCEPA$_0$	ΔDC-12	ΔCCSD	ΔOCEPA$_0$	ΔODC-12	ΔCCSD(T)	CCSD(T)+δQ
$^{\cdot}CH_2NO_2$	0.78	1.24	0.95	0.66	0.16	0.27	0.32	-3.50
$^{\cdot}CH_2OCHO$	0.76	1.16	1.12	0.63	0.40	0.48	0.10	-4.84
$^{\cdot}CH_2SCH_3$	0.76	1.89	1.70	0.81	0.63	0.72	0.15	-11.01
$^{\cdot}CF{=}CH_2$	0.94	6.12	3.71	0.96	0.42	0.64	0.46	6.26
$^{\cdot}CH_2CH_2F$	0.76	0.30	0.27	0.13	0.08	0.10	0.04	-1.53
$^{\cdot}CH_2CHO$	0.93	5.01	2.86	0.32	-0.16	0.02	0.46	-10.11
$^{\cdot}CH_2CN$	0.94	6.36	3.52	0.65	-0.02	0.21	0.46	-8.66
$^{\cdot}CH_2F$	0.76	1.03	1.00	0.52	0.55	0.57	0.06	-4.22
$^{\cdot}CH_2NH_2$	0.76	1.28	1.18	0.59	0.50	0.52	0.06	-12.06
$^{\cdot}CH_2NH_3^+$	0.76	0.16	0.10	0.08	0.06	0.03	0.02	4.58
$^{\cdot}CH_2NHOH$	0.77	1.76	1.57	0.78	0.58	0.64	0.15	-8.81
$^{\cdot}CH_2OH$	0.76	1.29	1.23	0.62	0.57	0.60	0.07	-9.27
$^{\cdot}CH_2PH_3^+$	0.76	0.21	0.14	0.01	0.01	-0.02	0.05	0.49
$^{\cdot}CH_2SH_2^+$	0.77	0.41	0.30	0.12	0.11	0.08	0.06	2.29
$^{\cdot}CH_2SH$	0.76	1.60	1.43	0.68	0.57	0.63	0.12	-9.68

$^{\cdot}$R	$\langle \hat{S}^2 \rangle_{\mathrm{SCF}}$	ΔCEPA$_0$	ΔDC-12	ΔCCSD	ΔOCEPA$_0$	ΔODC-12	ΔCCSD(T)	CCSD(T)+δQ
$^{\cdot}CH_2C{\equiv}CH$	1.00	6.23	3.47	0.82	-0.03	0.23	0.52	-13.17
$^{\cdot}CH_2CH_3$	0.76	0.30	0.26	0.11	0.08	0.10	0.03	-3.36
$^{\cdot}CH_2Cl$	0.77	1.13	1.02	0.50	0.48	0.51	0.09	-5.67
$^{\cdot}CH_2BH_2$	0.76	0.17	0.17	0.05	0.03	0.04	0.05	-11.66
$^{\cdot}CHO$	0.77	2.26	2.24	1.48	1.55	1.56	0.20	-17.61
$^{\cdot}CH_2PH_2$	0.76	1.17	1.02	0.39	0.36	0.39	0.12	-6.50
$^{\cdot}CHClF$	0.76	1.61	1.52	0.76	0.78	0.81	0.13	-6.61
$^{\cdot}CHFCH_3$	0.76	1.07	1.01	0.50	0.51	0.53	0.08	-5.87
$^{\cdot}CH(OH)_2$	0.76	1.30	1.22	0.60	0.60	0.61	0.08	-6.67
$^{\cdot}CHCl_2$	0.77	1.78	1.57	0.72	0.72	0.75	0.15	-9.56
$^{\cdot}CHF_2$	0.76	1.50	1.48	0.78	0.83	0.85	0.10	-4.07
$CH_2{=}C^{\cdot}{-}CN$	1.39	19.10	11.50	2.36	-0.31	0.29	1.80	1.98
$^{\cdot}C{\equiv}CH$	1.15	11.20	6.51	0.77	-0.78	-0.07	0.82	26.25
$^{\cdot}CH{=}CH_2$	0.94	5.42	3.01	0.58	0.11	0.31	0.40	5.49
$^{\cdot}CH_2{-}CH{=}CH_2$	0.97	4.98	3.17	0.51	0.11	0.31	0.48	-17.53
		Δ_{MAE}:	2.97	2.01	0.62	0.40	0.43	0.25
		Δ_{SD}:	3.97	2.27	0.45	0.43	0.35	0.35

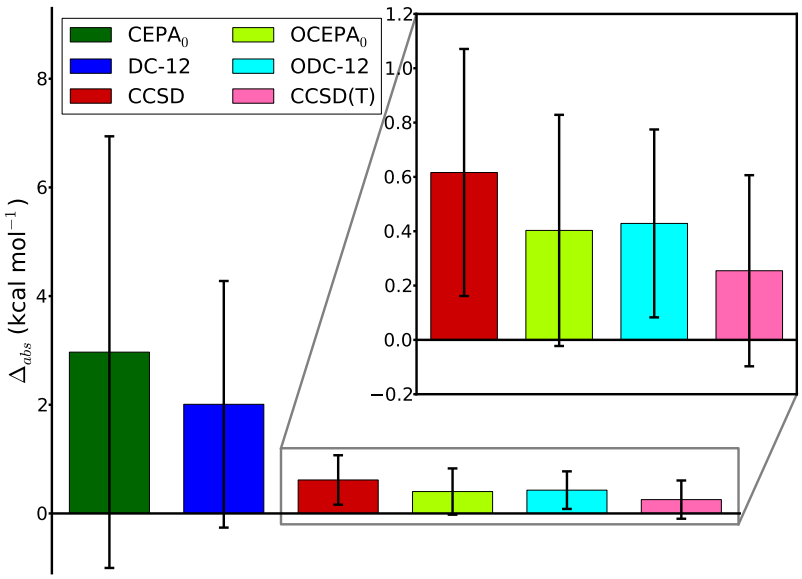

Figure 2.3: Mean absolute deviations (Δ_{MAE}, kcal mol^{-1}) and the standard deviations from the mean signed error (Δ_{SD}, kcal mol^{-1}) of the radical stabilization energies (RSEs) for 30 open-shell doublet species (RSE30 database) computed using six methods with the cc-pCVTZ basis set. The errors are relative to CCSD(T) with an added quadruples correction ($\delta\mathrm{Q} = E_{\mathrm{CCSDT(Q)}} - E_{\mathrm{CCSD(T)}}$). The δQ correction was computed using the cc-pCVDZ basis set. RSE is defined as the reaction enthalpy for the homodesmotic reaction $^{\cdot}\mathrm{CH_3} + \mathrm{RH} \rightarrow \mathrm{CH_4} + {}^{\cdot}\mathrm{R}$. The Δ_{MAE} value is represented as a height of each colored box, while the Δ_{SD} value is depicted as a radius of the black vertical bar. See Table 2.3 for data on individual database members.

for all database members and are omitted in the analysis below (see Supporting Information for incomplete DC-06 and ODC-06 data).

The relative performance of the DCFT, CEPA, and CC methods for the RSE30 dataset is shown in Figure 2.3. The effect of orbital-optimization on accuracy is now even more pronounced, reducing the large Δ_{MAE} errors of CEPA$_0$ (2.97 kcal mol^{-1})

and DC-12 (2.01 kcal mol^{-1}) to 0.40 and 0.43 kcal mol^{-1} for OCEPA$_0$ and ODC-12, respectively. CCSD has a slightly larger Δ_{MAE} value (0.62 kcal mol^{-1}), while CCSD(T) has the smallest overall Δ_{MAE} (0.25 kcal mol^{-1}). Both CEPA$_0$ and DC-12 show large standard deviations again (3.97 and 2.27 kcal mol^{-1}, respectively). For OCEPA$_0$, the standard deviation (0.43 kcal mol^{-1}) is similar to that of CCSD (0.45 kcal mol^{-1}). ODC-12 and CCSD(T) exhibit the most consistent performance with the same Δ_{SD} value of 0.35 kcal mol^{-1}.

Deviations from CCSD(T)+δQ for individual RSEs predicted by each method are tabulated in Table 2.3. In addition, Table 2.3 includes expectation values of the square-norm spin operator computed for the UHF wavefunction of ˙R ($\langle\hat{S}^2\rangle_{\mathrm{SCF}}$). The largest errors in computed RSEs were obtained for ˙R species with $\langle\hat{S}^2\rangle_{\mathrm{SCF}} > 0.9\ \hbar^2$ (radicals 4, 6, 7, 16, and 27-30 in Table 2.3). For these systems, the average CEPA$_0$ and DC-12 errors are 8.05 and 4.72 kcal mol^{-1}, and the average CCSD(T) error is 0.68 kcal mol^{-1}. OCEPA$_0$ and ODC-12 offer remarkably better performance for this subset, with average errors of 0.24 kcal mol^{-1} and 0.26 kcal mol^{-1}.

2.5.4 Adiabatic Ionization Energies in Electron-Dense Molecules

We conclude the assessment of DCFT methods for the description of thermodynamic properties by computing adiabatic ionization energies (AIEs) for a set of 10 di- and triatomic electron-dense molecules (Table 2.4), i.e. those that are composed of elements with small atomic radius, high electron affinity, and high electronegativity (N, O, F), in order to increase the magnitude of electron correla-

Table 2.4: Errors in adiabatic ionization energies (AIEs, eV) for 10 di- and triatomic molecules computed using six methods with the cc-pCVQZ basis set. The errors are relative to experimental values (IE_{ref}, eV) from Ref. 84, unless noted otherwise. For all AIEs the harmonic zero-point vibrational energy corrections were included. For each method the mean absolute deviations from IE_{ref} (Δ_{MAE}, eV) and the standard deviations from the mean signed error (Δ_{SD}, eV) are also shown.

Molecule	Transition	ΔCEPA$_0$	ΔDC-12	ΔCCSD	ΔOCEPA$_0$	ΔODC-12	ΔCCSD(T)	IE_{ref}
N_2	$^1\Sigma_g^+ \rightarrow {}^2\Sigma_g^+$	0.08	0.17	0.12	-0.05	0.07	-0.03	15.581 ± 0.008 [a]
O_2	$^3\Sigma_g^- \rightarrow {}^2\Pi_g$	-0.11	-0.03	0.04	-0.09	-0.02	-0.04	12.0697 ± 0.0002
F_2	$^1\Sigma_g^+ \rightarrow {}^2\Pi_g$	0.06	0.06	0.04	0.08	0.01	-0.03	15.697 ± 0.003
NO	$^2\Pi \rightarrow {}^1\Sigma^+$	-0.15	-0.05	-0.05	-0.05	-0.02	-0.09	9.26438 ± 0.00005
OF	$^2\Pi \rightarrow {}^3\Sigma^-$	0.11	0.12	-0.10	-0.03	-0.02	-0.11	12.77 ± 0.01 [b]
HNC	$^1\Sigma_g^+ \rightarrow {}^2\Sigma^+$	0.27	0.14	-0.12	-0.14	-0.08	-0.04	12.04 ± 0.01 [c]
HOF	$^1A' \rightarrow {}^2A''$	0.20	0.17	-0.10	-0.03	-0.04	-0.07	12.71 ± 0.01
FNO	$^1A' \rightarrow {}^2A''$	0.51	0.10	-0.02	-0.02	-0.00	0.04	12.63 ± 0.03
F_2N	$^2B_1 \rightarrow {}^1A_1$	0.07	0.10	0.07	0.01	0.03	-0.08	11.63± 0.01
F_2O	$^1A_1 \rightarrow {}^2B_1$	0.49	0.37	-0.01	0.05	0.04	-0.04	13.11 ± 0.01
	Δ_{MAE}:	0.21	0.13	0.06	0.05	0.03	0.06	
	Δ_{SD}:	0.22	0.12	0.08	0.06	0.04	0.04	

[a] Reference 85.

[b] Reference 86.

[c] Reference 87.

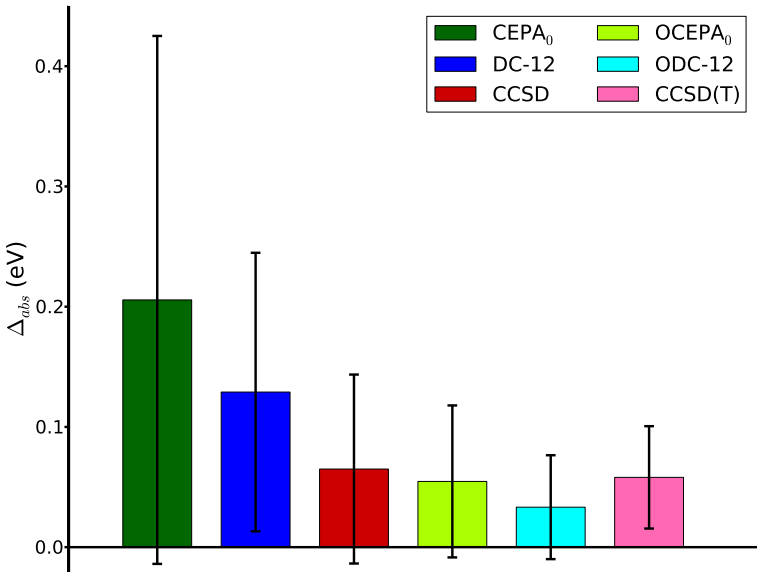

Figure 2.4: Mean absolute deviations (Δ_{MAE}, eV) and the standard deviations from the mean signed error (Δ_{SD}, eV) of adiabatic ionization energies for 10 di- and triatomic molecules computed using six methods with the cc-pCVQZ basis set. The errors are relative to experimental values.[84–87] The Δ_{MAE} value is represented as a height of each colored box, while the Δ_{SD} value is depicted as a radius of the black vertical bar. See Table 2.4 for data on individual molecules.

tion effects. We use experimentally measured ionization energies reported to high precision ($\sim$0.01 eV)[84–87] as reference values for our benchmark ($\mathrm{IE_{ref}}$, Table 2.4). The AIEs were computed using the cc-pCVQZ basis set, with harmonic ZPVE corrections applied to each neutral and cationic system.

The Δ_{MAE} and Δ_{SD} values for our computed AIEs relative to experiment are plotted in Figure 2.4. Of the six methods, $\mathrm{CEPA_0}$ and DC-12 exhibit the largest Δ_{MAE} values (0.21 and 0.13 eV, respectively). The closest agreement with experiment is given by ODC-12, with $\Delta_{\mathrm{MAE}} = 0.03$ eV. $\mathrm{OCEPA_0}$, CCSD, and CCSD(T)

show somewhat poorer performance ($\Delta_{\mathrm{MAE}} = 0.05$, 0.06 and 0.06 eV, respectively). The Δ_{SD} for ODC-12 matches that of CCSD(T) (0.04 eV). For the other methods, the Δ_{SD} values decrease in the order CEPA_0 (0.22 eV) > DC-12 (0.12) > CCSD (0.08) > OCEPA_0 (0.06).

Individual errors for each system are shown in Table 2.4. Both DC-12 and CEPA_0 exhibit large deviations for F_2O (0.49 and 0.37 eV), and CEPA_0 also gives a large error for FNO (0.51 eV) which is the maximum error for this dataset. Both DC-12 and CEPA_0 give errors exceeding 0.1 eV for seven of the ten systems, whereas CCSD exhibits errors in excess of 0.1 eV for only three systems (OF, HNC, and HOF). CCSD(T) has only one such error (0.11 eV for OF), as does OCEPA_0 (0.14 eV for HNC). ODC-12 does the best of the methods considered, with a maximum error of 0.08 eV, found for the AIE of HNC.

2.5.5 Covalent Bond Stretching in Diatomic Molecules

Finally, we benchmark DCFT methods for covalent bond stretching. Although accurate description of bond stretching demands the use of multireference methods, our aim here is to explore the limits of DCFT away from equilibrium. For this purpose, we compute the energy as a function of bond distance for diatomic molecules with single (HF and BH), double (BeO), and triple (N_2) bonds using the CEPA_0, OCEPA_0, DC-12, ODC-12, CCSD, and CCSD(T) methods. We restrict ourselves to modest basis sets in order to use full CI (FCI) as a reference, and plot the errors with respect to FCI (ΔE) as a function of internuclear distance for each molecule. The relative performance of the methods is described below using

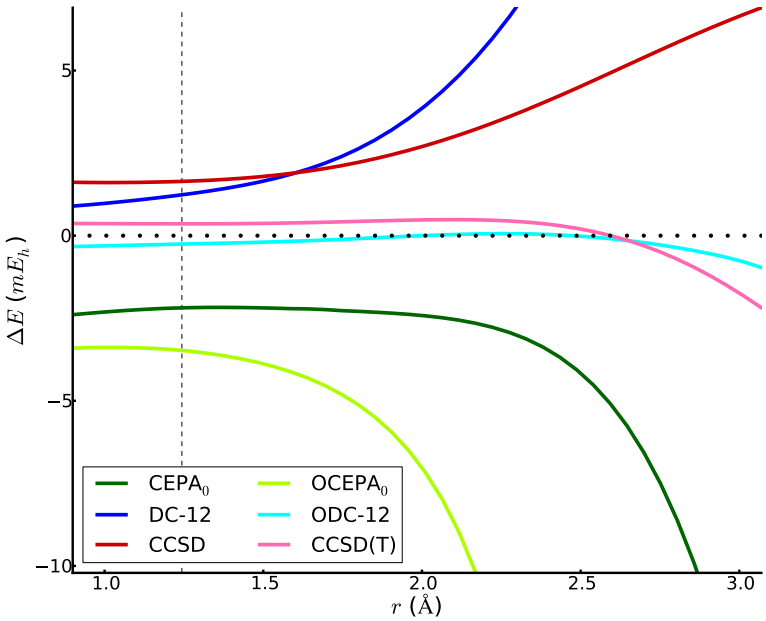

Figure 2.5: Error in the total energy (mE_h), relative to full CI, as a function of B–H internuclear separation (Å) computed using six methods with the DZP basis set. The full CI reference is depicted with a horizontal dotted line. The dashed vertical line indicates the full CI equilibrium bond distance.

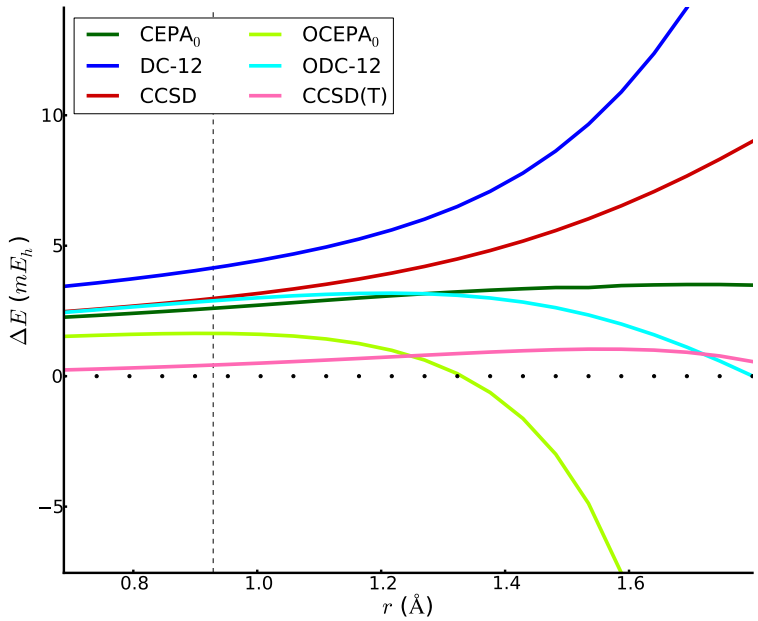

Figure 2.6: Error in the total energy (mE_h), relative to full CI, as a function of H–F internuclear separation (Å) computed using six methods with the DZP basis set. The full CI reference is depicted with a horizontal dotted line. The dashed vertical line indicates the full CI equilibrium bond distance.

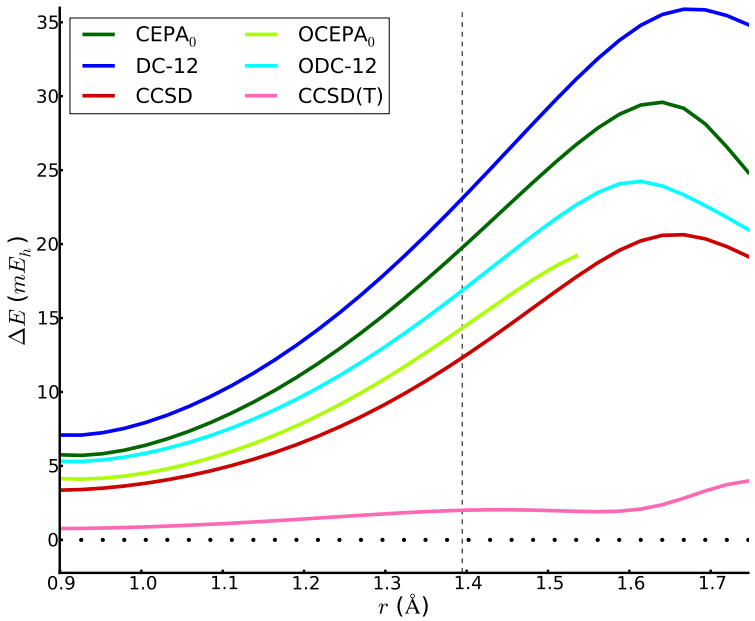

Figure 2.7: Error in the total energy (mE_h), relative to full CI, as a function of Be–O internuclear separation (Å) computed using six methods with the 6-31G basis set. The full CI reference is depicted with a horizontal dotted line. The dashed vertical line indicates the full CI equilibrium bond distance.

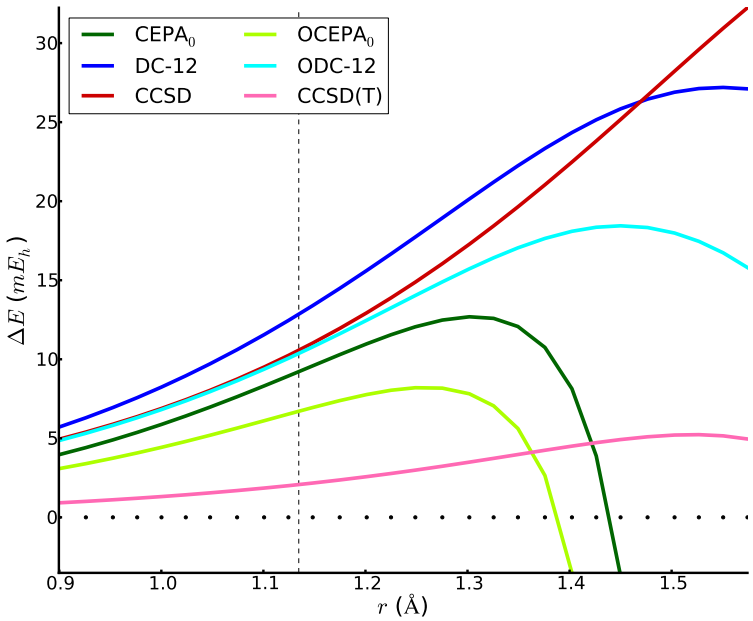

Figure 2.8: Error in the total energy (mE_h), relative to full CI, as a function of N–N internuclear separation (Å) computed using six methods with the 6-31G basis set. The full CI reference is depicted with a horizontal dotted line. The dashed vertical line indicates the full CI equilibrium bond distance.

non-parallelity errors (NPE = $\Delta E_{\max} - \Delta E_{\min}$, m$E_{\mathrm{h}}$) computed for specific bond distance ranges.

BH Figure 2.5 shows errors relative to FCI for the BH molecule. DC-12 and CCSD increasingly overestimate the energy at larger internuclear distances, whereas the CEPA_0 error curve is concave down. Orbital optimization lowers the binding energy for OCEPA_0 even further compared to CEPA_0, leading to large errors with respect to FCI for r(B–H) ¿ 1.5 r_{e}, where r_{e} is the FCI equilibrium bond distance ($r_{\mathrm{e}} = 1.244$ Å). At 1.87 r_{e}, OCEPA_0 encounters convergence problems, which originate from numerical instabilities due to the method's deficiencies in the description of N-representability. The ODC-12 method exhibits much more stable behavior with respect to bond stretching in this case, fortuitously showing smaller errors and better parallelity than CCSD(T). For the range [0.72 r_{e}, 2.47 r_{e}], the NPEs decrease in the order DC-12 (24 mE_{h}) > CEPA_0 (15) > CCSD (5) > CCSD(T) (3) > ODC-12 (1).

HF Errors for HF bond stretching are plotted in Figure 2.6. The ΔE values of CCSD and DC-12 increase as a function of r(H–F), while CEPA_0 fortuitously maintains parallelity similar to CCSD(T) over the range [0.74 r_{e}, 1.94 r_{e}] ($r_{\mathrm{e}} =$ 0.929 Å). OCEPA_0 increasingly overestimates the HF binding energy away from equilibrium, failing to converge past 1.82 r_{e}. The ODC-12 method exhibits larger NPE than was observed for BH, and encounters convergence problems past 1.94 r_{e}. CCSD(T) shows the best overall performance, with errors between 0 and 1 mE_{h}. In the range [0.74 r_{e}, 1.94 r_{e}] the computed NPE values are: DC-12 (15 mE_{h}) >

CCSD (7) > ODC-12 (3) > $CEPA_0$ (1) ≈ CCSD(T) (1). Recently, the orbital-optimized variants of CCSD(T) have been shown to yield good performance for HF bond stretching.[88]

BeO The double bond of BeO presents a more challenging test for the single-reference methods under consideration (Figure 2.7). All methods but CCSD(T) show qualitatively similar error curves, with inflection points near the FCI equilibrium ($r_e = 1.394$ Å) and valleys/peaks around 0.6 r_e/1.2 r_e. $OCEPA_0$ encounters convergence problems past 1.10 r_e. The ODC-12 method performs similarly to CCSD. Overall, the NPEs for the range $[0.65\ r_e, 1.10\ r_e]$ decrease in the following order: DC-12 (29 mE_h) > $CEPA_0$ (24) > ODC-12 (19) > CCSD (17) > CCSD(T) (3).

N_2 Figure 2.8 depicts the errors relative to FCI for triple bond stretching in N_2. Here, $OCEPA_0$ fails to converge past 1.24 r_e ($r_e = 1.135$ Å). The ODC-12 method significantly overestimates the binding energy, possibly due to the lack of three-body correlation effects, but shows much more stable performance compared to methods other than CCSD(T). NPEs in the range $[0.79\ r_e, 1.39\ r_e]$ decrease in the order: $CEPA_0$ (802 mE_h)[‡]> CCSD (27) > DC-12 (21) > ODC-12 (14) > CCSD(T) (4).

[‡]$CEPA_0$ exhibits a vertical asymptote at 1.36 r_e for N_2 stretching.

2.6 Conclusions

We have presented the benchmark study of four density cumulant functional theory (DCFT) methods (DC-06, DC-12, ODC-06, and ODC-12) developed recently in our group.[62;63;65;66] Specifically we have compared the performance of DCFT to that of coupled electron pair methods ($CEPA_0$ and $OCEPA_0$), as well as coupled-cluster theory [CCSD and CCSD(T)] for predicting a variety of chemical properties relevant to thermochemistry and kinetics, with a particular focus on open-shell, electron-dense, and non-equilibrium systems.

Our results indicate that among the four DCFT methods, the best agreement with available reference data is obtained for the ODC-12 method. While all four DCFT formulations yield similar results for the description of noncovalent interactions, DC-06, DC-12, and ODC-06 exhibit worse performance than ODC-12 for thermodynamic and kinetic properties of reactions involving open-shell molecules. In particular, DC-06 and ODC-06 frequently encounter convergence problems that originate from poor description of N-representability. In comparing ODC-12 to other methods, several trends can be observed:

(i) For all benchmark datasets, ODC-12 outperforms CCSD with errors smaller by almost a factor of two, on average. ODC-12 is also superior to CCSD for the description of single bond stretching in BH and HF, although it does not converge for all bond distances.

(ii) The performance of ODC-12 and $OCEPA_0$ is comparable. In particular, for hydrogen-transfer reaction barrier heights, the $OCEPA_0$ method yields smaller percent errors than ODC-12, whereas, for the radical stabilization energies (RSE)

and adiabatic ionization energies (AIE) in electron-dense molecules, the ODC-12 method smaller standard deviations than $OCEPA_0$. For AIEs, ODC-12 gives smaller mean absolute deviations by almost a factor of two. ODC-12 also shows significantly smaller non-parallelity errors than $OCEPA_0$ for covalent bond stretching, and can be converged for a larger range of distances for all diatomic molecules studied.

(iii) For the two most challenging datasets, RSE and AIE, the standard deviation of ODC-12 and CCSD(T) are similar. While CCSD(T) yields smaller mean absolute errors for the RSE database, the ODC-12 method significantly outperforms CCSD(T) for the AIE test case. However, for bond stretching ODC-12 is competitive with CCSD(T) only for the BH dissociation and shows worse results for other molecules.

Overall, the data presented herein indicates that the ODC-12 method can be used as an efficient $\mathcal{O}(n^6)$ alternative to CCSD, capable of predicting thermodynamic and kinetic quantities that are competitive in accuracy with the "gold-standard" $\mathcal{O}(n^7)$ CCSD(T). Although our current implementation of ODC-12 is far from optimal, the ODC-12 equations have reduced non-linearities compared to CCSD, which makes them more amenable to parallel implementation. The efficiency of ODC-12 can also greatly benefit from spin-adaptation,[55;89;90] local approximations,[47;91–93] and density fitting.[91;94–96] Another important advantage of ODC-12 over CCSD is its stationarity, which makes the computation of first-order properties and analytic gradients more efficient and easily accessible. In particu-

lar, ODC-12 has potential to be used for computing accurate response properties which do not suffer from a lack of gauge-invariance.[97;98]

Chapter 3

Linear-Response Density Cumulant Theory for Excited Electronic States*

*A. V. Copan and A. Yu. Sokolov, arXiv:1804.02141 [physics.chem-ph] (2018).
Reprinted here with permission of the publisher.

3.1 Abstract

We present a linear-response formulation of density cumulant theory (DCT) that provides a balanced and accurate description of many electronic states simultaneously. In the original DCT formulation, only information about a single electronic state (usually, the ground state) is obtained. We discuss the derivation of linear-response DCT, present its implementation for the ODC-12 method (LR-ODC-12), and benchmark its performance for excitation energies in small molecules (N_2, CO, HCN, HNC, C_2H_2, and H_2CO), as well as challenging excited states in ethylene, butadiene, and hexatriene. For small molecules, LR-ODC-12 shows smaller mean absolute errors in excitation energies than equation-of-motion coupled cluster theory with single and double excitations (EOM-CCSD), relative to the reference data from EOM-CCSDT. In a study of butadiene and hexatriene, LR-ODC-12 correctly describes the relative energies of the singly-excited 1^1B_u and the doubly-excited 2^1A_g states, in excellent agreement with highly accurate semistochastic heat-bath configuration interaction results, while EOM-CCSD overestimates the energy of the 2^1A_g state by almost 1 eV. Our results demonstrate that linear-response DCT is a promising theoretical approach for excited states of molecules.

3.2 Introduction

Accurate simulation of excited electronic states remains one of the major challenges in modern electronic structure theory. *Ab initio* methods for excited states can be divided into single-reference and multi-reference categories, based on their

ability to treat static electron correlation. Multi-reference methods[99–116] can correctly describe static correlation in near-degenerate valence orbitals and electronic states with multiple-excitation character, but often lack accurate treatment of important dynamic correlation effects or become computationally very costly when the number of strongly correlated orbitals is large. Meanwhile, single-reference methods[34;36;117–129] often provide a compromise between the computational cost and accuracy, and can be used to reliably compute properties of molecules in low-lying electronic states near the equilibrium geometries. In these situations, single-reference equation-of-motion coupled cluster theory (EOM-CC)[34;36;119–122] is usually the method of choice, especially when high accuracy is desired.

The EOM-CC methods yield size-intensive excitation energies[124;125] and can be systematically improved by increasing the excitation rank of the cluster operator in the exponential parametrization of the wavefunction. Although EOM-CC is usually formulated in the context of a similarity-transformed Hamiltonian, its excitation energies are equivalent to those obtained from linear-response coupled cluster theory (LR-CC).[123–125] Both EOM-CC and LR-CC are based on non-Hermitian eigenvalue problems, which complicates the computation of molecular properties (e.g., transition dipoles) by requiring evaluation of left and right eigenvectors,[130–133] and may result in an incorrect description of potential energy surfaces in the vicinity of conical intersections where complex excitation energies may be obtained.[134–136] Several Hermitian alternatives to EOM-CC and LR-CC have been proposed to avoid these problems, such as algebraic diagrammatic construc-

tion[137–139], unitary and variational LR-CC,[140–142] similarity-constrained CC,[143] and propagator-based LR-CC.[144;145]

In this work, we present a linear-response formulation of density cumulant theory for excited electronic states. In density cumulant theory (DCT),[48;62;63;65;66;146–148] the electronic energy is determined directly in terms of the one-particle reduced density matrix and the density cumulant, i.e. the fully connected part of the two-body reduced density matrix (2-RDM).[52–55;57;61;149–152] In this regard, DCT is related to approaches based on the variational optimization[54;153–158] or parametrization[49–51] of the 2-RDM. On the other hand, DCT has a close relationship with wavefunction-based electronic structure theories,[65;66] such as linearized, unitary, and variational coupled cluster theory.[18;159–166] In contrast to variational 2-RDM theory[58–60] and traditional coupled cluster methods,[34;36] DCT naturally combines size-extensivity and a Hermitian energy functional. In addition, the DCT electronic energy is fully optimized with respect to all of its parameters, which greatly simplifies computation of the first-order molecular properties.[167–170] We have successfully applied DCT to a variety of chemical systems with different electronic structure effects (e.g., open-shell, symmetry-breaking, and multi-reference).[1;66;146;147;171] One limitation of the original DCT formulation is the ability to describe only the lowest-energy state of a particular symmetry (usually, the ground state). By combining DCT with linear response theory, we remove this limitation, providing access to many electronic states simultaneously.

We begin with a brief overview of DCT (Section 3.3.1) and linear response theory (Section 3.3.2). In Section 3.3.3, we describe the derivation of the linear-

response equations for the ODC-12 model (LR-ODC-12). In Section 3.3.4, we compare the LR-ODC-12 method with linear-response orbital-optimized linearized coupled cluster theory with double excitations (LR-OLCCD), which we derive by linearizing the LR-ODC-12 equations. We outline the computational details in Section 3.4. In Section 3.5, we demonstrate that the LR-ODC-12 excitation energies are size-intensive (Section 3.5.1), test the performance of LR-ODC-12 for the dissociation of H_2 (Section 3.5.2), benchmark its accuracy for vertical excitation energies of small molecules (Section 3.5.3), and apply LR-ODC-12 to challenging excited states in ethylene, butadiene, and hexatriene (Section 3.5.4). We present our conclusions in Section 3.6.

3.3 Theory

3.3.1 Overview of Density Cumulant Functional Theory

We begin with a brief overview of density cumulant theory (DCT) for a single electronic state. Our starting point is to express the electronic energy as a trace of the one- and antisymmetrized two-electron integrals (h^q_p and $\overline{g}^{rs}_{pq}$) with the reduced one- and two-body density matrices (γ^p_q and γ^{pq}_{rs}):

$$E = h^q_p \gamma^p_q + \tfrac{1}{4} \overline{g}^{rs}_{pq} \gamma^{pq}_{rs} \tag{3.1}$$

where summation over the repeated indices is implied. In DCT, the two-body density matrix γ^{pq}_{rs} is expanded in terms of its connected part, the two-body density cumulant (λ^{pq}_{rs}), and its disconnected part, which is given by an antisymmetrized

product of one-body density matrices:[48]

$$\gamma_{rs}^{pq} = \langle \Psi | a_{rs}^{pq} | \Psi \rangle = \lambda_{rs}^{pq} + P_{(r/s)} \gamma_r^p \gamma_s^q \tag{3.2}$$

where $P_{(r/s)} v_{rs} = v_{rs} - v_{sr}$ denotes antisymmetrization and $a_{rs}^{pq} = a_p^\dagger a_q^\dagger a_s a_r$ is the two-body operator in second quantization. The one-body density matrix γ_q^p is determined from its non-linear relationship to the cumulant's partial trace:[65]

$$\gamma_q^p = \gamma_r^p \gamma_q^r - \lambda_{qr}^{pr} \tag{3.3}$$

This allows us to determine the energy (3.1) from the two-body density cumulant and the spin-orbitals, thereby defining the DCT energy functional. The density cumulant is parametrized by choosing a specific Ansatz for the wavefunction $|\Psi\rangle$ such that[146]

$$\lambda_{rs}^{pq} = \langle \Psi | a_{rs}^{pq} | \Psi \rangle_c \tag{3.4}$$

where c indicates that only fully connected terms are included in the parametrization. Eq. (3.4) can be considered as a set of n-representability conditions that ensure that the resulting one- and two-body density matrices represent a physical n-electron wavefunction. To compute the DCT energy, the functional (3.1) is made stationary with respect to all of its parameters. Importantly, due to the connected nature of Eq. (3.4), DCT is both size-consistent and size-extensive for any parametrization of $|\Psi\rangle$, and is exact in the limit of a complete parametrization.[146]

In this work, we consider the ODC-12 method,[65;66] which parametrizes the cumulant through a unitary treatment of single excitations and a linear expansion of double excitations:

$$|\Psi\rangle = e^{\hat{T}_1 - \hat{T}_1^\dagger}(1 + \hat{T}_2)|\Phi\rangle \tag{3.5}$$

$$\hat{T}_1 = \mathbf{t}_1 \cdot \mathbf{a}_1 = t_a^i a_i^a \tag{3.6}$$

$$\hat{T}_2 = \mathbf{t}_2 \cdot \mathbf{a}_2 = \tfrac{1}{4} t_{ab}^{ij} a_{ij}^{ab} \tag{3.7}$$

The exponential singles operator $e^{\hat{T}_1 - \hat{T}_1^\dagger}$ has the effect of a unitary transformation of the spin-orbital basis and is incorporated in our ODC-12 implementation by optimizing the orbitals.[66] The $\mathbf{t}_1$ and $\mathbf{t}_2$ parameters are obtained from the stationarity conditions

$$\frac{\partial E}{\partial \mathbf{t}_1^\dagger} \stackrel{!}{=} 0 \;, \qquad \frac{\partial E}{\partial \mathbf{t}_2^\dagger} \stackrel{!}{=} 0 \tag{3.8}$$

and are used to compute the ODC-12 energy. Explicit equations for the stationarity conditions are given in Refs. 65 and 66. Although in ODC-12 the wavefunction parametrization is linear with respect to double excitations (Eq. (3.5)), the ODC-12 energy stationarity conditions are non-linear in $\mathbf{t}_2$ due to the non-linear relationship between the one-particle density matrix and the density cumulant (Eq. (3.3)).[65] Neglecting the non-linear $\mathbf{t}_2$ terms in Eq. (3.8) results in the equations that define the linearized orbital-optimized coupled cluster doubles method (OLCCD). This method is equivalent to the orbital-optimized coupled electron pair approximation zero (OCEPA_0).[43]

3.3.2 Linear Response Theory

We now briefly review linear response theory in the quasi-energy formulation.[172] The quasi-energy of a system perturbed by a time-dependent interaction $\hat{V}f(t)$ is defined as

$$Q(t) = \langle \Psi(t)|\hat{H} + \hat{V}f(t) - i\tfrac{\partial}{\partial t}|\Psi(t)\rangle \tag{3.9}$$

where $\Psi(t)$ is the phase-isolated wavefunction, from which the usual Schrödinger wavefunction can be recovered as $e^{-i\int_0^t dt' Q(t')}\Psi(t)$. Assuming that the perturbation is periodic

$$f(t) = \sum_{\omega} f(\omega)e^{-i\omega t} \tag{3.10}$$

the time average of the quasi-energy over a period of oscillation, denoted as $\{Q(t)\}$, is variational with respect to the exact dynamic state.[173] The independent parameters $\mathbf{u}(t)$ that define such a state can be written using a Fourier expansion

$$\mathbf{u}(t) = \sum_{n=0}^{\infty} \sum_{\omega_1 \cdots \omega_n} \mathbf{u}(\omega_1, \ldots, \omega_n)e^{-i(\omega_1 + \cdots + \omega_n)t} \tag{3.11}$$

where the outer sum runs over polynomial orders in $f(t)$. The stationarity of the time-averaged quasi-energy then implies the following relationship[174]

$$\begin{aligned} 0 = \frac{d}{df(\omega)}\frac{\partial\{Q(t)\}}{\partial\mathbf{u}^\dagger(\omega)}\bigg|_{f=0} = \\ \frac{\partial^2\{Q(t)\}}{\partial\mathbf{u}^\dagger(\omega)\partial\mathbf{u}(\omega)}\frac{\partial\mathbf{u}(\omega)}{\partial f(\omega)}\bigg|_{f=0} + \frac{\partial^2\{Q(t)\}}{\partial\mathbf{u}^\dagger(\omega)\partial f(\omega)}\bigg|_{f=0} \end{aligned} \tag{3.12}$$

which constitutes a linear equation for the first-order response of the system to the perturbation. When the frequency ω is in resonance with an excitation energy of the system, Eq. (3.12) will result in an infinite first-order response $\dfrac{\partial \mathbf{u}(\omega)}{\partial f(\omega)}$. From Eq. (3.12), we find that these poles occur when the Hessian matrix of the quasi-energy with respect to the wavefunction parameters $\mathbf{u}(\omega)$ becomes singular. We can express this Hessian matrix in the form:

$$\left.\frac{\partial^2\{Q(t)\}}{\partial \mathbf{u}^\dagger(\omega)\partial \mathbf{u}(\omega)}\right|_{f=0} \equiv \mathbf{E} - \omega\,\mathbf{M} \tag{3.13}$$

where $\mathbf{E}$ is the Hessian of the time-averaged electronic energy $\{\langle\Psi(t)|\hat{H}|\Psi(t)\rangle\}$ and $\omega\mathbf{M}$ is the Hessian of the time-derivative overlap $\{\langle\Psi(t)|i\dot{\Psi}(t)\rangle\}$. The excitation energies of the system ω_k can therefore be determined by solving the following generalized eigenvalue equation:

$$\mathbf{E}\mathbf{z}_k = \omega_k \mathbf{M}\mathbf{z}_k \tag{3.14}$$

where $\mathbf{M}$ serves as the metric matrix. Eq. (3.14) allows the determination of excitation energies for an arbitrary parametrization of $|\Psi(t)\rangle$.

The generalized eigenvectors $\mathbf{z}_k$ can be used to compute transition properties for excited states. In particular, in the exact linear response theory,[175] the transition strength of the perturbing interaction, $|\langle\Psi|\hat{V}|\Psi_k\rangle|^2$, is equal to the complex residue of the following quantity at $\omega \to \omega_k$:

$$\langle\langle \hat{V}; \hat{V} \rangle\rangle_\omega \equiv \mathbf{v}'^\dagger \cdot \left.\frac{\partial \mathbf{u}(\omega)}{\partial f(\omega)}\right|_{f=0} \tag{3.15}$$

This quantity is known as the linear response function and $\mathbf{v}'$ is termed the property gradient vector,[176] which is defined as follows:

$$\mathbf{v}' \equiv \left.\frac{\partial^2\{Q(t)\}}{\partial\mathbf{u}^\dagger(\omega)\partial f(\omega)}\right|_{f=0} \tag{3.16}$$

Substituting Eqs. (3.13) and (3.16) into Eq. (3.12) and decomposing the quasi-energy Hessian as

$$\mathbf{E} - \omega\mathbf{M} = (\mathbf{Z}^\dagger)^{-1}(\mathbf{Z}^\dagger\mathbf{M}\mathbf{Z})(\mathbf{\Omega} - \omega\mathbf{1})(\mathbf{Z})^{-1} \tag{3.17}$$

where $\mathbf{Z}$ is the matrix of generalized eigenvectors (Eq. (3.14)) diagonalizing matrices $\mathbf{E}$ and $\mathbf{M}$, and $\mathbf{\Omega}$ is the diagonal matrix of eigenvalues, we obtain the general formula for the transition strengths:

$$\lim_{\omega\to\omega_k}(\omega - \omega_k)\langle\langle\hat{V};\hat{V}\rangle\rangle_\omega = \frac{|\mathbf{z}_k^\dagger\mathbf{v}'|^2}{\mathbf{z}_k^\dagger\mathbf{M}\mathbf{z}_k} \tag{3.18}$$

In Section 3.3.3, we will use the quasi-energy formalism to derive equations for the linear-response ODC-12 method (LR-ODC-12).

3.3.3 Linear-Response ODC-12

In the ODC-12 method, the electronic energy Hessian can be written in the following form

$$\mathbf{E} = \begin{pmatrix} \mathbf{A}_{11} & \mathbf{A}_{12} & \mathbf{B}_{11} & \mathbf{B}_{12} \\ \mathbf{A}_{21} & \mathbf{A}_{22} & \mathbf{B}_{21} & \mathbf{B}_{22} \\ \mathbf{B}_{11}^* & \mathbf{B}_{12}^* & \mathbf{A}_{11}^* & \mathbf{A}_{12}^* \\ \mathbf{B}_{21}^* & \mathbf{B}_{22}^* & \mathbf{A}_{21}^* & \mathbf{A}_{22}^* \end{pmatrix} \tag{3.19}$$

where the submatrices are defined in general as

$$\mathbf{A}_{nm} = \left.\frac{\partial^2 E}{\partial \mathbf{t}_n^\dagger \partial \mathbf{t}_m}\right|_{f=0}, \; \mathbf{B}_{nm} = \left.\frac{\partial^2 E}{\partial \mathbf{t}_n^\dagger \partial \mathbf{t}_m^*}\right|_{f=0} \tag{3.20}$$

These complex derivatives relate to the second derivatives of the electronic energy with respect to variations of the orbitals ($\mathbf{A}_{11}$, $\mathbf{B}_{11}$) and cumulant parameters ($\mathbf{A}_{22}$, $\mathbf{B}_{22}$). Similarly, the mixed second derivatives couple variations in the orbitals and cumulant parameters ($\mathbf{A}_{12}$, $\mathbf{B}_{12}$). The metric matrix $\mathbf{M}$ has a block-diagonal structure, as a consequence of the linear parametrization of the wavefunction in Eq. (3.5):

$$\mathbf{M} = \begin{pmatrix} \mathbf{S}_{11} & \mathbf{0} & \mathbf{0} & \mathbf{0} \\ \mathbf{0} & \mathbf{1}_2 & \mathbf{0} & \mathbf{0} \\ \mathbf{0} & \mathbf{0} & -\mathbf{S}_{11}^* & \mathbf{0} \\ \mathbf{0} & \mathbf{0} & \mathbf{0} & -\mathbf{1}_2 \end{pmatrix} \tag{3.21}$$

where $\mathbf{1}_2 = \langle \Phi | \mathbf{a}_2^\dagger \mathbf{a}_2 | \Phi \rangle$ is an identity matrix over the space of unique two-body excitations and the orbital metric is defined as follows:

$$\omega \mathbf{S}_{11} = \left.\frac{\partial^2 \{ \langle \Psi(t) | i \dot{\Psi}(t) \rangle \}}{\partial \mathbf{t}_1^\dagger(\omega) \partial \mathbf{t}_1(\omega)}\right|_{f=0} \tag{3.22}$$

Equations for all blocks of $\mathbf{E}$, $\mathbf{M}$, and the property gradient vector $\mathbf{v}'$ are shown explicitly in the Supporting Information. The computational cost of solving the LR-ODC-12 equations has $\mathcal{O}(O^2V^4)$ scaling (where O and V are the numbers of occupied and virtual orbitals, respectively), which is the same as the computational scaling of the single-state ODC-12 method. We note that, due to the Hermitian nature of the DCT energy functional (3.1), the ODC-12 energy Hessian $\mathbf{E}$ is always

symmetric. As a result, in the absence of instabilities (i.e., as long as the Hessian is positive semi-definite), the LR-ODC-12 excitation energies are guaranteed to have real values.

To illustrate the derivation of the LR-ODC-12 energy Hessian, let us consider the diagonal two-body block of $\mathbf{E}$. Expressing the energy (3.1) using the cumulant expansion (3.2) and differentiating with respect to $\mathbf{t}_2$, we obtain:

$$\begin{aligned}\mathbf{A}_{22} = \frac{\partial^2 E}{\partial \mathbf{t}_2^\dagger \partial \mathbf{t}_2} = f_p^q \frac{\partial^2 \gamma_q^p}{\partial \mathbf{t}_2^\dagger \partial \mathbf{t}_2} + \overline{g}_{pr}^{qs} \frac{\partial \gamma_q^p}{\partial \mathbf{t}_2^\dagger} \frac{\partial \gamma_s^r}{\partial \mathbf{t}_2} \\ + \tfrac{1}{4} \overline{g}_{pq}^{rs} \frac{\partial^2 \lambda_{rs}^{pq}}{\partial \mathbf{t}_2^\dagger \partial \mathbf{t}_2}\end{aligned} \tag{3.23}$$

where we have introduced the generalized Fock matrix $f_p^q \equiv h_p^q + \overline{g}_{pr}^{qs} \gamma_s^r$. The derivatives of the one-body density matrix can be expressed in terms of the derivatives of the density cumulant

$$\begin{aligned}\mathbf{A}_{22} = \mathcal{F}_p^q \frac{\partial^2 \lambda_{qt}^{pt}}{\partial \mathbf{t}_2^\dagger \partial \mathbf{t}_2} + \mathcal{G}_{pr}^{qs} \frac{\partial \lambda_{qt}^{pt}}{\partial \mathbf{t}_2^\dagger} \frac{\partial \lambda_{su}^{ru}}{\partial \mathbf{t}_2} \\ + \tfrac{1}{4} \overline{g}_{pq}^{rs} \frac{\partial^2 \lambda_{rs}^{pq}}{\partial \mathbf{t}_2^\dagger \partial \mathbf{t}_2}\end{aligned} \tag{3.24}$$

where the intermediates $\mathcal{F}_p^q$ and $\mathcal{G}_{pr}^{qs}$ can be computed using a transformation of the one- and two-electron integrals to the natural spin-orbital basis (see Section 3.A for details). These cumulant derivatives are straightforward to evaluate from Eqs. (3.4) and (3.5) using either algebraic or diagrammatic techniques.

Next, let us outline the derivation of the one-body metric. Substituting Eq. (3.5) into Eq. (3.22) gives

$$\begin{aligned}\omega\mathbf{S}_{11} = \frac{1}{2}\frac{\partial^2\{\langle\Psi|[i\hat{\hat{T}}_1^\dagger(t), \hat{T}_1(t)]|\Psi\rangle\}}{\partial\mathbf{t}_1^\dagger(\omega)\partial\mathbf{t}_1(\omega)}\bigg|_{f=0} \\ - \frac{1}{2}\frac{\partial^2\{\langle\Psi|[\hat{T}_1^\dagger(t), i\hat{\hat{T}}_1(t)]|\Psi\rangle\}}{\partial\mathbf{t}_1^\dagger(\omega)\partial\mathbf{t}_1(\omega)}\bigg|_{f=0}\end{aligned} \tag{3.25}$$

where we have assumed that we are working in the variational orbital basis so that $\hat{T}_1(t)|_{f=0} = 0$, and $\Psi = \Psi(t)|_{f=0}$ denotes the ground state wavefunction. Using the Fourier expansion of the $\mathbf{t}_1(t)$ parameters (Eq. (3.11)), the gradients of the time derivatives can be evaluated as:

$$\frac{\partial i\hat{\hat{T}}_1^\dagger(t)}{\partial\mathbf{t}_1^\dagger(\omega)}\bigg|_{f=0} = -\omega\mathbf{a}_1^\dagger e^{+i\omega t} \tag{3.26}$$

$$\frac{\partial i\hat{\hat{T}}_1(t)}{\partial\mathbf{t}_1(\omega)}\bigg|_{f=0} = +\omega\mathbf{a}_1 e^{-i\omega t} \tag{3.27}$$

Substituting Eqs. (3.26) and (3.27) into Eq. (3.25) and evaluating the gradients of $\hat{T}_1$ and $\hat{T}_1^\dagger$ similarly gives the final working equation for the one-body metric:

$$\begin{aligned}\omega(\mathbf{S}_{11})_{ia,jb} &= \omega\langle\Psi|[a_a^i, a_j^b]|\Psi\rangle \\ &= \omega(\delta_a^b\gamma_j^i - \delta_j^i\gamma_a^b)\end{aligned} \tag{3.28}$$

3.3.4 Linear-Response OLCCD

As we discussed in Section 3.3.1, the orbital-optimized linearized coupled cluster doubles method (OLCCD) can be considered as an approximation to the ODC-12 method where all of the non-linear $\mathbf{t}_2$ terms are neglected in the stationarity conditions. Similarly, we can formulate the linear-response OLCCD method (LR-OLCCD) by linearizing the LR-ODC-12 equations. This simplifies the expressions for the electronic Hessian blocks that involve the second derivatives with respect to $\mathbf{t}_2$. For example, for the $\mathbf{A}_{22}$ block, we obtain:

$$\mathbf{A}_{22} = (f_0)_i^j \frac{\partial^2 \lambda_{jr}^{ir}}{\partial \mathbf{t}_2^\dagger \partial \mathbf{t}_2} - (f_0)_a^b \frac{\partial^2 \lambda_{br}^{ar}}{\partial \mathbf{t}_2^\dagger \partial \mathbf{t}_2} + \tfrac{1}{4} \overline{g}_{pq}^{rs} \frac{\partial^2 \lambda_{rs}^{pq}}{\partial \mathbf{t}_2^\dagger \partial \mathbf{t}_2} \tag{3.29}$$

where $(f_0)_p^q = h_p^q + \overline{g}_{pi}^{qi}$ is the usual (mean-field) Fock operator. Comparing Eq. (3.29) with Eq. (3.24) from the LR-ODC-12 method, we observe that the former equation can be obtained from the latter by replacing the $\mathcal{F}_p^q$ intermediates with the mean-field Fock matrix elements and ignoring the term that depends on $\mathcal{G}_{pr}^{qs}$. These simplifications arise from the fact that the $\mathcal{F}_p^q$ and $\mathcal{G}_{pr}^{qs}$ intermediates contain high-order $\mathbf{t}_2$ contributions that are not included in the linearized LR-OLCCD formulation (see Section 3.A and Ref. 65 for details). For the $\mathbf{B}_{22}$ block, we find that all of the Hessian elements are zero. A complete set of working equations for LR-OLCCD is given in the Supporting Information.

3.4 Computational Details

The LR-ODC-12 and LR-OLCCD methods were implemented as a standalone Python program, which was interfaced with Psi4[177] and Pyscf[178] to obtain the one- and two-electron integrals. To compute excitation energies, our implementation utilizes the multi-root Davidson algorithm,[179;180] which solves the generalized eigenvalue problem (3.14) by progressively growing an expansion space for the n_{root} lowest generalized eigenvectors of the electronic Hessian and the metric matrix. A key feature of this algorithm is that it avoids storing the Hessian and metric matrices, significantly reducing the amount of memory required by the computations. Our implementation of the energy Hessian was validated by computing the static response function for a dipole perturbation (i.e., the dipole polarizability):

$$\langle\langle \hat{V}; \hat{V} \rangle\rangle_0 = -\mathbf{v}'^{\dagger} \mathbf{E}^{-1} \mathbf{v}' \tag{3.30}$$

This quantity can be evaluated numerically as a derivative of the ground state energy

$$\langle\langle \hat{V}; \hat{V} \rangle\rangle_0 = \left. \frac{d^2 E}{df^2} \right|_{f=0} \tag{3.31}$$

by perturbing the one-electron integrals $h_p^q \leftarrow h_p^q + f v_p^q$ with the integrals of the perturbing dipole operator (v_p^q), and solving the ODC-12 (or OLCCD) equations for different values of f. For the dipole polarizability of the water molecule along its C_2 symmetry axis, the values of $\langle\langle \hat{V}; \hat{V} \rangle\rangle_0$ Computed using Eqs. (3.30) and (3.31) matched to 10^{-9} a.u.

We used Q-Chem 4.4[181] to obtain results from equation-of-motion coupled cluster theory with single and double excitations (EOM-CCSD) and EOM-CCSD with triple excitations in the EOM part [EOM-CC(2,3)]. The MRCC program[182] was used to obtain results for equation-of-motion coupled cluster theory with up to full triple excitations (EOM-CCSDT). All electrons were correlated in all computations. We used tight convergence parameters in all ground-state (10^{-8} E_h) and excited-state computations (10^{-5} E_h). In Sections 3.5.2 and 3.5.3, the augmented aug-cc-pVTZ and d-aug-cc-pVTZ basis sets of Dunning and co-workers were employed.[73] For alkenes (Section 3.5.4), the ANO-L-pVXZ (X = D, T) basis sets[183] were used as in Ref. 184. To compute vertical excitation energies in Section 3.5.3, geometries of molecules were optimized using ODC-12 (for LR-ODC-12), OLCCD (for LR-OLCCD), or CCSD [for EOM-CCSD, EOM-CC(2,3), and EOM-CCSDT]. For the alkenes in Section 3.5.4, frozen-core MP2/cc-pVQZ geometries were used as in Refs. 184 and 185.

3.5 Results

3.5.1 Size-Intensivity of the LR-ODC-12 Energies

In Section 3.3.1, we mentioned that all DCT methods are by construction *size-extensive*, meaning that their electronic energies scale linearly with the number of electrons. In this section, we demonstrate that the LR-ODC-12 excitation energies are *size-intensive*, i.e. they satisfy the following property: $E(A^* + B) = E(A^*) + E(B)$, where A and B are two noninteracting fragments in their corresponding ground states and A^* is the fragment A in an excited state. Table 3.1 shows

Table 3.1: Ground-state energies (in E_h) and vertical excitation energies (in eV) for the four lowest-energy excited states of the CO molecule and noninteracting systems of CO with Ne atoms (CO + nNe, $n = 1, 2, 3$) computed using the ODC-12 and LR-ODC-12 methods (cc-pVDZ basis set). The noninteracting systems were separated from each other by 10000 Å and the C–O bond distance was set to 1.12547 Å. Results demonstrate size-intensivity of the LR-ODC-12 excitation energies.

	CO	CO + Ne	CO + 2Ne	CO + 3Ne
$X\,^1\Sigma_g^+$	−113.051282	−241.730913	−370.410543	−499.090174
$^3\Pi$	6.48596	6.48596	6.48596	6.48596
$^3\Sigma^+$	8.41225	8.41225	8.41225	8.41225
$^1\Pi$	8.90866	8.90866	8.90866	8.90866
$^3\Delta$	9.33189	9.33189	9.33189	9.33189

the ODC-12 ground-state energies and the LR-ODC-12 excitation energies for the CO molecule and noninteracting systems composed of CO and the neon atoms separated by 10000 Å (CO + nNe, $n = 1, 2, 3$). The scaling of the ODC-12 energies with the number of electrons for the ground $X\,^1\Sigma_g^+$ electronic state is perfectly linear up to 10^{-8} E_h, which is the convergence parameter used in our ODC-12 computations. Upon the addition of the neon atoms, the excitation energies of the CO molecule remain constant up to the convergence threshold set in LR-ODC-12 (10^{-6} eV). These results provide numerical evidence that the LR-ODC-12 excitation energies are size-intensive.

3.5.2 H_2 Dissociation

One of the desirable properties of an electronic structure method is exactness for two-electron systems. While the ODC-12 method is not exact for two-electron

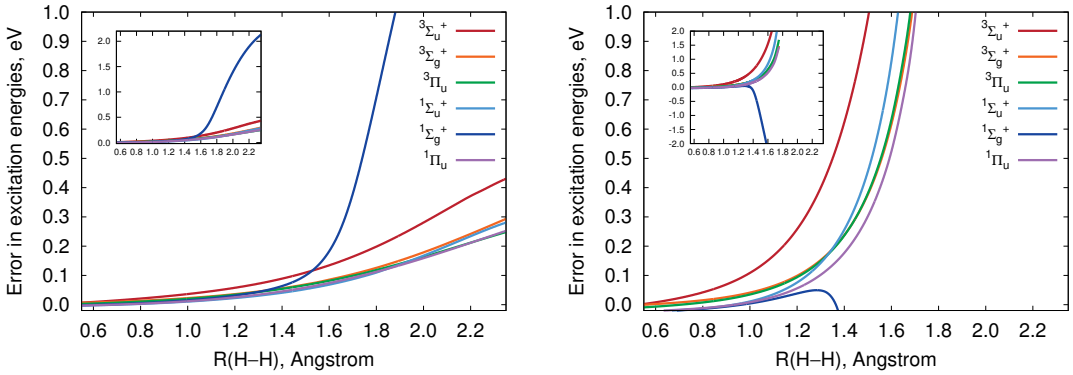

(a) (b)

Figure 3.1: Errors in vertical excitation energies (eV) for six lowest-lying electronic states of H_2 computed using LR-ODC-12 (3.1a) and LR-OLCCD (3.1b) as a function of the H–H bond length, relative to full configuration interaction. All methods employed the d-aug-cc-pvtz basis set. In each figure, the inset shows the same plot for a larger range of errors.

systems, it has been shown to provide a very good description of the ground-state H_2 dissociation curve, with errors of $\sim$ 1 kcal mol^{-1} with respect to full configuration interaction (FCI) near the dissociation limit.[66] Here, we investigate the performance of LR-ODC-12 for the excited states of H_2. Figure 3.1a shows the errors in vertical excitation energies for six lowest-lying electronic states as a function of the H−H distance, relative to FCI. The FCI energies were computed using the EOM-CCSD method, which is exact for two-electron systems. At the equilibrium geometry ($r_e = 0.742$ Å) the errors in excitation energies for all states do not exceed 0.02 eV. Between 0.6 and 1.45 Å ($r \approx 2r_e$), the LR-ODC-12 excitation energies remain in good agreement with FCI, with errors less than 0.1 eV for all states. In this range, the largest error is observed for the $^3\Sigma_u^+$ state. For

$r \geq 1.5$ Å, the error in the $^1\Sigma_g^+$ excited state energy rapidly increases from 0.10 eV (at 1.5 Å) to 2.13 eV (at 2.35 Å), while for other states the errors increase much more slowly. Analysis of the FCI wavefunction for the $^1\Sigma_g^+$ state shows a significant contribution from the $(1\sigma_g)^2 \rightarrow (1\sigma_u)^2$ double excitation already at $r =$ 1.55 Å. This contribution becomes dominant for $r \geq 1.75$ Å. Thus, the large LR-ODC-12 errors observed for the $^1\Sigma_g^+$ state are likely due to the increasingly large double-excitation character of this electronic state at long H−H bond distances. The second largest error near the dissociation is observed for the $^3\Sigma_u^+$ state (0.43 eV). For other electronic states, smaller errors of ~ 0.25 eV are observed near the dissociation.

The importance of the non-linear terms in the LR-ODC-12 equations can be investigated by comparing the LR-ODC-12 and LR-OLCCD results. Figure 3.1b shows the errors in the LR-OLCCD vertical excitation energies as a function of the H−H bond length. Although near the equilibrium geometry the performance of LR-OLCCD and LR-ODC-12 is similar, the LR-OLCCD errors increase much faster with increasing H−H distance compared to LR-ODC-12. At $r = 1.3$ Å, the LR-OLCCD error for the $^3\Sigma_u^+$ state (0.4 eV) is almost six times larger than the corresponding error from LR-ODC-12 (0.07 eV). For $r \geq 1.35$ Å, the LR-OLCCD errors for all excitation energies show very steep increase in magnitude, ranging from 1.5 to 4.7 eV already at $r = 1.75$ Å. We were unable to converge the LR-OLCCD equations for $r \geq 1.80$ Å. Overall, our results demonstrate that the non-linear terms in LR-ODC-12 significantly improve the description of the

excited states at long H−H distances where the electron correlation effects are stronger.

3.5.3 Benchmark: Small Molecules

Here, we benchmark the performance of LR-ODC-12 for vertical excitation energies in several small molecules: N_2, CO, HCN, HNC, C_2H_2, and H_2CO. Tables 3.2 and 3.3 show the errors in excitation energies computed using EOM-CCSD, LR-OLCCD, and LR-ODC-12 for the singlet and triplet excited states, respectively, relative to the results from EOM-CCSDT. To measure the performance of each method, we computed the mean absolute errors (Δ_{MAE}) and the standard deviations from the average signed error (Δ_{SD}), shown in Figure 3.2.

For the singlet electronic states (Table 3.2), the excitation energies computed using LR-ODC-12 are in better agreement with EOM-CCSDT than those obtained from EOM-CCSD, on average. This is evidenced by Δ_{MAE}, which is smaller for LR-ODC-12 compared to EOM-CCSD by a factor of two ($\Delta_{\mathrm{MAE}} = 0.08$ and 0.17 eV, respectively). The LR-ODC-12 errors exceed 0.10 eV for only four states, with a maximum error of 0.20 eV. EOM-CCSD has a minimum error of 0.10 eV, shows errors greater than 0.10 eV for 14 states, and has a maximum error of 0.26 eV. EOM-CCSD shows a somewhat smaller Δ_{SD} compared to that of LR-ODC-12 ($\Delta_{\mathrm{SD}} = 0.05$ and 0.08 eV, respectively).

For the triplet states (Table 3.3), LR-ODC-12 is again superior to EOM-CCSD, on average, with $\Delta_{\mathrm{MAE}} = 0.06$ and 0.11 eV for the two methods, respectively. LR-ODC-12 has errors larger than 0.10 eV for five states with a maximum error of

Table 3.2: Errors in vertical excitation energies (eV) for singlet states computed using LR-OLCCD, LR-ODC-12, and EOM-CCSD, relative to EOM-CCSDT (aug-cc-pVTZ basis set). All electrons were correlated in all computations. Also shown are mean absolute errors (Δ_{MAE}) and standard deviations (Δ_{SD}) computed for each method.

		ΔEOM-CCSD	ΔLR-OLCCD	ΔLR-ODC-12	EOM-CCSDT
N_2	$^1\Pi_g$	0.18	0.08	0.20	9.29
	$^1\Sigma_u^-$	0.23	0.15	0.09	9.84
	$^1\Delta_u$	0.26	0.14	0.10	10.26
CO	$^1\Pi$	0.16	0.09	0.17	8.46
	$^1\Sigma^-$	0.19	−0.10	−0.01	9.89
	$^1\Delta$	0.19	−0.22	−0.05	10.03
HCN	$^1\Sigma^-$	0.16	0.05	0.00	8.25
	$^1\Delta$	0.17	0.04	0.01	8.61
	$^1\Pi$	0.17	0.05	0.20	9.12
HNC	$^1\Pi$	0.15	−0.01	0.10	8.13
	$^1\Sigma^+$	0.24	0.05	0.12	8.46
	$^1\Sigma^-$	0.15	−0.09	0.04	8.67
	$^1\Delta$	0.15	−0.18	−0.03	8.84
C_2H_2	$^1\Sigma_u^-$	0.12	0.06	0.02	7.11
	$^1\Delta_u$	0.10	0.07	0.03	7.45
H_2CO	$^1A_2$	0.10	−0.07	0.02	3.95
Δ_{MAE}		0.17	0.09	0.08	
Δ_{SD}		0.05	0.11	0.08	

Table 3.3: Errors in vertical excitation energies (eV) for triplet states computed using LR-OLCCD, LR-ODC-12, and EOM-CCSD, relative to EOM-CCSDT (aug-cc-pVTZ basis set). All electrons were correlated in all computations. Also shown are mean absolute errors (Δ_{MAE}) and standard deviations (Δ_{SD}) computed for each method.

		ΔEOM-CCSD	ΔLR-OLCCD	ΔLR-ODC-12	EOM-CCSDT
N_2	$^3\Sigma_u^+$	0.11	0.04	−0.02	7.63
	$^3\Pi_g$	0.15	0.06	0.11	8.00
	$^3\Delta_u$	0.17	0.08	0.03	8.82
	$^3\Sigma_u^-$	0.28	0.03	0.01	9.63
	$^3\Pi_u$	0.14	−0.01	0.10	11.18
CO	$^3\Pi$	0.12	0.06	0.08	6.27
	$^3\Sigma^+$	0.05	−0.03	−0.03	8.38
	$^3\Delta$	0.11	−0.07	−0.03	9.21
	$^3\Sigma^-$	0.19	−0.18	−0.06	9.72[a]
HCN	$^3\Sigma^+$	0.05	−0.04	−0.10	6.40
	$^3\Delta$	0.13	−0.02	−0.06	7.40
	$^3\Pi$	0.10	0.08	0.06	8.01
	$^3\Sigma^-$	0.16	−0.10	−0.05	8.15[a]
HNC	$^3\Pi$	0.09	0.00	0.03	6.06
	$^3\Sigma^+$	0.04	−0.09	−0.11	7.20
	$^3\Delta$	0.10	−0.14	−0.11	8.02
	$^3\Sigma^+$	0.22	−0.05	0.04	8.38
	$^3\Sigma^-$	0.15	−0.02	0.11	8.56[a]
C_2H_2	$^3\Sigma_u^+$	0.01	−0.02	−0.08	5.52
	$^3\Delta_u$	0.08	−0.02	−0.05	6.41
	$^3\Sigma_u^-$	0.10	−0.03	−0.05	7.10[a]
H_2CO	$^3A_2$	0.04	−0.02	0.01	3.56
	$^3A_1$	0.02	−0.06	−0.14	6.06
Δ_{MAE}		0.11	0.05	0.06	
Δ_{SD}		0.06	0.07	0.07	

[a] For CO, HCN, HNC, and C_2H_2, the $^3\Sigma^-$ ($^3\Sigma_u^-$) excitation energies were obtained from EOM-CC(2,3), which energies were shifted to reproduce the EOM-CCSDT energy for the $^1\Sigma^-$ ($^1\Sigma_u^-$) state.

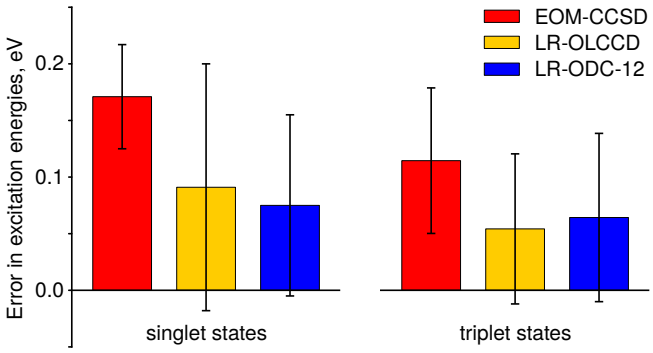

Figure 3.2: Mean absolute deviations (Δ_{MAE}) and standard deviations from the mean signed error (Δ_{SD}) for vertical excitation energies (Tables 3.2 and 3.3) computed using LR-OLCCD, LR-ODC-12, and EOM-CCSD, relative to EOM-CCSDT (aug-cc-pVTZ basis set). The Δ_{MAE} value is represented as a height of each colored box, while the Δ_{SD} value is depicted as a radius of the black vertical bar.

0.14 eV, whereas EOM-CCSD exceeds 0.10 eV error for 12 states and shows a maximum error of 0.28 eV. For linear molecules, EOM-CCSD exhibits consistently poor results for the $^3\Sigma^-$ electronic states, while the performance of LR-ODC-12 for different electronic states is similar. Notably, all EOM-CCSD excitation energies overestimate the EOM-CCSDT values, while the LR-ODC-12 energies are centered around the reference energies, suggesting that LR-ODC-12 provides a more balanced description of the ground and excited states.

Comparing LR-ODC-12 with LR-OLCCD, we see that both methods show very similar results for the triplet states ($\Delta_{\mathrm{MAE}} = 0.06$ and 0.05 eV, respectively), with noticeable differences observed only for the $^3\Sigma^-$ states. For the singlet electronic states, LR-OLCCD shows a somewhat larger $\Delta_{\mathrm{MAE}} = 0.09$ eV and $\Delta_{\mathrm{SD}} = 0.11$ eV compared to LR-ODC-12 ($\Delta_{\mathrm{MAE}} = 0.08$ eV and $\Delta_{\mathrm{SD}} = 0.08$ eV). In this case, significant differences are observed for the $^1\Pi$ states of N_2 and HCN, $^1\Sigma^-$ of HNC,

Table 3.4: Vertical excitation energies computed using LR-OLCCD, LR-ODC-12, and EOM-CCSD for the low-lying electronic states of ethylene (C_2H_4), butadiene (C_4H_6), and hexatriene (C_6H_8). Computations employed the ANO-L-pVDZ (for C_4H_6 and C_6H_8) and ANO-L-pVTZ (for C_2H_4) basis sets and the MP2/cc-pVQZ optimized geometries. For LR-OLCCD and LR-ODC-12, oscillator strengths of the allowed transitions are given in parentheses. All electrons were correlated in all computations.

		EOM-CCSD	LR-OLCCD	LR-ODC-12	SHCI[a]
C_2H_4	1^3B_{1u}	4.46	4.66	4.52	4.59
	1^1B_{1u}	8.14	8.20 (1.8)	8.13 (1.9)	8.05
C_4H_6	1^3B_u	3.20	3.58	3.43	3.37
	1^1B_u	6.53	6.76 (4.2)	6.67 (4.4)	6.45
	2^1A_g	7.28	7.14	6.81	6.58
C_6H_8	1^3B_u	2.64	3.01	2.83	2.77
	1^1B_u	5.60	5.89 (6.5)	5.74 (8.1)	5.59
	2^1A_g	6.55	4.21	5.73	5.58

[a] Also shown are the excitation energies from the semistochastic heat-bath CI (SHCI) method, extrapolated to full CI limit.[186] The $1s$ orbitals of carbon atoms were not included in the SHCI correlation treatment. The SHCI computations used the same basis sets and optimized geometries as those used for LR-OLCCD, LR-ODC-12, and EOM-CCSD.

and $^1\Delta$ of CO and HNC, indicating that the non-linear terms included in LR-ODC-12 are important for these electronic states.

3.5.4 Ethylene, Butadiene, and Hexatriene

Finally, we apply the LR-ODC-12 method to challenging excited states of ethylene (C_2H_4), butadiene (C_4H_6), and hexatriene (C_6H_8). A reliable description of these electronic states requires an accurate treatment of electron correlation.[184;185;187–201] All three molecules feature a dipole-allowed 1^1B_u (or 1^1B_{1u}) state that is well

described as a $\pi-\pi^*$ excitation, but requires a very accurate description of dynamic correlation between the σ and π electrons. In butadiene and hexatriene, the 1^1B_u state is near-degenerate with a dipole-forbidden 2^1A_g state that has a substantial double-excitation character, requiring the description of static correlation in the π and π^* orbitals.[195–197] For this reason, the relative energies and ordering of the 1^1B_u and 2^1A_g states are very sensitive to various levels of theory. For example, single-reference methods truncated to single and double excitations describe the 1^1B_u state more accurately than the 2^1A_g state, while multi-reference methods are more reliable for the 2^1A_g state, missing important dynamic correlation for the 1^1B_u state. Very recently, Chien et al.[186] reported accurate vertical excitation energies for the low-lying states of ethylene, butadiene, and hexatriene computed using semistochastic heat-bath configuration interaction (SHCI) extrapolated to the full CI limit. In this section, we will use the SHCI results to benchmark the accuracy of the LR-ODC-12 method.

Table 3.4 reports the vertical excitation energies of ethylene, butadiene, and hexatriene computed using the EOM-CCSD, LR-OLCCD, and LR-ODC-12 methods, along with the SHCI results from Ref. 186. All methods employed the same optimized geometries and basis sets (see Table 3.4 for details). We refer to the B_{1u} states of C_2H_4 as B_u for brevity. All excitation energies decrease as the number of double bonds in a molecule increases. For butadiene and hexatriene, the (1^1B_u; 2^1A_g) excitation energies computed using the SHCI method are (6.45; 6.58) and (5.59; 5.58) eV, respectively, indicating that the two states are nearly degenerate for the longer polyene. This feature is not reproduced by the EOM-CCSD method,

which predicts the 1^1B_u state energies in close agreement with SHCI, but significantly overestimates the energies for the doubly-excited 2^1A_g state. As a result, the EOM-CCSD method overestimates the energy spacing between the 1^1B_u and 2^1A_g states by ~ 0.6 eV and 1.0 eV for butadiene and hexatriene, respectively.

The LR-ODC-12 method, by contrast, correctly describes the relative energies and ordering of the 1^1B_u and 2^1A_g states, predicting their energy spacing to be 0.14 and -0.01 eV for butadiene and hexatriene, respectively, in an excellent agreement with the SHCI results (0.13 and -0.01 eV). For the singlet excited states, the LR-ODC-12 method consistently overestimates the SHCI excitation energies by ~ 0.1 – 0.2 eV. For the 1^3B_u state, the LR-ODC-12 errors are smaller in magnitude (~ 0.06 eV). Importantly, these results suggest that the LR-ODC-12 method provides a balanced description of the excited states with different electronic structure effects, as illustrated by its consistent performance for the 1^3B_u, 1^1B_u, and 2^1A_g states in ethylene, butadiene, and hexatriene.

Comparing to LR-OLCCD shows that including the non-linear terms in LR-ODC-12 is crucial for the description of excited states with double-excitation character. While for the 1^3B_u and 1^1B_u states the LR-OLCCD errors exceed the LR-ODC-12 errors by ~ 0.15 eV, for the doubly-excited 2^1A_g state the LR-OLCCD errors are much worse: 0.56 and -1.37 eV for butadiene and hexatriene, respectively.

3.6 Conclusions

We have presented a new approach for excited electronic states based on the linear-response formulation of density cumulant theory (DCT). The resulting linear-response DCT model (LR-DCT) has the same computational scaling as the original (single-state) DCT formulation but can accurately predict energies and properties for many electronic states, simultaneously. We have described the general formulation of LR-DCT, derived equations for the linear-response ODC-12 method (LR-ODC-12), and presented its implementation. In LR-ODC-12, excited-state energies are obtained by solving the generalized eigenvalue equation that involves a symmetric Hessian matrix. This simplifies the computation of the excited-state properties (such as transition dipoles) and ensures that the excitation energies have real values, provided that the Hessian is positive semi-definite. In addition, the LR-ODC-12 excitation energies are size-intensive, which we have verified numerically for a system of noninteracting fragments.

Our preliminary results demonstrate that LR-ODC-12 yields very accurate excitation energies for a variety of excited states with different electronic structure effects. For a set of small molecules (N_2, CO, HCN, HNC, C_2H_2, and H_2CO), LR-ODC-12 outperforms equation-of-motion coupled cluster theory with single and double excitations (EOM-CCSD), with mean absolute errors in excitation energies of less than 0.1 eV, relative to reference data. Importantly, both LR-ODC-12 and EOM-CCSD have the same computational scaling. In a study of ethylene, butadiene, and hexatriene, we have compared the performance of LR-ODC-12 and EOM-CCSD with the results from highly-accurate semistochastic heat-bath config-

uration interaction (SHCI). For butadiene and hexatriene, LR-ODC-12 provides a balanced description of the singly-excited 1^1B_u and the doubly-excited 2^1A_g states, predicting that the two states become nearly-degenerate in hexatriene, in excellent agreement with SHCI. By contrast, EOM-CCSD drastically overestimates the energy of the 2^1A_g state, resulting in a ~ 1 eV error in the energy gap between these states of hexatriene.

Overall, our results demonstrate that linear-response density cumulant theory is a promising theoretical approach for spectroscopic properties of molecules and encourage its further development. Several research directions are worth exploring. One of them is the efficient implementation of LR-ODC-12 and its applications to chemical systems with challenging electronic states. Two classes of systems that are particularly worth exploring are open-shell molecules and transition metal complexes. Another direction is to extend LR-DCT to simulations of other spectroscopic properties, such as photoelectron or X-ray absorption spectra. In this regard, applying LR-DCT to the computation of optical rotation properties is of particular interest as it is expected to avoid gauge invariance problems due to the variational nature of the DCT orbitals.[202] We plan to explore these directions in the future.

3.A Derivatives of the One-Body Density Matrix in Density Cumulant Theory

Repeated differentiation of the one-body n-representability condition (Eq. (3.3)) gives the following formulas for the first and second derivatives of the cumulant

partial trace:

$$\frac{\partial \lambda_{qr}^{pr}}{\partial y} = \gamma_s^p \frac{\partial \gamma_q^s}{\partial y} + \frac{\partial \gamma_s^p}{\partial y}\gamma_q^s - \frac{\partial \gamma_q^p}{\partial y} \tag{3.32}$$

$$\begin{aligned}\frac{\partial^2 \lambda_{qr}^{pr}}{\partial x \partial y} =& \gamma_s^p \frac{\partial \gamma_q^s}{\partial x \partial y} + \frac{\partial \gamma_s^p}{\partial x \partial y}\gamma_q^s - \frac{\partial \gamma_q^p}{\partial x \partial y} \\ &+ \frac{\partial \gamma_s^p}{\partial x}\frac{\partial \gamma_q^s}{\partial y} + \frac{\partial \gamma_q^s}{\partial x}\frac{\partial \gamma_s^p}{\partial y}\end{aligned} \tag{3.33}$$

Transforming to the natural spin-orbital basis (NSO, denoted by prime indices) where the one-body density matrix is diagonal, the first and second derivatives of the one-body density matrix can be determined from the cumulant derivatives as follows:

$$\frac{\partial \gamma_{q'}^{p'}}{\partial y} = \theta_{p'q'} \frac{\partial \lambda_{q'r}^{p'r}}{\partial y} \tag{3.34}$$

$$\begin{aligned}\frac{\partial^2 \gamma_{q'}^{p'}}{\partial x \partial y} =& \theta_{p'q'} \frac{\partial^2 \lambda_{q'r}^{p'r}}{\partial x \partial y} - \delta_{r'}^{s'} \theta_{p'q'} \theta_{p's'} \theta_{q'r'} \frac{\partial \lambda_{s't}^{p't}}{\partial x}\frac{\partial \lambda_{q'u}^{r'u}}{\partial y} \\ &- \delta_{r'}^{s'} \theta_{p'q'} \theta_{p's'} \theta_{q'r'} \frac{\partial \lambda_{q'u}^{r'u}}{\partial x}\frac{\partial \lambda_{s't}^{p't}}{\partial y}\end{aligned} \tag{3.35}$$

Here, we have defined the following matrix:

$$\theta_{p'q'} \equiv \begin{cases} (\gamma_{p'} + \gamma_{q'} - 1)^{-1} & \text{if } p', q' \in \text{occ or vir} \\ 0 & \text{otherwise} \end{cases} \tag{3.36}$$

where $\gamma_{p'}$ denotes an eigenvalue of the one-body density matrix (i.e., an occupation number). The natural spin-orbital p' is considered occupied if $\gamma_{p'} > 0.5$.

Eqs. (3.34) and (3.35) can be used to derive expression for the two-body energy Hessian in Eq. (3.23). Simplifying the resulting equations allows us to determine the intermediates defined in Eq. (3.24). In the NSO basis, these intermediates are

given by

$$\mathcal{F}_{p'}^{q'} \equiv \theta_{p'q'} f_{p'}^{q'} \tag{3.37}$$

$$\mathcal{G}_{p'r'}^{q's'} \equiv \theta_{p'q'}\theta_{r's'}(\overline{g}_{p'r'}^{q's'} - \mathcal{F}_{p'}^{s'}\delta_{r'}^{q'} - \mathcal{F}_{r'}^{q'}\delta_{p'}^{s'}) \tag{3.38}$$

These quantities are computed in the NSO basis and back-transformed to the original spin-orbital basis using the eigenvectors of the one-particle density matrix (see Ref. 65 for more details).

3.B Supporting Information

Here, we present the working equations for the LR-ODC-12 and LR-OLCCD methods. We refer the reader to the main article for definitions and notation, and note that prime indices refer to the natural spin-orbital basis (NSO) where the one-particle density matrix is diagonal, $\gamma_{q'}^{p'} = \delta_{q'}^{p'}\gamma_{q'}$. Quantities computed in the NSO basis can be back-transformed to the original basis using the eigenvectors of the one-particle density matrix.

For the property gradient vectors, we define the block structure as follows

$$\mathbf{v}'^{\dagger} \equiv (\mathbf{p}_1\ \mathbf{p}_2\ \mathbf{p}_1^*\ \mathbf{p}_2^*)^{\dagger} \qquad \mathbf{p}_m \equiv \frac{\partial\langle\Psi|\hat{V}|\Psi\rangle}{\partial\mathbf{t}_m^{\dagger}} \tag{3.39}$$

where $\hat{V}$ can be any one-particle operator, defined through its spin-orbital integrals, $v_p^q = \langle\psi_p|\hat{v}|\psi_q\rangle$, as follows.

$$\hat{V} = v_p^q a_q^p \tag{3.40}$$

A typical example would be an electric dipole operator.

3.C Working Equations for LR-ODC-12

3.C.1 Density Matrices

$$\gamma^i_j = \tfrac{1}{2}(\mathbf{1} + \sqrt{\mathbf{1} + 4\mathbf{d}})^i_j \qquad d^i_j \equiv -\tfrac{1}{2} t^{ik}_{cd} t^{cd}_{jk} \tag{3.41}$$

$$\gamma^b_a = \tfrac{1}{2}(\mathbf{1} - \sqrt{\mathbf{1} + 4\mathbf{d}})^b_a \qquad d^b_a \equiv -\tfrac{1}{2} t^{kl}_{ac} t^{bc}_{kl} \tag{3.42}$$

$$\gamma^{ij}_{kl} = \tfrac{1}{2} t^{ij}_{cd} t^{cd}_{kl} + P_{(k/l)} \gamma^i_k \gamma^j_l \tag{3.43}$$

$$\gamma^{cd}_{ab} = \tfrac{1}{2} t^{kl}_{ab} t^{cd}_{kl} + P^{(c/d)} \gamma^c_a \gamma^d_b \tag{3.44}$$

$$\gamma^{ib}_{ja} = -t^{ik}_{ac} t^{bc}_{jk} + \gamma^i_j \gamma^b_a \tag{3.45}$$

$$\gamma^{ij}_{ab} = t^{ij}_{ab} \tag{3.46}$$

3.C.2 Blocks of the Energy Hessian

$$\begin{aligned}(\mathbf{A}_{11})_{ia,jb} = {} & h^i_j \gamma^b_a + h^b_a \gamma^i_j - \bar{F}^i_j \delta^b_a - \bar{F}^b_a \delta^i_j + \overline{g}^{mi}_{nj} \gamma^{nb}_{ma} + \overline{g}^{nb}_{ma} \gamma^{mi}_{nj} + \overline{g}^{ie}_{jf} \gamma^{bf}_{ae} + \overline{g}^{bf}_{ae} \gamma^{ie}_{jf} \\ & + \overline{g}^{ib}_{me} \gamma^{me}_{ja} + \overline{g}^{me}_{ja} \gamma^{ib}_{me}\end{aligned} \tag{3.47}$$

$$\bar{\mathbf{F}} \equiv \tfrac{1}{2}(\mathbf{F} + \mathbf{F}^\dagger) \qquad F_p^q \equiv h_p^t \gamma_t^q + \tfrac{1}{2}\overline{g}_{pt}^{uv}\gamma_{uv}^{qt} \tag{3.48}$$

$$\begin{aligned}(\mathbf{B}_{11})_{ia,jb} = &\overline{g}_{be}^{im}\gamma_{ma}^{je} + \overline{g}_{ma}^{je}\gamma_{be}^{im} + \overline{g}_{mb}^{ie}\gamma_{ae}^{jm} + \overline{g}_{ae}^{jm}\gamma_{mb}^{ie} + \tfrac{1}{2}\overline{g}_{mn}^{ij}\gamma_{ab}^{mn} + \tfrac{1}{2}\overline{g}_{ab}^{mn}\gamma_{mn}^{ij} \\ &+\tfrac{1}{2}\overline{g}_{ef}^{ij}\gamma_{ab}^{ef} + \tfrac{1}{2}\overline{g}_{ab}^{ef}\gamma_{ef}^{ij}\end{aligned} \tag{3.49}$$

$$\begin{aligned}(\mathbf{A}_{22})_{ijab,klcd} = &-P_{(a/b|k/l)}^{(c/d)}\mathcal{F}_a^c\delta_b^d\delta_k^i\delta_l^j - P_{(k/l)}^{(i/j|c/d)}\mathcal{F}_k^i\delta_l^j\delta_a^c\delta_b^d + P_{(k/l)}\overline{g}_{ab}^{cd}\delta_k^i\delta_l^j + P^{(c/d)}\overline{g}_{kl}^{ij}\delta_a^c\delta_b^d \\ &-P_{(a/b|k/l)}^{(i/j|c/d)}\overline{g}_{la}^{jc}\delta_b^d\delta_k^i + P_{(a/b)}^{(c/d)}\mathcal{G}_{af}^{ec}t_{eb}^{ij}t_{kl}^{fd} + P_{(a/b|k/l)}\mathcal{G}_{ka}^{me}t_{eb}^{ij}t_{ml}^{cd} \\ &+P^{(i/j|c/d)}\mathcal{G}_{me}^{ic}t_{ab}^{mj}t_{kl}^{ed} + P_{(k/l)}^{(i/j)}\mathcal{G}_{mk}^{in}t_{ab}^{mj}t_{nl}^{cd}\end{aligned} \tag{3.50}$$

$$\mathcal{F}_{p'}^{q'} \equiv \theta_{p'q'}f_{p'}^{q'} \qquad \mathcal{G}_{p'r'}^{q's'} \equiv \theta_{p'q'}\theta_{r's'}(\overline{g}_{p'r'}^{q's'} - \mathcal{F}_{p'}^{s'}\delta_{r'}^{q'} - \mathcal{F}_{r'}^{q'}\delta_{p'}^{s'}) \tag{3.51}$$

$$\theta_{p'q'} \equiv \begin{cases} (\gamma_{p'} + \gamma_{q'} - 1)^{-1} & \text{if } p,q \in \text{occ or vir} \\ 0 & \text{otherwise} \end{cases} \tag{3.52}$$

$$\begin{aligned}(\mathbf{B}_{22})_{ijab,klcd} = &P_{(a/b|c/d)}\mathcal{G}_{ac}^{ef}t_{eb}^{ij}t_{fd}^{kl} + P_{(a/b)}^{(k/l)}\mathcal{G}_{na}^{ke}t_{eb}^{ij}t_{cd}^{nl} + P_{(c/d)}^{(i/j)}\mathcal{G}_{mc}^{if}t_{ab}^{mj}t_{fd}^{kl} \\ &+P^{(i/j|k/l)}\mathcal{G}_{mn}^{ik}t_{ab}^{mj}t_{cd}^{nl}\end{aligned} \tag{3.53}$$

$$\begin{aligned}(\mathbf{A}_{12})_{ia,klcd} = &-P_{(k/l)}\overline{g}_{la}^{cd}\delta_k^i - P^{(c/d)}\overline{g}_{kl}^{id}\delta_a^c - P_{(k/l)}(\mathcal{I}_a^i)_k^m t_{ml}^{cd} - P^{(c/d)}(\mathcal{I}_a^i)_e^c t_{kl}^{ed} \\ &-P_{(k/l)}^{(c/d)}\overline{g}_{ae}^{mc}t_{ml}^{ed}\delta_k^i - P_{(k/l)}^{(c/d)}\overline{g}_{ke}^{im}t_{ml}^{ed}\delta_a^c - \tfrac{1}{2}P_{(k/l)}\overline{g}_{la}^{mn}t_{mn}^{cd}\delta_k^i - \tfrac{1}{2}P^{(c/d)}\overline{g}_{ef}^{id}t_{kl}^{ef}\delta_a^c\end{aligned} \tag{3.54}$$

$$(\mathbf{B}_{12})_{ia,klcd} = -P^{(k/l)}(\mathcal{I}_a^i)_m^k t_{cd}^{ml} - P_{(c/d)}(\mathcal{I}_a^i)_c^e t_{ed}^{kl} - P_{(c/d)}^{(k/l)}\overline{g}_{ad}^{le} t_{ce}^{ki} - P_{(c/d)}^{(k/l)}\overline{g}_{md}^{il} t_{ca}^{km} - \overline{g}_{ma}^{kl} t_{cd}^{im} - \overline{g}_{cd}^{ie} t_{ae}^{kl} \tag{3.55}$$

$$(\mathcal{I}_a^i)_{k'}^{l'} \equiv \theta_{k'l'}(I_a^i)_{k'}^{l'} \qquad (I_a^i)_k^l \equiv +f_a^l \delta_k^i - \overline{g}_{ka}^{ml}\gamma_m^i + \overline{g}_{ke}^{il}\gamma_a^e \tag{3.56}$$

$$(\mathcal{I}_a^i)_{d'}^{c'} \equiv \theta_{c'd'}(I_a^i)_{d'}^{c'} \qquad (I_a^i)_d^c \equiv -f_d^i \delta_a^c + \overline{g}_{ad}^{mc}\gamma_m^i - \overline{g}_{ed}^{ic}\gamma_a^e \tag{3.57}$$

3.C.3 Blocks of the Metric Matrix

$$(\mathbf{S}_{11})_{ia,jb} = (\delta_a^b \gamma_j^i - \delta_j^i \gamma_a^b) \tag{3.58}$$

3.C.4 Blocks of the Property Gradient Vector

$$(\mathbf{p}_1)_{ia} = v_a^m \gamma_m^i - v_e^i \gamma_a^e \tag{3.59}$$

$$(\mathbf{p}_2)_{ijab} = -P_{(a/b)}\mathcal{V}_a^e t_{eb}^{ij} - P^{(i/j)}\mathcal{V}_m^i t_{ab}^{mj} \tag{3.60}$$

$$\mathcal{V}_{p'}^{q'} \equiv \theta_{p'q'} v_{p'}^{q'} \tag{3.61}$$

3.D Working Equations for LR-OLCCD

3.D.1 Density Matrices

$$\gamma_j^i = \delta_j^i - \tfrac{1}{2} t_{cd}^{ik} t_{jk}^{cd} \tag{3.62}$$

$$\gamma_a^b = \tfrac{1}{2} t_{ac}^{kl} t_{kl}^{bc} \tag{3.63}$$

$$\gamma_{kl}^{ij} = \tfrac{1}{2} t_{cd}^{ij} t_{kl}^{cd} + P_{(k/l)} \delta_k^i \delta_l^j - \tfrac{1}{2} P_{(k/l)}^{(i/j)} \delta_k^i t_{cd}^{jm} t_{lm}^{cd} \tag{3.64}$$

$$\gamma_{ab}^{cd} = \tfrac{1}{2} t_{ab}^{kl} t_{kl}^{cd} \tag{3.65}$$

$$\gamma_{ja}^{ib} = -t_{ac}^{ik} t_{jk}^{bc} + \tfrac{1}{2} \delta_j^i t_{ac}^{kl} t_{kl}^{bc} \tag{3.66}$$

$$\gamma_{ab}^{ij} = t_{ab}^{ij} \tag{3.67}$$

3.D.2 Blocks of the Energy Hessian

$$(\mathbf{A}_{11})_{ia,jb} = \text{Eq. (3.47) with OLCCD density matrices.} \tag{3.68}$$

$$(\mathbf{B}_{11})_{ia,jb} = \text{Eq. (3.49) with OLCCD density matrices.} \tag{3.69}$$

$$\begin{aligned}(\mathbf{A}_{22})_{ijab,klcd} = {} & P_{(a/b|k/l)}^{(c/d)} (f_0)_a^c \delta_b^d \delta_k^i \delta_l^j - P_{(k/l)}^{(i/j|c/d)} (f_0)_k^i \delta_l^j \delta_a^c \delta_b^d + P_{(k/l)} \overline{g}_{ab}^{cd} \delta_k^i \delta_l^j \\ & + P^{(c/d)} \overline{g}_{kl}^{ij} \delta_a^c \delta_b^d - P_{(a/b|k/l)}^{(i/j|c/d)} \overline{g}_{la}^{jc} \delta_b^d \delta_k^i\end{aligned} \tag{3.70}$$

$$(f_0)_p^q = h_p^q + \overline{g}_{pi}^{qi} \tag{3.71}$$

$$(\mathbf{B}_{22})_{ijab,klcd} = 0 \tag{3.72}$$

$$\begin{aligned}(\mathbf{A}_{12})_{ia,klcd} = &-P_{(k/l)}\overline{g}^{cd}_{la}\delta^i_k - P^{(c/d)}\overline{g}^{id}_{kl}\delta^c_a - P_{(k/l)}(I^i_a)^m_k t^{cd}_{ml} + P^{(c/d)}(I^i_a)^c_e t^{ed}_{kl} \\ &-P^{(c/d)}_{(k/l)}\overline{g}^{mc}_{ae}t^{ed}_{ml}\delta^i_k - P^{(c/d)}_{(k/l)}\overline{g}^{im}_{ke}t^{ed}_{ml}\delta^c_a - \tfrac{1}{2}P_{(k/l)}\overline{g}^{mn}_{la}t^{cd}_{mn}\delta^i_k - \tfrac{1}{2}P^{(c/d)}\overline{g}^{id}_{ef}t^{ef}_{kl}\delta^c_a\end{aligned} \tag{3.73}$$

$$(I^i_a)^l_k \equiv +f^l_a\delta^i_k - \overline{g}^{il}_{ka} \qquad (I^i_a)^c_d \equiv -f^i_d\delta^c_a + \overline{g}^{ic}_{ad} \tag{3.74}$$

$$\begin{aligned}(\mathbf{B}_{12})_{ia,klcd} = &-P^{(k/l)}(I^i_a)^k_m t^{ml}_{cd} + P_{(c/d)}(I^i_a)^e_c t^{kl}_{ed} - P^{(k/l)}_{(c/d)}\overline{g}^{le}_{ad}t^{ki}_{ce} - P^{(k/l)}_{(c/d)}\overline{g}^{il}_{md}t^{km}_{ca} - \overline{g}^{kl}_{ma}t^{im}_{cd} \\ &-\overline{g}^{ie}_{cd}t^{kl}_{ae}\end{aligned} \tag{3.75}$$

3.D.3 Blocks of the Metric Matrix

$$(\mathbf{S}_{11})_{ia,jb} = \text{Eq. (3.58) with OLCCD density matrices.} \tag{3.76}$$

3.D.4 Blocks of the Property Gradient Vector

$$(\mathbf{p}_1)_{ia} = \text{Eq. (3.59) with OLCCD density matrices.} \tag{3.77}$$

$$(\mathbf{p}_2)_{ijab} = P_{(a/b)}v^e_a t^{ij}_{eb} - P^{(i/j)}v^i_m t^{mj}_{ab} \tag{3.78}$$

Chapter 4

Algorithms for Linear-Response Density Cumulant Theory

Chapter 3 presented the LR-ODC-12 model for electronic excited states, where excitation energies and transition properties are computed by diagonalizing the parameter Hessian of the ODC-12 energy functional, with respect to a metric that arises from the time-dependence of the parameter responses. Since number of parameters in the ODC-12 model scales as $\mathcal{O}(o^2v^2)$ with the number of occupied (o) and virtual (v) orbitals, the memory requirement for the Hessian matrix scales with the fourth power of o and v, and the number of floating point operations needed to diagonalize it scales with the sixth power of these dimensions. Such a brute-force approach will rapidly overwhelm available computing resources even for relatively small molecules. For the common scenario in which we only care about states within a narrow energy range, the cost of diagonalization can be drastically reduced through the use of so-called *direct algorithms* which enable the determination of subsets of eigenvectors and eigenvalues without explicitly constructing the Hessian matrix in computer memory. This chapter will explore the use of the Davidson algorithm[179;180] in solving the LR-ODC-12 model. Section 4.1 describes

the Davidson algorithm in general terms and describes strategies employed in the present implementation to reduce memory usage for large calculations. Section 4.2 discusses the structure of the LR-ODC-12 eigenvalue equations, which is followed by a comparison of several alternative strategies for solving the LR-ODC-12 model in section Section 4.3.

4.1 The Davidson Algorithm

Direct algorithms represent linear transformations as functions mapping vectors $\mathbf{v}$ in their domain to vectors $\mathbf{L}(\mathbf{v})$ in their codomain, rather than as coefficient arrays $[L_{ij}] = [\mathbf{e}_i \cdot \mathbf{L}(\mathbf{e}_j)]$ over a complete basis. That is, the result of the transformation is determined *directly*, without explicitly forming its matrix representation in computer memory. The Davidson algorithm applies this technique in the context of a matrix diagonalization, by progressively growing a basis $\{\mathbf{u}_1, \ldots, \mathbf{u}_d\}$ to span the lowest or highest eigenvectors of a matrix to some threshold of accuracy. For a transformation on $\mathbb{R}^n$, this allows us to reduce our computational effort from $\mathcal{O}(n^3)$ to $\mathcal{O}(n^2 d)$ or even less when $\mathbf{L}$ is constructed from lower-dimensional arrays. Memory requirements are reduced from $\mathcal{O}(n^2)$ to $\mathcal{O}(nd)$ in the Davidson algorithm, so that, as long as the dimension of the transformation is large relative to the desired number of roots, we can gain considerable savings.

The procedure for the generalized Davidson algorithm is presented in Algorithm 1, which solves for the eigenvalues and right eigenvectors of a generalized eigenvalue problem, which may or may not be symmetric. The strategy of the algorithm is as follows. We expand our transformations in the reduced expansion

Algorithm 1 Canonical multiroot Davidson algorithm for a generic eigenvalue problem, $\mathbf{L}\mathbf{v}_j = \lambda_j \mathbf{G}\mathbf{v}_j$, with periodic subspace collapse. Requires linear transformation functions and diagonal approximations (indicated by tildes) for $\mathbf{L}$ and $\mathbf{G}$ and solves for the lowest k eigenvalues and eigenvectors.

procedure DAVIDSON($\mathbf{L}(\cdot), \mathbf{G}(\cdot), \tilde{\mathbf{L}}, \tilde{\mathbf{G}}, \mathbf{U}^{(0)}, k, d_{\max}, i_{\max}, r_{\text{tol}}$)
  Initialize the expansion space with a set of guess vectors, $\mathbf{U} \leftarrow \mathbf{U}^{(0)}$.
  for $1 \leq i \leq i_{\max}$ **do**
    Construct subspace representation and solve the lowest k eigenvalues.

$$\mathbf{L}^{\text{sub}} = \mathbf{U}^\dagger \mathbf{L}(\mathbf{U})$$

$$\mathbf{G}^{\text{sub}} = \mathbf{U}^\dagger \mathbf{G}(\mathbf{U})$$

$$\mathbf{L}^{\text{sub}} \mathbf{v}_j^{\text{sub}} = \lambda_j \mathbf{G}^{\text{sub}} \mathbf{v}_j^{\text{sub}}$$

    Calculate the eigenvector residuals over the full space.

$$\mathbf{r}_j = (\mathbf{L}(\mathbf{U}) - \lambda_j \mathbf{G}(\mathbf{U}))\mathbf{v}_j^{\text{sub}}$$

    if $\max(\mathbf{r}_j) < r_{\text{tol}}$ for all j **then**
      Set $\mathbf{v}_j \leftarrow \mathbf{U}\mathbf{v}_j^{\text{sub}}$ and quit the loop. The eigenvectors are converged.
    end if
    Determine new direction vectors by preconditioning the residual.

$$\mathbf{d}_j^{(i)} = -(\tilde{\mathbf{L}} - \lambda_j \tilde{\mathbf{G}})^{-1} \mathbf{r}_j$$

    Project out the span of $\mathbf{U}$ and orthogonalize via SVD compression.

$$\widehat{\mathbf{U}}^{(i)} = (\mathbf{1} - \mathbf{U}^\dagger \mathbf{U})\mathbf{D}^{(i)}$$

$$\widehat{\mathbf{U}}^{(i)} \approx \mathbf{U}^{(i)} \mathbf{\Sigma}^{(i)} \mathbf{W}^{(i)\dagger}$$

    if $\text{rank}(\mathbf{U}) + \text{rank}(\mathbf{U}^{(i)}) < d_{\max}$ **then**
      Extend the expansion space, $\mathbf{U} \leftarrow (\mathbf{U}\ \mathbf{U}^{(i)})$
    else
      Collapse the expansion space, $\mathbf{U} \leftarrow (\mathbf{U}\mathbf{v}_1^{\text{sub}}\ \cdots\ \mathbf{U}\mathbf{v}_k^{\text{sub}})$.
    end if
  end for
  return $\lambda_j, \mathbf{v}_j$
end procedure

space, $[L_{ij}^{\text{sub}}] = [\mathbf{u}_i \cdot \mathbf{L}(\mathbf{u}_j)]$, and solve the eigenvalue equation in this subspace.

$$\mathbf{L}^{\text{sub}}\mathbf{v}_j^{\text{sub}} = \lambda_j^{\text{trial}}\mathbf{G}^{\text{sub}}\mathbf{v}_j^{\text{sub}} \tag{4.1}$$

This trial solution is expressed in the full space as $\mathbf{v}_j^{\text{trial}} = \mathbf{U}\mathbf{v}_j^{\text{sub}}$. The correction vector $\mathbf{d}_j = \mathbf{v}_j^{\text{trial}} - \mathbf{v}_j$ taking us to the exact solution can be approximated as

$$\mathbf{d}_j \approx -(\tilde{\mathbf{L}} - \lambda_j^{\text{trial}}\tilde{\mathbf{G}})^{-1}\mathbf{r}_j \tag{4.2}$$

where $\mathbf{r}_j \equiv (\mathbf{L} - \lambda_j^{\text{trial}}\mathbf{G})\mathbf{v}_j^{\text{trial}}$ is the residual vector and $(\tilde{\mathbf{L}} - \lambda^{\text{trial}}\tilde{\mathbf{G}})^{-1}$ is called the preconditioner, which is constructed from diagonal approximations to $\mathbf{L}$ and $\mathbf{G}$. This correction vector can be motivated as an approximate solution to the following identity.

$$\mathbf{0} = (\mathbf{L} - \lambda_j\mathbf{G})\mathbf{v}_j = (\mathbf{L} - \lambda_j\mathbf{G})(\mathbf{v}_j^{\text{trial}} + \mathbf{d}_j) \tag{4.3}$$

By repeatedly adding these correction vectors to the subspace, one can iteratively grow the expansion space until it spans the desired eigenvector, $\mathbf{v}_j$. At convergence, the residual and the correction vectors become vanishingly small. A key assumption of this algorithm is that the matrices are diagonally dominant, otherwise the diagonal approximation in Eq. (4.2) breaks down and the procedure will fail to converge on the desired roots. When the expansion space becomes large, we can periodically replace the expansion vectors with the current set of trial eigenvectors in order to keep the memory requirements more manageable. For very

large matrices, frequent collapses every second or third iteration can be used to keep I/O requirements to a minimum, at the cost of slower convergence.[203] This approach is quite general and can be adapted to other large matrix problems, such as the linear equation $\mathbf{Lx} = \mathbf{b}$, where it yields a variant of the conjugate gradient method.

Figure 4.1 presents memory profiles for the Davidson algorithm, as implemented for the present study. The red trace represents the most straight-forward implementation of Algorithm 1. Note that the images $\mathbf{L}(\mathbf{u}_i)$ are only evaluated once as these vectors are added to the expansion space and are reused on future iterations. The large spike in memory between 0 and 3 minutes in the runtime comes from the initial evaluation of the transformation on the guess vectors. This can be mitigated by breaking the expansion space into blocks of no more than 20 vectors, so that the guess vector evaluations have the same cost as the latter transformations. The result is depicted as the purple trace, where we see that the early memory spike has been smoothed at negligible cost to the runtime. The sawtooth shape of the red and purple traces between 3 and 18 minutes depicts the periodic collapse of the expansion space, which would otherwise continue to build indefinitely as the algorithm proceeds. Storing the Davidson vectors and the all-virtual integral arrays, $\overline{g}_{ab}^{cd}$ and $\mathcal{G}_{ab}^{cd}$, on disk produces the green trace, which irons out the sawtooth shape in the trajectory at the cost of some additional runtime for retrieving arrays that are stored on disk. Finally, the blue trace shows that the memory usage can be reduced below 1 GB by shrinking the block sizes even further, albeit at the cost of some additional I/O overhead.

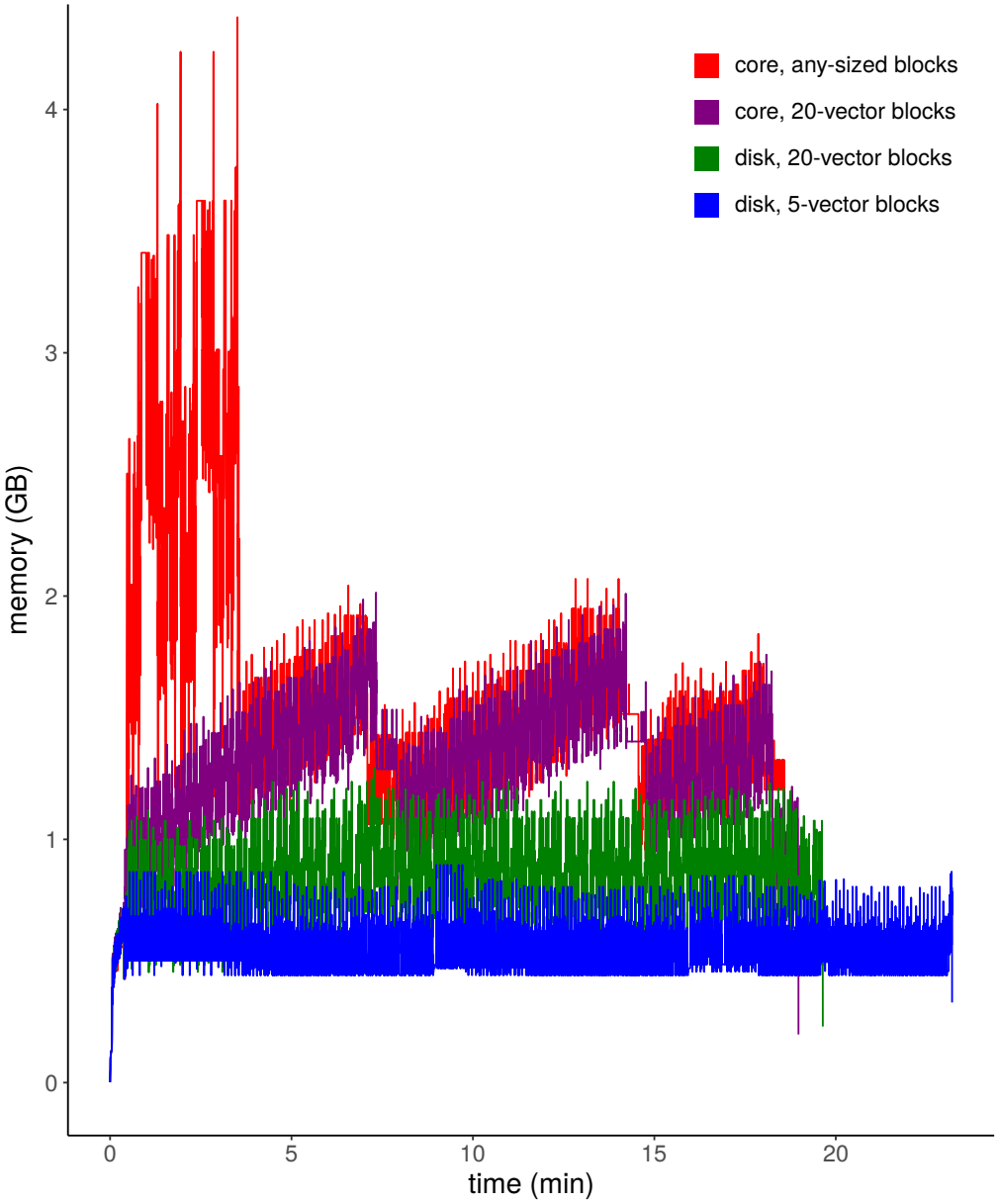

Figure 4.1: Memory profiles for calculating the lowest 20 states of ethylene with the def2-SV(P) basis set on an Intel® Core™ i7-5600U processor using Eqs. (4.14) and (4.16) below. Starts from a set of 100 guess vectors and periodically collapses the expansion space to keep the number of vectors under 200. The green and blue trace result from storing vectors and integral arrays on disk, whereas the red and purple ones use only RAM.

4.2 The LR-ODC-12 Eigenvalue Equation

The LR-ODC-12 eigenvalue equation has a two-by-two block structure which describes the independent variation of the parameters and their complex conjugates.

$$\mathbf{E}\mathbf{z}_k = \omega_k \mathbf{M}\mathbf{z}_k, \quad \mathbf{E} = \begin{pmatrix} \mathbf{A} & \mathbf{B} \\ \mathbf{B}^* & \mathbf{A}^* \end{pmatrix}, \quad \mathbf{M} = \begin{pmatrix} \mathbf{S} & \mathbf{0} \\ \mathbf{0} & -\mathbf{S}^* \end{pmatrix}, \quad \mathbf{z}_k = \begin{pmatrix} \mathbf{x}_k \\ \mathbf{y}_k \end{pmatrix} \tag{4.4}$$

This block symmetry leads to a paired system of eigenvalues, $\{\pm\omega_k\}$. The submatrices in Eq. (4.4) are further blocked according to whether they describe variations of the one-body ($\mathbf{t}_1$) or two-body ($\mathbf{t}_2$) parameters.

$$\mathbf{A} = \begin{pmatrix} \mathbf{A}_{11} & \mathbf{A}_{12} \\ \mathbf{A}_{21} & \mathbf{A}_{22} \end{pmatrix} \quad \mathbf{B} = \begin{pmatrix} \mathbf{B}_{11} & \mathbf{B}_{12} \\ \mathbf{B}_{21} & \mathbf{B}_{22} \end{pmatrix} \quad \mathbf{S} = \begin{pmatrix} \mathbf{S}_{11} & \mathbf{0} \\ \mathbf{0} & \mathbf{1}_2 \end{pmatrix} \quad \mathbf{x}_k = \begin{pmatrix} \mathbf{x}_{k,1} \\ \mathbf{x}_{k,2} \end{pmatrix} \tag{4.5}$$

Following Ref. 204, we can can add and subtract the block rows of Eq. (4.4) to arrive at the following pair of equations (assuming real coefficients).

$$(\mathbf{A} + \mathbf{B})(\mathbf{x}_k + \mathbf{y}_k) = \omega_k \mathbf{S}(\mathbf{x}_k - \mathbf{y}_k) \tag{4.6}$$

$$(\mathbf{A} - \mathbf{B})(\mathbf{x}_k - \mathbf{y}_k) = \omega_k \mathbf{S}(\mathbf{x}_k + \mathbf{y}_k) \tag{4.7}$$

Multiplying both equations by $\mathbf{S}^{-1}$ and substituting one into the other yields the following non-symmetric eigenvalue equation for the squares of the excitation energies, reducing the dimension of the transformation by a factor of two.

$$\mathbf{S}^{-1}(\mathbf{A} - \mathbf{B})\mathbf{S}^{-1}(\mathbf{A} + \mathbf{B})(\mathbf{x}_k + \mathbf{y}_k) = \omega_k^2(\mathbf{x}_k + \mathbf{y}_k) \tag{4.8}$$

Solving this equation only gives us the sum $\mathbf{x}_k + \mathbf{y}_k$, not the individual blocks, but these can be recovered by using Eq. (4.6) to compute $\mathbf{x}_k - \mathbf{y}_k$, so we can still calculate transition from the reduced eigenvalue equation.

The bottleneck in evaluating these transformations is in the diagonal two-body Hessian, $\mathbf{A}_{22}$. The image of an arbitrary two-body vector $\mathbf{u}_{\mu,2} = [u^{ij}_{\mu,ab}]$ under this transformation is given by

$$\begin{aligned}(\mathbf{A}_{22}(\mathbf{u}_{\mu,2}))_{ijab} = &-P_{(a/b)}\mathcal{F}^c_a u^{ij}_{\mu,cb} - P^{(i/j)}\mathcal{F}^i_k u^{kj}_{\mu,ab} + \tfrac{1}{2}\overline{g}^{cd}_{ab} u^{ij}_{\mu,cd} + \tfrac{1}{2}\overline{g}^{ij}_{kl} u^{kl}_{\mu,ab} \\ &-P^{(i/j)}_{(a/b)}\overline{g}^{jc}_{la} u^{il}_{\mu,cb} + \tfrac{1}{2}P_{(a/b)}\mathcal{G}^{ec}_{af} t^{ij}_{eb} t^{fd*}_{kl} u^{kl}_{\mu,cd} + \tfrac{1}{2}P_{(a/b)}\mathcal{G}^{me}_{ka} t^{ij}_{eb} t^{cd*}_{ml} u^{kl}_{\mu,cd} \\ &+\tfrac{1}{2}P^{(i/j)}\mathcal{G}^{ic}_{me} t^{mj}_{ab} t^{ed*}_{kl} u^{kl}_{\mu,cd} + \tfrac{1}{2}P^{(i/j)}\mathcal{G}^{in}_{mk} t^{mj}_{ab} t^{cd*}_{nl} u^{kl}_{\mu,cd}\end{aligned} \tag{4.9}$$

where the i, j, k, l, m, n run over occupied spin-orbitals and a, b, c, d, e, f run over virtual (un-occupied) spin-orbitals with implicit summation over pairs of upper and lower indices. See Chapter 3 for the definitions of these intermediates. For reasonably sized basis sets, the rate limiting step is the contraction of the v^4 integrals with the expansion vector, $\mathrm{g}^{cd}_{ab} u^{ij}_{\mu,cd}$, which scales as $\mathcal{O}(d_\mu o^2 v^4)$ in the number of floating point operations. This term is the rate limiting step in EOM-CCSD as well. The full set of linear transformation formulas for the LR-ODC-12 Hessian and metric blocks is given in the appendix (Section 4.A).

The reduced eigenvalue equation, Eq. (4.8), requires us to invert the metric, which is an identity matrix but for the orbital block, $\mathbf{S}_{11}$. This matrix is given by

$$(\mathbf{S}_{11})_{ia,jb} = \gamma^i_j \delta^b_a - \delta^i_j \gamma^b_a \tag{4.10}$$

where γ_j^i and γ_a^b are occupied and virtual blocks of the one-body density matrix. For systems of moderate size this metric could be numerically inverted, but we can derive a simple and inexpensive formula for the inverse by expanding the density matrices in the natural spin-orbital (NSO) basis where they are diagonal.

$$\gamma_j^i = (\mathbf{Y})_j^{j'}(\mathbf{Y}^\dagger)_{i'}^i \delta_{j'}^{i'} \gamma_{j'} \qquad \gamma_a^b = (\mathbf{Y})_a^{a'}(\mathbf{Y}^\dagger)_{b'}^b \delta_{a'}^{b'} \gamma_{a'} \tag{4.11}$$

Inverting in the NSO basis and transforming back to the original basis yields

$$(\mathbf{S}_{11}^{-1})_{ia,jb} = \frac{(\mathbf{Y}^\dagger)_{j'}^i (\mathbf{Y})_a^{b'}}{\gamma_{j'} - \gamma_{b'}} (\mathbf{Y}^\dagger)_{b'}^b (\mathbf{Y})_j^{j'} \tag{4.12}$$

which scales as $\mathcal{O}(o^2v^3)$ in the number of floating point operations. The same strategy can be used to evaluate other analytic functions of the metric.

4.3 Strategies for Solving the LR-ODC-12 Model

We explore three strategies for solving for the excitation energies and transition properties of the LR-ODC-12 model using the Davidson algorithm. A direct solution of the full eigenvalue equation (Eq. (4.4)) is not possible with the Davidson algorithm, because the presence of negative roots means that the eigenvalues of interest are in the middle of the spectrum. Instead, we can solve for the *highest* roots of the full inverse (FI) eigenvalue equation

$$\mathbf{M}(\mathbf{z}_k) = \omega_k^{-1} \mathbf{E}(\mathbf{z}_k) \tag{4.13}$$

which are the reciprocals of the excitation energies. Alternatively, we can solve the reduced eigenvalue equation, Eq. (4.8), for the squares of the lowest excitation energies, which we will call the canonical reduced (CR) equation.

$$\mathbf{H}^{-}(\mathbf{H}^{+}(\mathbf{c}_k^{+})) = \omega_k^2 \mathbf{c}_k^{+} \qquad \mathbf{H}^{\pm} \equiv \mathbf{S}^{-1}(\mathbf{A} \pm \mathbf{B}) \qquad \mathbf{c}_k^{\pm} \equiv \mathbf{x}_k \pm \mathbf{y}_k \tag{4.14}$$

Lastly, we consider the following symmetrized reduced (SR) eigenvalue equation

$$\bar{\mathbf{H}}^{-}(\bar{\mathbf{H}}^{+}(\bar{\mathbf{c}}_k^{+})) = \omega_k^2 \bar{\mathbf{c}}_k^{+} \qquad \bar{\mathbf{H}}^{\pm} \equiv \mathbf{S}^{-\frac{1}{2}}(\mathbf{A} \pm \mathbf{B})\mathbf{S}^{-\frac{1}{2}} \qquad \bar{\mathbf{c}}_k^{\pm} \equiv \mathbf{S}^{\frac{1}{2}}(\mathbf{x}_k \pm \mathbf{y}_k) \tag{4.15}$$

which is approximately Hermitian when the elements of $\mathbf{B}$ are small in magnitude.

For each of these variants of the LR-ODC-12 eigenvalue equation we can use different diagonal approximations to define the preconditioner. Here we will consider two possibilities. One option is to only use the Fock-like terms in the $\mathbf{A}$ matrix and approximate the metric as an identity matrix, which will here be called the Fock diagonal (FD) approximation.

$$(\tilde{\mathbf{S}}_{11}^{\mathrm{FD}})_{ia,ia} \equiv 1 \qquad (\tilde{\mathbf{A}}_{11}^{\mathrm{FD}})_{ia,ia} \equiv -f_i^i + f_a^a \qquad (\tilde{\mathbf{A}}_{22}^{\mathrm{FD}})_{ijab,ijab} \equiv -\mathcal{F}_i^i - \mathcal{F}_j^j - \mathcal{F}_a^a - \mathcal{F}_b^b \tag{4.16}$$

These generalized Fock matrices take the place of the mean-field Fock matrix in a linearized theory, where this would constitute the zeroth order perturbative approximation to the Hessian. Alternatively, we can approximate diagonals of our transformation matrices as products of the exact diagonals of $\mathbf{A}$, $\mathbf{S}$, and, for the reduced eigenvalue equations, also $\mathbf{B}$. I will call this the product of exact

diagonals (PED) approximation. Evaluating these diagonal elements from the transformation function is computationally inefficient because it requires $\mathcal{O}(o^2v^2)$ function evaluations, each of which scales as $\mathcal{O}(o^2v^4)$, so it is important to have analytic formulae for the diagonals. The two-body diagonals are given by

$$\begin{aligned}(\tilde{\mathbf{A}}_{22}^{\mathrm{PED}})_{ijab,ijab} \equiv & -\mathcal{F}_i^i - \mathcal{F}_j^j - \mathcal{F}_a^a - \mathcal{F}_b^b + \overline{g}_{ij}^{ij} + \overline{g}_{ab}^{ab} - S(i/j|a/b)\overline{g}_{ia}^{ia} \\ & + S(a/b)\mathcal{G}_{af}^{ea} t_{eb}^{ij} t_{ij}^{fb} - S(a/b)\mathcal{G}_{af}^{eb} t_{eb}^{ij} t_{ij}^{fa} + 2S(i/j|a/b)\mathcal{G}_{ia}^{me} t_{eb}^{ij} t_{mj}^{ab} \\ & + S(i/j)\mathcal{G}_{mi}^{in} t_{ab}^{mj} t_{nj}^{ab} - S(i/j)\mathcal{G}_{mj}^{jn} t_{ab}^{mi} t_{nj}^{ab} \end{aligned} \tag{4.17}$$

$$\begin{aligned}(\tilde{\mathbf{B}}_{22}^{\mathrm{PED}})_{ijab,ijab} \equiv & + S(a/b)\mathcal{G}_{aa}^{ef} t_{eb}^{ij} t_{fb}^{ij} - S(a/b)\mathcal{G}_{ba}^{ef} t_{eb}^{ij} t_{fb}^{ij} + 2S(i/j|a/b)\mathcal{G}_{ma}^{ia} t_{eb}^{ij} t_{ab}^{mj} \\ & + S(i/j)\mathcal{G}_{mn}^{ii} t_{ab}^{mj} t_{ab}^{nj} - S(i/j)\mathcal{G}_{mn}^{ij} t_{ab}^{mj} t_{ab}^{ni} \end{aligned} \tag{4.18}$$

where $S(p/q)v_{pq}^{pq} = v_{pq}^{pq} + v_{qp}^{qp}$ denotes an index symmetrizer. Formulae for the diagonals of the one-body blocks of $\mathbf{A}$, $\mathbf{B}$, and $\mathbf{S}$ are included in the appendix, Section 4.A.

Table 4.1 shows the results for each solution strategy on five small molecules, ranging in size from water to ethylene, using the def2-SV(P) basis set[205] of Weigend and Ahlrichs. The Davidson algorithm and the LR-ODC-12 were implemented as part of a standalone Python code interfaced to the Psi4[177] and Pyscf[178] packages, which performed the integral evaluations. In this code the order of operations of the tensor contractions is optimized before passing the operations off to the appropriate BLAS linear algebra kernels, which use multithreading for performance enhancement. Comparing the three strategies, we see that the FI strategy consistently achieves the best convergence, with the CR and SR strategies requiring $\sim$ 50% more iterations in most cases. This comes at the cost of a 2–3 times

Table 4.1: A comparison of three different solution strategies for the LR-ODC-12 model for five molecules using the def2-SV(P) basis set. In each case 10 eigenvectors are converged to 10^{-5} a.u., starting from an initial expansion space of 100 guess vectors and collapsing the subspace very 200 vectors. The second and third columns show the number of singles and doubles parameters for each system, which determine the dimensions of the matrix equation, and the remaining columns give the number of iterations, the run-time, and the number of low-lying roots obtained for each strategy. The first row for each molecule shows the results for the FD preconditioner and the second row shows the results for the PED preconditioner. All computations were run on an Intel® Core™ i7-5600U processor using four threads.

			Full Inverse			Canonical Reduced			Symmetrized Reduced		
	n_1	n_2	iter	time (s)	roots	iter	time (s)	roots	iter	time (s)	roots
H_2O	260	14,625	11	23	10/10	16	29	10/10	16	30	10/10
			11	23	10/10	24	38	10/10	24	40	10/10
N_2	588	78,351	14	186	10/10	17	213	9/10	17	216	9/10
			10	156	10/10	15	179	9/10	15	202	9/10
HCN	644	94,185	15	251	9/10	21	281	9/10	21	331	9/10
			10	205	9/10	18	252	9/10	19	308	9/10
H_2CO	768	135,360	20	478	7/10	28	638	6/10	27	650	6/10
			11	362	7/10	23	442	7/10	25	614	7/10
C_2H_4	896	184,800	17	640	9/10	25	874	9/10	25	891	9/10
			10	500	9/10	19	574	9/10	20	722	9/10

greater memory requirement which will require the vectors to be stored on disk for larger systems. This likely owes to the fact that the diagonal approximations of the preconditioner are more appropriate for the full transformation than the reduced ones, so the convergence gap could likely be closed by developing better preconditioners for the latter. The performance of the SR strategy is consistently similar or marginally worse than that of the CR strategy, suggesting that the symmetrization is not worth it. Comparing the rows for each strategy shows that the PED preconditioner consistently reduces the number of iterations to convergence with the exception of water, where the reduced algorithms perform slightly worse with the alternative preconditioner. The FI strategy is helped more than the reduced strategies by the PED preconditioner, which further widens the gap in their convergence rates. Taken together, these results suggest that the FI/PED combination is to be preferred if it can be afforded, and the CR/PED combination presents a second best option.

4.A LR-ODC-12 Linear Transformation Formulas

$$\begin{aligned}(\mathbf{A}_{11}(\mathbf{u}_{\mu,1}))_{ia} = & h^i_j \gamma^b_a u^j_{\mu,b} + h^b_a \gamma^i_j u^j_{\mu,b} - \bar{F}^i_j u^j_{\mu,a} - \bar{F}^b_a u^i_{\mu,b} + \overline{g}^{mi}_{nj} \gamma^{nb}_{ma} u^j_{\mu,b} \\ & + \overline{g}^{nb}_{ma} \gamma^{mi}_{nj} u^j_{\mu,b} + \overline{g}^{ie}_{jf} \gamma^{bf}_{ae} u^j_{\mu,b} + \overline{g}^{bf}_{ae} \gamma^{ie}_{jf} u^j_{\mu,b} + \overline{g}^{ib}_{me} \gamma^{me}_{ja} u^j_{\mu,b} \\ & + \overline{g}^{me}_{ja} \gamma^{ib}_{me} u^j_{\mu,b}\end{aligned} \tag{4.19}$$

$$\begin{aligned}(\mathbf{B}_{11}(\mathbf{u}_{\mu,1}))_{ia} = & \overline{g}^{im}_{be} \gamma^{je}_{ma} u^b_{\mu,j} + \overline{g}^{je}_{ma} \gamma^{im}_{be} u^b_{\mu,j} + \overline{g}^{ie}_{mb} \gamma^{jm}_{ae} u^b_{\mu,j} + \overline{g}^{jm}_{ae} \gamma^{ie}_{mb} u^b_{\mu,j} \\ & + \tfrac{1}{2} \overline{g}^{ij}_{mn} \gamma^{mn}_{ab} u^b_{\mu,j} + \tfrac{1}{2} \overline{g}^{mn}_{ab} \gamma^{ij}_{mn} u^b_{\mu,j} + \tfrac{1}{2} \overline{g}^{ij}_{ef} \gamma^{ef}_{ab} u^b_{\mu,j} + \tfrac{1}{2} \overline{g}^{ef}_{ab} \gamma^{ij}_{ef} u^b_{\mu,j}\end{aligned} \tag{4.20}$$

$$
\begin{aligned}
(\mathbf{A}_{12}(\mathbf{u}_{\mu,2}))_{ia} = & -\tfrac{1}{2}\overline{g}^{cd}_{la}u^{il}_{\mu,cd} - \tfrac{1}{2}\overline{g}^{id}_{kl}u^{kl}_{\mu,ad} - \tfrac{1}{2}(\mathcal{I}^{i}_{a})^{m}_{k}t^{cd*}_{ml}u^{kl}_{\mu,cd} - \tfrac{1}{2}(\mathcal{I}^{i}_{a})^{c}_{e}t^{ed*}_{kl}u^{kl}_{\mu,cd} \\
& -\overline{g}^{mc}_{ae}t^{ed*}_{ml}u^{il}_{\mu,cd} - \overline{g}^{im}_{ke}t^{ed*}_{ml}u^{kl}_{\mu,ad} - \tfrac{1}{4}\overline{g}^{mn}_{la}t^{cd*}_{mn}u^{il}_{\mu,cd} \\
& -\tfrac{1}{4}\overline{g}^{id}_{ef}t^{ef*}_{kl}u^{kl}_{\mu,ad}
\end{aligned}
\tag{4.21}
$$

$$
\begin{aligned}
(\mathbf{B}_{12}(\mathbf{u}_{\mu,2}))_{ia} = & -\tfrac{1}{2}(\mathcal{I}^{i}_{a})^{k}_{m}t^{ml}_{cd}u^{cd}_{\mu,kl} - \tfrac{1}{2}(\mathcal{I}^{i}_{a})^{e}_{c}t^{kl}_{ed}u^{cd}_{\mu,kl} - \overline{g}^{le}_{ad}t^{ki}_{ce}u^{cd}_{\mu,kl} - \overline{g}^{il}_{md}t^{km}_{ca}u^{cd}_{\mu,kl} \\
& -\tfrac{1}{4}\overline{g}^{kl}_{ma}t^{im}_{cd}u^{cd}_{\mu,kl} - \tfrac{1}{4}\overline{g}^{ie}_{cd}t^{kl}_{ae}u^{cd}_{\mu,kl}
\end{aligned}
\tag{4.22}
$$

$$
\begin{aligned}
(\mathbf{A}_{21}(\mathbf{u}_{\mu,1}))_{ijab} = & -P^{(i/j)}\overline{g}^{jc}_{ab}u^{i}_{\mu,c} - P_{(a/b)}\overline{g}^{ij}_{kb}u^{k}_{\mu,a} - P^{(i/j)}(\mathcal{I}^{c}_{k})^{i}_{m}t^{mj}_{ab}u^{k}_{\mu,c} \\
& -P_{(a/b)}(\mathcal{I}^{c}_{k})^{e}_{a}t^{ij}_{eb}u^{k}_{\mu,c} - P^{(i/j)}_{(a/b)}\overline{g}^{ce}_{ma}t^{mj}_{eb}u^{i}_{\mu,c} - P^{(i/j)}_{(a/b)}\overline{g}^{ie}_{km}t^{mj}_{eb}u^{k}_{\mu,a} \\
& -\tfrac{1}{2}P^{(i/j)}\overline{g}^{jc}_{mn}t^{mn}_{ab}u^{i}_{\mu,c} - \tfrac{1}{2}P_{(a/b)}\overline{g}^{ef}_{kb}t^{ij}_{ef}u^{k}_{\mu,a}
\end{aligned}
\tag{4.23}
$$

$$
\begin{aligned}
(\mathbf{B}_{21}(\mathbf{u}_{\mu,1}))_{ijab} = & -P^{(i/j)}(\mathcal{I}^{k}_{c})^{i}_{m}t^{mj}_{ab}u^{c}_{\mu,k} - P_{(a/b)}(\mathcal{I}^{k}_{c})^{e}_{a}t^{ij}_{eb}u^{c}_{\mu,k} - P^{(i/j)}_{(a/b)}\overline{g}^{je}_{cb}t^{ik}_{ae}u^{c}_{\mu,k} \\
& -P^{(i/j)}_{(a/b)}\overline{g}^{mb}_{kj}t^{im}_{ac}u^{c}_{\mu,k} - \overline{g}^{ij}_{mc}t^{km}_{ab}u^{c}_{\mu,k} - \overline{g}^{ke}_{ab}t^{ij}_{ce}u^{c}_{\mu,k}
\end{aligned}
\tag{4.24}
$$

$$
\begin{aligned}
(\mathbf{A}_{22}(\mathbf{u}_{\mu,2}))_{ijab} = & -P_{(a/b)}\mathcal{F}^{c}_{a}u^{ij}_{\mu,cb} - P^{(i/j)}\mathcal{F}^{i}_{k}u^{kj}_{\mu,ab} + \tfrac{1}{2}\overline{g}^{cd}_{ab}u^{ij}_{\mu,cd} + \tfrac{1}{2}\overline{g}^{ij}_{kl}u^{kl}_{\mu,ab} \\
& -P^{(i/j)}_{(a/b)}\overline{g}^{jc}_{la}u^{il}_{\mu,cb} + \tfrac{1}{2}P_{(a/b)}\mathcal{G}^{ec}_{af}t^{ij}_{eb}t^{fd*}_{kl}u^{kl}_{\mu,cd} + \tfrac{1}{2}P_{(a/b)}\mathcal{G}^{me}_{ka}t^{ij}_{eb}t^{cd*}_{ml}u^{kl}_{\mu,cd} \\
& +\tfrac{1}{2}P^{(i/j)}\mathcal{G}^{ic}_{me}t^{mj}_{ab}t^{ed*}_{kl}u^{kl}_{\mu,cd} + \tfrac{1}{2}P^{(i/j)}\mathcal{G}^{in}_{mk}t^{mj}_{ab}t^{cd*}_{nl}u^{kl}_{\mu,cd}
\end{aligned}
\tag{4.25}
$$

$$(\mathbf{B}_{22}(\mathbf{u}_{\mu,2}))_{ijab} = \tfrac{1}{2}P_{(a/b)}\mathcal{G}^{ef}_{ac}t^{ij}_{eb}t^{kl}_{fd}u^{cd}_{\mu,kl} + \tfrac{1}{2}P_{(a/b)}\mathcal{G}^{ke}_{na}t^{ij}_{eb}t^{nl}_{cd}u^{cd}_{\mu,kl} + \tfrac{1}{2}P^{(i/j)}\mathcal{G}^{if}_{mc}t^{mj}_{ab}t^{kl}_{fd}u^{cd}_{\mu,kl} + \tfrac{1}{2}P^{(i/j)}\mathcal{G}^{ik}_{mn}t^{mj}_{ab}t^{nl}_{cd}u^{cd}_{\mu,kl} \tag{4.26}$$

$$(\mathbf{S}_{11}(\mathbf{u}_{\mu,1}))_{ia} = \gamma^i_j u^j_{\mu,a} - \gamma^b_a u^i_{\mu,b} \tag{4.27}$$

$$(\mathbf{S}^{-1}_{11}(\mathbf{u}_{\mu,1}))_{ia} = \frac{(\mathbf{Y}^\dagger)^i_{j'}(\mathbf{Y})^{b'}_a}{\gamma_{j'} - \gamma_{b'}}(\mathbf{Y}^\dagger)^b_{b'}(\mathbf{Y})^{j'}_j u^j_{\mu,b} \tag{4.28}$$

$$(\mathbf{Y}^\dagger)^q_{q'}\gamma^p_q(\mathbf{Y})^{p'}_p = \delta^{p'}_{q'}\gamma_{q'} \tag{4.29}$$

$$(\tilde{\mathbf{A}}^{\mathrm{PED}}_{11})_{ia,ia} = f^i_i\gamma^a_a + f^a_a\gamma^i_i - \bar{F}^i_i - \bar{F}^a_a - \overline{g}^{na}_{ma}\gamma^m_i\gamma^i_n - \overline{g}^{if}_{ie}\gamma^a_f\gamma^e_a + 2\overline{g}^{me}_{ia}\gamma^i_m\gamma^a_e - \overline{g}^{ni}_{mi}t^{nk}_{ac}t^{ac}_{mk} \tag{4.30}$$

$$\begin{aligned}(\tilde{\mathbf{A}}^{\mathrm{PED}}_{22})_{ijab,ijab} \equiv & -\mathcal{F}^i_i - \mathcal{F}^j_j - \mathcal{F}^a_a - \mathcal{F}^b_b + \overline{g}^{ij}_{ij} + \overline{g}^{ab}_{ab} - S(i/j|a/b)\overline{g}^{ia}_{ia} \\ & + S(a/b)\mathcal{G}^{ea}_{af}t^{ij}_{eb}t^{fb}_{ij} - S(a/b)\mathcal{G}^{eb}_{af}t^{ij}_{eb}t^{fa}_{ij} + 2S(i/j|a/b)\mathcal{G}^{me}_{ia}t^{ij}_{eb}t^{ab}_{mj} \\ & + S(i/j)\mathcal{G}^{in}_{mi}t^{mj}_{ab}t^{ab}_{nj} - S(i/j)\mathcal{G}^{jn}_{mj}t^{mi}_{ab}t^{ab}_{nj}\end{aligned} \tag{4.31}$$

$$\begin{aligned}(\tilde{\mathbf{B}}^{\mathrm{PED}}_{22})_{ijab,ijab} \equiv & +S(a/b)\mathcal{G}^{ef}_{aa}t^{ij}_{eb}t^{ij}_{fb} - S(a/b)\mathcal{G}^{ef}_{ba}t^{ij}_{eb}t^{ij}_{fb} + 2S(i/j|a/b)\mathcal{G}^{ia}_{ma}t^{ij}_{eb}t^{mj}_{ab} \\ & + S(i/j)\mathcal{G}^{ii}_{mn}t^{mj}_{ab}t^{nj}_{ab} - S(i/j)\mathcal{G}^{ij}_{mn}t^{mj}_{ab}t^{ni}_{ab}\end{aligned} \tag{4.32}$$

Chapter 5

Conclusion

We have presented comprehensive benchmarks to demonstrate that orbital-optimized density cumulant theory with double excitations (ODC-12) consistently outperforms coupled-cluster theory with singles and doubles (CCSD) for the description of noncovalent interactions, hydrogen-transfer barrier heights, radical stabilization energies, ionization energies, and covalent bond stretching. Having established the promising performance of this model for ground state calculations, we have extended the theory for the calculation of excitation energies and transition properties through the use of linear response theory. After numerically demonstrating that our initial working equations and implementation are correct, we have empirically shown this method to be size-intensive, i.e. displaying the correct qualitative behavior with respect to excited states of independent systems. Next, we have shown that this method is more stable with respect to strong electron correlation than its linearized variant, LR-OLCCD, which often achieves impressive error cancellation in the absence of strong correlation. This demonstrates that the infinite order one-particle n-representability conditions defining the ODC-12 method con-

tribute to a robust description of the electron distribution for more challenging states. Our initial benchmark study of the vertical excitation energies predicted by this method shows that it reduces the mean absolute error by roughly a factor of two relative to the popular equation-of-motion coupled-cluster with singles and doubles (EOM-CCSD) method, similar to our findings for ground states. For well-behaved systems we find that the linearized model, LR-OLCCD, is an effective approximation to LR-ODC-12 with a lower cost prefactor. Finally, we develop some improvements to the algorithms used for solving the LR-ODC-12 equations using disk-based direct matrix algorithms (variants of the Davidson algorithm). These developments allow us to study polyene systems as large as hexatriene with a natural orbital basis of double-zeta quality. This calculation involves 44 electrons and 124 spatial orbitals withnearly 20 million unique wavefunction parameters, which would not be feasible without the new algorithms. The advantages of LR-ODC-12 over EOM-CCSD and LR-OLCCD for these polyene systems are even more stark than for our previous benchmarks. Whereas EOM-CCSD overestimates the energy of the challenging 2^1A_g state of hexatriene and its gap with the neighboring 1^1B_u state by close to 1 eV each, LR-ODC-12 matches its energy to within 0.15 eV and matches the energy gap to within 0.01 eV. Given the relative sparsity of inexpensive alternatives to EOM-CCSD, we believe that these results merit further development of algorithms for the LR-ODC-12 method to expand our toolkit for studying excited electronic states.

Bibliography

[1] A. V. Copan, A. Y. Sokolov, and H. F. Schaefer, J. Chem. Theory Comput. **10**, 2389 (2014).

[2] W. Heisenberg, Z. Phys. **33**, 879 (1925).

[3] E. Schrödinger, Ann. Phys. **384**, 361 (1926).

[4] E. Schrödinger, Ann. Phys. **384**, 489 (1926).

[5] E. Schrödinger, Ann. Phys. **384**, 734 (1926).

[6] W. Pauli, Z. Phys. **36**, 336 (1926).

[7] G. E. Uhlenbeck and S. Goudsmit, Naturwissenschaften , 953 (1925).

[8] W. Pauli, Z. Phys. **31**, 373 (1925).

[9] W. Gerlach and O. Stern, Z. Phys. **9**, 349 (1922).

[10] W. Pauli, Z. Phys. **31**, 765 (1925).

[11] W. Heisenberg, Z. Phys. **38**, 411 (1926).

[12] S. N. Bose, Z. Phys. **26**, 178 (1924).

[13] A. Einstein, Sitzber. Preuss. Akad. **22**, 261 (1924).

[14] A. Einstein, Sitzber. Preuss. Akad. **1**, 3 (1925).

[15] M. Nooijen, K. R. Shamasundar, and D. Mukherjee, Mol. Phys. **103**, 2277 (2005).

[16] J. A. Pople, J. S. Binkley, and R. Seeger, Int. J. Quantum Chem. **10**, 1 (1976).

[17] R. J. Bartlett, Annu. Rev. Phys. Chem. **32**, 359 (1981).

[18] P. G. Szalay, M. Nooijen, and R. J. Bartlett, J. Chem. Phys. **103**, 281 (1995).

[19] H. P. Kelly and A. M. Sessler, Phys. Rev. **132**, 2091 (1963).

[20] H. P. Kelly, Phys. Rev. A **134**, 1450 (1964).

[21] W. Meyer, J. Chem. Phys. **58**, 1017 (1973).

[22] R. Ahlrichs, Comput. Phys. Commun. **17**, 31 (1979).

[23] S. Koch and W. Kutzelnigg, Theor. Chim. Acta **59**, 387 (1981).

[24] M. Gelus, R. Ahlrichs, V. Staemmler, and W. Kutzelnigg, Chem. Phys. Lett. **7**, 503 (1970).

[25] V. Staemmler and M. Jungen, Chem. Phys. Lett. **16**, 187 (1972).

[26] R. Ahlrichs, F. Driessler, H. Lischka, V. Staemmler, and W. Kutzelnigg, J. Chem. Phys. **62**, 1235 (1975).

[27] H. Kollmar and V. Staemmler, J. Am. Chem. Soc. **99**, 3583 (1977).

[28] J. Wasilewski, V. Staemmler, and S. Koch, Phys. Rev. A **38**, 1289 (1988).

[29] A. G. Taube and R. J. Bartlett, J. Chem. Phys. **130**, 144112 (2009).

[30] F. Coester, Nucl. Phys. **7**, 421 (1958).

[31] F. Coester and H. Kümmel, Nucl. Phys. **17**, 477 (1960).

[32] J. Čížek, J. Chem. Phys. **45**, 4256 (1966).

[33] R. J. Bartlett and G. D. Purvis, Int. J. Quantum Chem. **14**, 561 (1978).

[34] T. D. Crawford and H. F. Schaefer, Rev. Comp. Chem. **14**, 33 (2000).

[35] R. J. Bartlett and M. Musiał, Rev. Mod. Phys. **79**, 291 (2007).

[36] I. Shavitt and R. J. Bartlett, *Many-Body Methods in Chemistry and Physics* (Cambridge University Press, Cambridge, UK, 2009).

[37] C. Kollmar and F. Neese, Mol. Phys. **108**, 2449 (2010).

[38] J. P. Daudey, J. L. Heully, and J. P. Malrieu, J. Chem. Phys. **99**, 1240 (1993).

[39] J. P. Malrieu, H. Zhang, and J. Ma, Chem. Phys. Lett. **493**, 179 (2010).

[40] M. Nooijen and R. J. Le Roy, J. Mol. Struct. **768**, 25 (2006).

[41] C. Kollmar and F. Neese, J. Chem. Phys. **135**, 84102 (2011).

[42] C. Kollmar and A. Heßelmann, Theor. Chem. Acc. **127**, 311 (2010).

[43] U. Bozkaya and C. D. Sherrill, J. Chem. Phys. **139**, 054104 (2013).

[44] E. SoydaÅ§ and U. Bozkaya, J. Comput. Chem. **35**, 1073 (2014).

[45] U. Bozkaya, J. Chem. Phys. **139**, 154105 (2013).

[46] F. Wennmohs and F. Neese, Chem. Phys. **343**, 217 (2008).

[47] F. Neese, F. Wennmohs, and A. Hansen, J. Chem. Phys. **130**, 114108 (2009).

[48] W. Kutzelnigg, J. Chem. Phys. **125**, 171101 (2006).

[49] D. A. Mazziotti, Phys. Rev. Lett. **101**, 253002 (2008).

[50] D. A. Mazziotti, Phys. Rev. A **81**, 62515 (2010).

[51] A. E. DePrince and D. A. Mazziotti, Mol. Phys. **110**, 1917 (2012).

[52] W. Kutzelnigg and D. Mukherjee, J. Chem. Phys. **107**, 432 (1997).

[53] D. A. Mazziotti, Chem. Phys. Lett. **289**, 419 (1998).

[54] D. A. Mazziotti, Phys. Rev. A **57**, 4219 (1998).

[55] W. Kutzelnigg and D. Mukherjee, J. Chem. Phys. **110**, 2800 (1999).

[56] L. Kong, Int. J. Quantum Chem. **111**, 3541 (2011).

[57] M. Hanauer and A. Köhn, Chem. Phys. **401**, 50 (2012).

[58] M. Nakata and K. Yasuda, Phys. Rev. A **80**, 42109 (2009).

[59] H. van Aggelen, B. Verstichel, P. Bultinck, D. Van Neck, P. W. Ayers, and D. L. Cooper, J. Chem. Phys. **132**, 114112 (2010).

[60] B. Verstichel, H. van Aggelen, D. Van Neck, P. W. Ayers, and P. Bultinck, J. Chem. Phys. **132**, 114113 (2010).

[61] J. M. Herbert and J. E. Harriman, Adv. Chem. Phys. **134**, 261 (2007).

[62] A. C. Simmonett, J. J. Wilke, H. F. Schaefer, and W. Kutzelnigg, J. Chem. Phys. **133**, 174122 (2010).

[63] A. Y. Sokolov, J. J. Wilke, A. C. Simmonett, and H. F. Schaefer, J. Chem. Phys. **137**, 054105 (2012).

[64] W. Kutzelnigg and D. Mukherjee, J. Chem. Phys. **120**, 7350 (2004).

[65] A. Y. Sokolov, A. C. Simmonett, and H. F. Schaefer, J. Chem. Phys. **138**, 024107 (2013).

[66] A. Y. Sokolov and H. F. Schaefer, J. Chem. Phys. **139**, 204110 (2013).

[67] D. A. Mazziotti, ed., *Reduced-Density-Matrix Mechanics: With Application to Many-Electron Atoms and Molecules*, Advances in Chemical Physics, Vol. 134 (John Wiley & Sons, Inc., Hoboken, NJ, 2007).

[68] J. M. Turney, A. C. Simmonett, R. M. Parrish, E. G. Hohenstein, F. A. Evangelista, J. T. Fermann, B. J. Mintz, L. A. Burns, J. J. Wilke, M. L. Abrams, N. J. Russ, M. L. Leininger, C. L. Janssen, E. T. Seidl, W. D.

Allen, H. F. Schaefer, R. A. King, E. F. Valeev, C. D. Sherrill, and T. D. Crawford, WIREs Comput. Mol. Sci. **2**, 556 (2012).

[69] K. Raghavachari, G. W. Trucks, J. A. Pople, and M. Head-Gordon, Chem. Phys. Lett. **157**, 479 (1989).

[70] J. F. Stanton, Chem. Phys. Lett. **281**, 130 (1997).

[71] T. H. Dunning, J. Chem. Phys. **90**, 1007 (1989).

[72] D. E. Woon and T. H. Dunning, J. Chem. Phys. **103**, 4572 (1995).

[73] R. A. Kendall, T. H. Dunning, and R. J. Harrison, J. Chem. Phys. **96**, 6796 (1992).

[74] J. ÅŸezáč and P. Hobza, J. Chem. Theory Comput. **9**, 2151 (2013).

[75] Y. Zhao, B. J. Lynch, and D. G. Truhlar, Phys. Chem. Chem. Phys. **7**, 43 (2005).

[76] E. SoydaÅ§ and U. Bozkaya, J. Chem. Theory Comput. **9**, 1452 (2013).

[77] B. J. Lynch, Y. Zhao, and D. G. Truhlar, "enquote "bibinfo title The Minnesota Databases for Chemistry and Solid-State Physics," .

[78] H. Zipse, Top. Curr. Chem. **263**, 163 (2006).

[79] E. F. C. Byrd, C. D. Sherrill, and M. Head-Gordon, J. Phys. Chem. A **105**, 9736 (2001).

[80] G. J. O. Beran, S. R. Gwaltney, and M. Head-Gordon, Phys. Chem. Chem. Phys. **5**, 2488 (2003).

[81] R. C. Lochan and M. Head-Gordon, J. Chem. Phys. **126**, 164101 (2007).

[82] W. Kurlancheek and M. Head-Gordon, Mol. Phys. **107**, 1223 (2009).

[83] U. Bozkaya, J. Chem. Phys. **135**, 224103 (2011).

[84] S. G. Lias, J. E. Bartmess, J. F. Liebman, J. L. Holmes, R. D. Levin, and W. G. Mallard, J. Phys. Chem. Ref. Data **17**, 1 (1988).

[85] T. Trickl, E. F. Cromwell, Y. T. Lee, and A. H. Kung, J. Chem. Phys. **91**, 6006 (1989).

[86] Z. Zhang, S. C. Kuo, R. B. Klemm, P. S. Monks, and L. J. Stief, Chem. Phys. Lett. **229**, 377 (1994).

[87] A. Hansel, C. Scheiring, M. Glantschnig, W. Lindinger, and E. E. Ferguson, J. Chem. Phys. **109**, 1748 (1998).

[88] U. Bozkaya and H. F. Schaefer, J. Chem. Phys. **136**, 204114 (2012).

[89] W. Kutzelnigg and D. Mukherjee, J. Chem. Phys. **116**, 4787 (2002).

[90] W. Kutzelnigg, K. R. Shamasundar, and D. Mukherjee, Mol. Phys. **108**, 433 (2010).

[91] H.-J. Werner, F. R. Manby, and P. J. Knowles, J. Chem. Phys. **118**, 8149 (2003).

[92] A. G. Taube and R. J. Bartlett, Collect. Czech. Chem. Commun. **70**, 837 (2005).

[93] F. Neese, A. Hansen, and D. G. Liakos, J. Chem. Phys. **131**, 64103 (2009).

[94] O. Vahtras, J. Almlöf, and M. W. Feyereisen, Chem. Phys. Lett. **213**, 514 (1993).

[95] G. Hetzer, M. Schütz, H. Stoll, and H.-J. Werner, J. Chem. Phys. **113**, 9443 (2000).

[96] M. Schütz and H.-J. Werner, J. Chem. Phys. **114**, 661 (2001).

[97] T. B. Pedersen, H. Koch, and C. Hättig, J. Chem. Phys. **110**, 8318 (1999).

[98] T. B. Pedersen, B. Fernández, and H. Koch, J. Chem. Phys. **114**, 6983 (2001).

[99] P. J. Knowles and H.-J. Werner, Chem. Phys. Lett. **115**, 259 (1985).

[100] K. Wolinski, H. L. Sellers, and P. Pulay, Chem. Phys. Lett. **140**, 225 (1987).

[101] K. Hirao, Chem. Phys. Lett. **190**, 374 (1992).

[102] J. P. Finley, P. Å. Malmqvist, B. O. Roos, and L. Serrano-Andrés, Chem. Phys. Lett. **288**, 299 (1998).

[103] K. Andersson, P. Å. Malmqvist, B. O. Roos, A. J. Sadlej, and K. Wolinski, J. Phys. Chem. **94**, 5483 (1990).

[104] K. Andersson, P. Å. Malmqvist, and B. O. Roos, J. Chem. Phys. **96**, 1218 (1992).

[105] C. Angeli, R. Cimiraglia, S. Evangelisti, T. Leininger, and J.-P. Malrieu, J. Chem. Phys. **114**, 10252 (2001).

[106] C. Angeli, R. Cimiraglia, and J.-P. Malrieu, Chem. Phys. Lett. **350**, 297 (2001).

[107] D. Mukherjee, R. K. Moitra, and A. Mukhopadhyay, Mol. Phys. **33**, 955 (1977).

[108] B. Jeziorski and H. J. Monkhorst, Phys. Rev. A **24**, 1668 (1981).

[109] H.-J. Werner and P. J. Knowles, J. Chem. Phys. **89**, 5803 (1988).

[110] U. S. Mahapatra, B. Datta, and D. Mukherjee, Mol. Phys. **94**, 157 (1998).

[111] J. Pittner, J. Chem. Phys. **118**, 10876 (2003).

[112] F. A. Evangelista, W. D. Allen, and H. F. Schaefer, J. Chem. Phys. **127**, 24102 (2007).

[113] D. Datta, L. Kong, and M. Nooijen, J. Chem. Phys. **134**, 214116 (2011).

[114] F. A. Evangelista and J. Gauss, J. Chem. Phys. **134**, 114102 (2011).

[115] A. Köhn, M. Hanauer, L. A. Mück, T.-C. Jagau, and J. Gauss, Wiley Interdiscip. Rev.: Comput. Mol. Sci. **3**, 176 (2013).

[116] M. Nooijen, O. Demel, D. Datta, L. Kong, K. R. Shamasundar, V. Lotrich, L. M. Huntington, and F. Neese, J. Chem. Phys. **140**, 81102 (2014).

[117] J. B. Foresman, M. Head-Gordon, J. A. Pople, and M. J. Frisch, J. Phys. Chem. **96**, 135 (1992).

[118] C. D. Sherrill and H. F. Schaefer, Adv. Quant. Chem. **34**, 143 (1999).

[119] J. Geertsen, M. Rittby, and R. J. Bartlett, Chem. Phys. Lett. **164**, 57 (1989).

[120] D. C. Comeau and R. J. Bartlett, Chem. Phys. Lett. **207**, 414 (1993).

[121] J. F. Stanton and R. J. Bartlett, J. Chem. Phys. **98**, 7029 (1993).

[122] A. I. Krylov, Annu. Rev. Phys. Chem. **59**, 433 (2008).

[123] H. Sekino and R. J. Bartlett, Int. J. Quantum Chem. **26**, 255 (1984).

[124] H. Koch, H. J. A. Jensen, P. Jørgensen, and T. Helgaker, J. Chem. Phys. **93**, 3345 (1990).

[125] H. Koch and P. Jørgensen, J. Chem. Phys. **93**, 3333 (1990).

[126] M. Nooijen and R. J. Bartlett, J. Chem. Phys. **106**, 6441 (1997).

[127] M. Nooijen and R. J. Bartlett, J. Chem. Phys. **107**, 6812 (1997).

[128] H. Nakatsuji and K. Hirao, J. Chem. Phys. **68**, 2053 (1978).

[129] H. Nakatsuji, Chem. Phys. Lett. **67**, 329 (1979).

[130] J. F. Stanton, J. Chem. Phys. **99**, 8840 (1993).

[131] J. F. Stanton and J. Gauss, J. Chem. Phys. **100**, 4695 (1994).

[132] J. F. Stanton and J. Gauss, J. Chem. Phys. **101**, 8938 (1994).

[133] S. V. Levchenko, T. Wang, and A. I. Krylov, J. Chem. Phys. **122**, 224106 (2005).

[134] C. Hättig, Adv. Quantum Chem. **50**, 37 (2005).

[135] A. Köhn and A. Tajti, J. Chem. Phys. **127**, 044105 (2007).

[136] E. F. Kjønstad, R. H. Myhre, T. J. Martínez, and H. Koch, J. Chem. Phys. **147**, 164105 (2017).

[137] J. Schirmer, Phys. Rev. A **26**, 2395 (1982).

[138] J. Schirmer, Phys. Rev. A **43**, 4647 (1991).

[139] A. Dreuw and M. Wormit, WIREs Comput. Mol. Sci. **5**, 82 (2014).

[140] A. G. Taube and R. J. Bartlett, Int. J. Quantum Chem. **106**, 3393 (2006).

[141] D. Kats, D. Usvyat, and M. Schütz, Phys. Rev. A **83**, 62503 (2011).

[142] G. Wälz, D. Kats, D. Usvyat, T. Korona, and M. Schütz, Phys. Rev. A **86**, 52519 (2012).

[143] E. F. Kjønstad and H. Koch, J. Phys. Chem. Lett. **8**, 4801 (2017).

[144] R. Moszynski, P. S. Żuchowski, and B. Jeziorski, Collect. Czech. Chem. Commun. **70**, 1109 (2005).

[145] T. Korona, Phys. Chem. Chem. Phys. **12**, 14977 (2010).

[146] A. Y. Sokolov, H. F. Schaefer, and W. Kutzelnigg, J. Chem. Phys. **141**, 74111 (2014).

[147] X. Wang, A. Y. Sokolov, J. M. Turney, and H. F. Schaefer, J. Chem. Theory Comput. **12**, 4833 (2016).

[148] We note that early on DCT was referred to as "density cumulant functional theory" (DCFT).

[149] P. Fulde, *Electron Correlations in Molecules and Solids* (Springer, Berlin, 1991).

[150] P. Ziesche, Solid State Commun **82**, 597 (1992).

[151] P. Ziesche, in *Many-Electron Densities and Reduced Density Matrices*, edited by J. Cioslowski (Springer US, Boston, MA, 2000) pp. 33–56.

[152] L. Kong and E. F. Valeev, J. Chem. Phys. **134**, 214109 (2011).

[153] F. Colmenero and C. Valdemoro, Phys. Rev. A **47**, 979 (1993).

[154] H. Nakatsuji and K. Yasuda, Phys. Rev. Lett. **76**, 1039 (1996).

[155] D. A. Mazziotti, Phys. Rev. Lett. **97**, 143002 (2006).

[156] C. Kollmar, J. Chem. Phys. **125**, 84108 (2006).

[157] A. E. DePrince and D. A. Mazziotti, Phys. Rev. A **76**, 42501 (2007).

[158] A. E. DePrince, J. Chem. Phys. **145**, 164109 (2016).

[159] W. Kutzelnigg, Theor. Chim. Acta **80**, 349 (1991).

[160] W. Kutzelnigg, Mol. Phys. **94**, 65 (1998).

[161] T. Van Voorhis and M. Head-Gordon, J. Chem. Phys. **113**, 8873 (2000).

[162] W. Kutzelnigg, J. Chem. Phys. **77**, 3081 (1982).

[163] R. J. Bartlett, S. A. Kucharski, and J. Noga, Chem. Phys. Lett. **155**, 133 (1989).

[164] J. D. Watts, G. W. Trucks, and R. J. Bartlett, Chem. Phys. Lett. **157**, 359 (1989).

[165] B. Cooper and P. J. Knowles, J. Chem. Phys. **133**, 234102 (2010).

[166] F. A. Evangelista, J. Chem. Phys. **134**, 224102 (2011).

[167] A. C. Scheiner, G. E. Scuseria, J. E. Rice, T. J. Lee, and H. F. Schaefer, J. Chem. Phys. **87**, 5361 (1987).

[168] E. A. Salter, G. W. Trucks, and R. J. Bartlett, J. Chem. Phys. **90**, 1752 (1989).

[169] J. Gauss, J. F. Stanton, and R. J. Bartlett, J. Chem. Phys. **95**, 2623 (1991).

[170] J. Gauss, W. J. Lauderdale, J. F. Stanton, J. D. Watts, and R. J. Bartlett, Chem. Phys. Lett. **182**, 207 (1991).

[171] J. W. Mullinax, A. Y. Sokolov, and H. F. Schaefer, J. Chem. Theory Comput. **11**, 2487 (2015).

[172] P. Norman, Phys. Chem. Chem. Phys. **13**, 20519 (2011).

[173] T. Helgaker, S. Coriani, P. Jørgensen, K. Kristensen, J. Olsen, and K. Ruud, Chem. Rev. **112**, 543 (2012).

[174] K. Kristensen, J. Kauczor, T. Kjærgaard, and P. Jørgensen, J. Chem. Phys. **131**, 044112 (2009).

[175] J. Olsen and P. Jørgensen, J. Chem. Phys. **82**, 3235 (1985).

[176] S. P. A. Sauer, *Molecular Electromagnetism: A Computational Chemistry Approach* (Oxford University Press, Oxford, 2011).

[177] R. M. Parrish, L. A. Burns, D. G. A. Smith, A. C. Simmonett, A. E. DePrince, E. G. Hohenstein, U. Bozkaya, A. Y. Sokolov, R. Di Remigio, R. M. Richard, J. F. Gonthier, A. M. James, H. R. McAlexander, A. Kumar, M. Saitow, X. Wang, B. P. Pritchard, P. Verma, H. F. Schaefer, K. Patkowski, R. A. King, E. F. Valeev, F. A. Evangelista, J. M. Turney, T. D. Crawford, and C. D. Sherrill, J. Chem. Theory Comput. **13**, 3185 (2017).

[178] Q. Sun, T. C. Berkelbach, N. S. Blunt, G. H. Booth, S. Guo, Z. Li, J. Liu, J. D. McClain, E. R. Sayfutyarova, S. Sharma, S. Wouters, and G. K.-L. Chan, WIREs Comput. Mol. Sci. **8**, e1340 (2018).

[179] E. R. Davidson, J. Comput. Phys. **17**, 87 (1975).

[180] B. Liu, "The Simultaneous Expansion Method for the Iterative Solution of Several of the Lowest-Lying Eigenvalues and Corresponding Eigenvectors of Large Real-Symmetric Matrices," Tech. Rep. (Lawrence Berkeley Laboratory, University of California, Berkeley, CA, USA, 1978).

[181] Y. Shao, Z. Gan, E. Epifanovsky, A. T. Gilbert, M. Wormit, J. Kussmann, A. W. Lange, A. Behn, J. Deng, X. Feng, D. Ghosh, M. Goldey, P. R. Horn, L. D. Jacobson, I. Kaliman, R. Z. Khaliullin, T. KuÅŻ, A. Landau, J. Liu, E. I. Proynov, Y. M. Rhee, R. M. Richard, M. A. Rohrdanz, R. P. Steele, E. J. Sundstrom, H. L. W. III, P. M. Zimmerman, D. Zuev, B. Albrecht, E. Alguire, B. Austin, G. J. O. Beran, Y. A. Bernard, E. Berquist, K. Brandhorst, K. B. Bravaya, S. T. Brown, D. Casanova, C.-M. Chang, Y. Chen, S. H. Chien, K. D. Closser, D. L. Crittenden, M. Diedenhofen, R. A. D. Jr., H. Do, A. D. Dutoi, R. G. Edgar, S. Fatehi, L. Fusti-Molnar, A. Ghysels, A. Golubeva-Zadorozhnaya, J. Gomes, M. W. Hanson-Heine, P. H. Harbach, A. W. Hauser, E. G. Hohenstein, Z. C. Holden, T.-C. Jagau, H. Ji, B. Kaduk, K. Khistyaev, J. Kim, J. Kim, R. A. King, P. Klunzinger, D. Kosenkov, T. Kowalczyk, C. M. Krauter, K. U. Lao, A. D. Laurent, K. V. Lawler, S. V. Levchenko, C. Y. Lin, F. Liu, E. Livshits, R. C. Lochan, A. Luenser, P. Manohar, S. F. Manzer, S.-P. Mao, N. Mardirossian, A. V. Marenich, S. A. Maurer, N. J. Mayhall, E. Neuscamman, C. M. Oana, R. Olivares-Amaya, D. P. OâĂŹNeill, J. A. Parkhill, T. M. Perrine, R. Peverati, A. Prociuk, D. R. Rehn, E. Rosta, N. J. Russ, S. M. Sharada, S. Sharma, D. W. Small, A. Sodt,

T. Stein, D. StÃijck, Y.-C. Su, A. J. Thom, T. Tsuchimochi, V. Vanovschi, L. Vogt, O. Vydrov, T. Wang, M. A. Watson, J. Wenzel, A. White, C. F. Williams, J. Yang, S. Yeganeh, S. R. Yost, Z.-Q. You, I. Y. Zhang, X. Zhang, Y. Zhao, B. R. Brooks, G. K. Chan, D. M. Chipman, C. J. Cramer, W. A. G. III, M. S. Gordon, W. J. Hehre, A. Klamt, H. F. S. III, M. W. Schmidt, C. D. Sherrill, D. G. Truhlar, A. Warshel, X. Xu, A. Aspuru-Guzik, R. Baer, A. T. Bell, N. A. Besley, J.-D. Chai, A. Dreuw, B. D. Dunietz, T. R. Furlani, S. R. Gwaltney, C.-P. Hsu, Y. Jung, J. Kong, D. S. Lambrecht, W. Liang, C. Ochsenfeld, V. A. Rassolov, L. V. Slipchenko, J. E. Subotnik, T. V. Voorhis, J. M. Herbert, A. I. Krylov, P. M. Gill, and M. Head-Gordon, Mol. Phys. **113**, 184 (2015).

[182] M. Kállay, Z. Rolik, J. Csontos, P. Nagy, G. Samu, D. Mester, J. Csóka, B. Szabó, I. LadjÃąnszki, L. Szegedy, B. Ladóczki, K. Petrov, M. Farkas, P. D. Mezei, and B. HÃľgely., "Mrcc, a quantum chemical program suite." See also: Z. Rolik, L. Szegedy, I. Ladjánszki, B. Ladóczki, and M. Kállay, J. Chem. Phys. 139, 094105 (2013), as well as: www.mrcc.hu.

[183] P.-O. Widmark, P. Å. Malmqvist, and B. O. O. Roos, Theoret. Chim. Acta **77**, 291 (1990).

[184] C. Daday, S. Smart, G. H. Booth, A. Alavi, and C. Filippi, J. Chem. Theory Comput. **8**, 4441 (2012).

[185] P. M. Zimmerman, J. Phys. Chem. A **121**, 4712 (2017).

[186] A. D. Chien, A. A. Holmes, M. Otten, C. J. Umrigar, S. Sharma, and P. M. Zimmerman, J. Phys. Chem. A **122**, 2714 (2018).

[187] P. Tavan and K. Schulten, J. Chem. Phys. **85**, 6602 (1986).

[188] P. Tavan and K. Schulten, Phys. Rev. B **36**, 4337 (1987).

[189] K. Nakayama, H. Nakano, and K. Hirao, Int. J. Quantum Chem. **66**, 157 (1998).

[190] E. R. Davidson, J. Phys. Chem. **100**, 6161 (1996).

[191] J. D. Watts, S. R. Gwaltney, and R. J. Bartlett, J. Chem. Phys. **105**, 6979 (1998).

[192] T. Müller, M. Dallos, and H. Lischka, J. Chem. Phys. **110**, 7176 (1999).

[193] X. Li and J. Paldus, Int. J. Quantum Chem. **74**, 177 (1999).

[194] J. H. Starcke, M. Wormit, J. Schirmer, and A. Dreuw, Chem. Phys. **329**, 39 (2006).

[195] Y. Kurashige, H. Nakano, Y. Nakao, and K. Hirao, Chem. Phys. Lett. **400**, 425 (2004).

[196] D. Ghosh, J. Hachmann, T. Yanai, and G. K.-L. Chan, J. Chem. Phys. **128**, 144117 (2008).

[197] A. Y. Sokolov, S. Guo, E. Ronca, and G. K.-L. Chan, J. Chem. Phys. **146**, 244102 (2017).

[198] M. Schreiber, M. R. Silva-Junior, S. P. A. Sauer, and W. Thiel, J. Chem. Phys. **128**, 134110 (2008).

[199] D. Zgid, D. Ghosh, E. Neuscamman, and G. K.-L. Chan, J. Chem. Phys. **130**, 194107 (2009).

[200] C. Angeli, Int. J. Quantum Chem. **110**, 2436 (2010).

[201] M. A. Watson and G. K.-L. Chan, J. Chem. Theory Comput. **8**, 4013 (2012).

[202] G. D. Lindh, T. J. Mach, and T. D. Crawford, Chem. Phys. **401**, 125 (2012).

[203] M. L. Leininger, C. D. Sherrill, W. D. Allen, and H. F. Schaefer, J. Comp. Chem. **22**, 1574 (2001).

[204] J. Oddershede, P. Jørgensen, and D. L. Yeager, Comput. Phys. Rep. **2**, 33 (1984).

[205] F. Weigend and R. Ahlrichs, Phys. Chem. Chem. Phys. **7**, 3297 (2005).